

# Diamond machining of silicon: A review of advances in molecular dynamics simulation

Saurav Goel<sup>a\*</sup>, Xichun Luo<sup>b</sup>, Anupam Agrawal<sup>c</sup> and Robert L Reuben<sup>d</sup>

<sup>a</sup> School of Mechanical and Aerospace Engineering, Queen's University, Belfast, BT95AH, UK

<sup>b</sup> Department of Design, Manufacture and Engineering Management, University of Strathclyde, Glasgow, G11XQ, UK

<sup>c</sup> Department of Business Administration, University of Illinois at Urbana-Champaign, USA

<sup>d</sup> School of Engineering and Physical Sciences, Heriot-Watt University, Edinburgh, EH144AS, UK

\* Corresponding author Tel.: +44 28 9097 5625, Email address: s.goel@qub.ac.uk, Fax: +44 028 9097 4148

## **Abstract:**

Molecular Dynamics (MD) simulation has enhanced our understanding about ductile-regime machining of brittle materials such as silicon and germanium. In particular, MD simulation has helped understand the occurrence of brittle-ductile transition due to the high-pressure phase transformation (HPPT), which induces Herzfeld-Mott transition. In this paper, relevant MD simulation studies in conjunction with experimental studies are reviewed with a focus on (i) The importance of machining variables: undeformed chip thickness, feed rate, depth of cut, geometry of the cutting tool in influencing the state of the deviatoric stresses to cause HPPT in silicon, (ii) The influence of material properties: role of fracture toughness and hardness, crystal structure and anisotropy of the material, and (iii) Phenomenological understanding of the wear of diamond cutting tools, which are all non-trivial for cost-effective manufacturing of silicon. The ongoing developmental work on potential energy functions is reviewed to identify opportunities for overcoming the current limitations of MD simulations. Potential research areas relating to how MD simulation might help improve existing manufacturing technologies are identified which may be of particular interest to early stage researchers.

**Keywords: MD simulation, silicon, diamond machining, high pressure phase transformation.**

## Abbreviations:

|              |  |
|--------------|--|
| <i>ABOP</i>  | Analytical bond order potential          |
| AMMPs        | Advanced micro-machining processes       |
| AMNFPs       | Advanced micro-/nano-finishing processes |
| BDT          | Brittle-ductile transition               |
| <i>BOP</i>   | Bond order potential function            |
| CIS          | Critical indent size                     |
| DBT          | Ductile to brittle transition            |
| DXA          | Dislocation extraction algorithm         |
| HPPT         | High pressure phase transformation       |
| IC           | Internal combustion                      |
| IR           | Infra red                                |
| MEMS         | Micro-electro-mechanical system          |
| MD           | Molecular dynamics                       |
| MNM          | Micro-/nano-machining                    |
| NEMS         | Nano-electro-mechanical system           |
| <i>NVE</i>   | Microcanonical ensemble                  |
| <i>OVITO</i> | Open Visualization tool                  |
| PBC          | Periodic boundary condition              |
| PCD          | Polycrystalline diamond                  |
| RDF / $g(r)$ | Radial distribution function             |
| SPDT         | Single point diamond turning             |
| UPL          | Ultra precision lathe machine            |
| UPM          | Ultra precision manufacturing            |

## Nomenclatures:

|                |   |                  |
|----------------|---|------------------|
| $\alpha$       | Nominal rake angle                                    | Lattice constant |
| $a_0$          | Depth of cut  |                  |
| $c$            | Critical crack length                                 |                  |
| $d_c$ or $t_c$ | Critical chip thickness                               |                  |
| $E$            | Elastic modulus of the material                       |                  |
| $G$            | Bulk modulus of the material                          |                  |
| $H$            | Hardness of the material                              |                  |
| $K_c$ / $R$    | Fracture toughness of the material                    |                  |
| $K_b$          | Boltzmann constant ( $1.3806503 \times 10^{-23}$ J/K) |                  |
| $l_c$          | Length of contact between cutting chip and tool       |                  |
| $R$            | Nose radius of the cutting tool                       |                  |
| $r$            | Inter-atomic distance                                 |                  |
| $S$            | Specific energy required to propagate a crack         |                  |
| $t_{max}$      | Maximum critical undeformed chip thickness            |                  |
| $V$            | Cutting speed   |                  |

|                 |                               |
|-----------------|-------------------------------|
| $V_p$           | Potential energy function     |
| $W$             | Width of cut                  |
| $W_d / Z_{eff}$ | Ductile width of cut          |
| $y_c$           | Critical crack length         |
| $\rho$          | Density of the material       |
| $\sigma_y$      | Yield stress for plastic flow |

## 1. Ultra-precision manufacturing and silicon

Ultra precision manufacturing has emerged as a powerful tool for manipulating optical, electrical and mechanical properties of components by changing their surface and sub-surface structure at the nanometre length scale [1]. During the 1980s, Taniguchi [2-3] proposed a predictive map of development in ultra precision manufacturing (figure 1), and this remains true as we approach 2020. Recently, Shore *et al.* [4] suggested that Taniguchi's chart is analogous to Moore's Law which is a mid-1960s prediction for the coming 50 years of microelectronics manufacturing precision. In both cases, a sharp distinction is made in the attainable accuracy between macro-, micro-, and nano-scale machining.

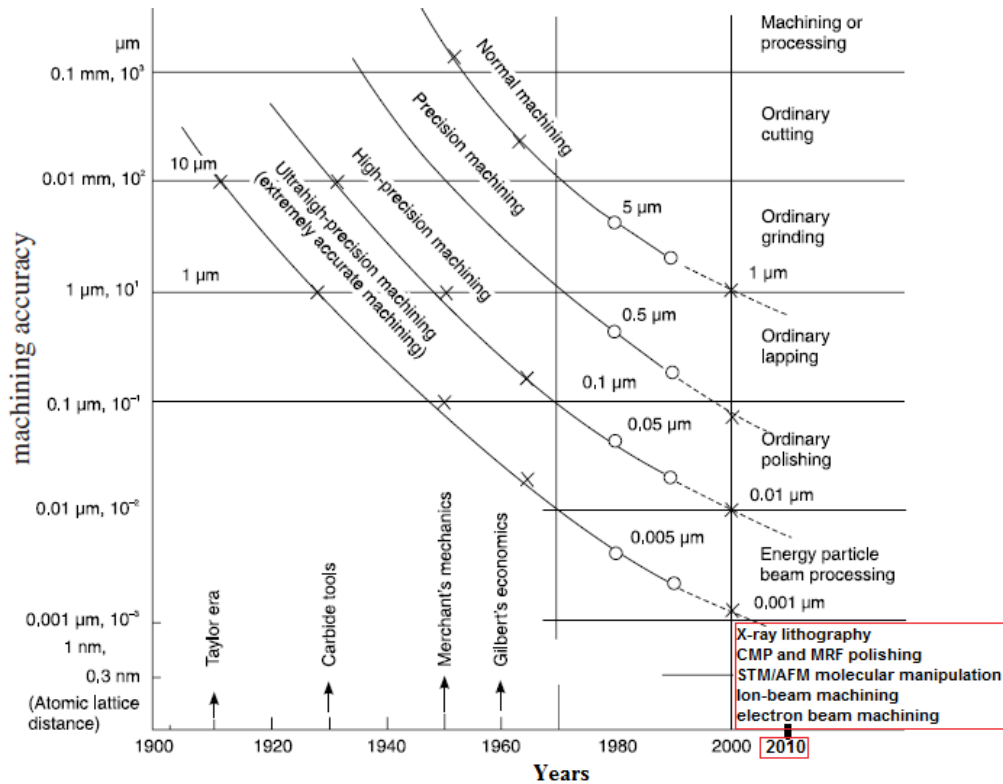


Figure 1: Evolution of machining accuracy - Taniguchi's predictions [3] updated beyond 2000 to include state-of-the-art manufacturing processes (shown in the red box)

The recent perspective has been that [5] “Ultra precision engineering is doing for light what integrated circuits did for electronics”. There is no clear distinction between ultra precision manufacturing and nanotechnology. Nobel laureate Richard Feynman’s early vision of atom-by-atom construction, revealed in his widely cited lecture “There’s plenty of room at the bottom,” would suggest that the second term is most often associated with additive manufacture. More recently, however, technologies capable of controlling a single point diamond turning tool and workpiece have made feasible the production of a deterministic finish on brittle materials with the precision envisioned by Feynman.

The 21<sup>st</sup> century witnessed the rapid emergence of a variety of non-conventional micro-/nano-machining (MNM) processes capable of being applied to a range of engineering materials, including metals, ceramics, plastics, and composites. Miniaturization has pushed manufacturing improvements related to attainable accuracies and tolerances to the sub-micron range, especially in the fields of optics, electronics, medicine, biotechnology, communications, and avionics. Further improvements are necessary for applications relating to fuel cells, microscale pumps, valves and mixing devices, fluidic microchemical reactors, microfluidic systems, micronozzles for high-temperature jets, microholes for fibre optics, micromoulds and deep X-ray lithography masks etc. [6]. Additionally, it has been used for several precision engineering applications such as micro-lens arrays, Fresnel lenses, pyramids array, polygon mirrors, aspheric lenses, multi- focal lenses, corner-cubes, two-dimensional planar encoders, and antireflective gratings or channels [7].

Micro-/nano-machining (MNM) processes can broadly be divided into two categories:

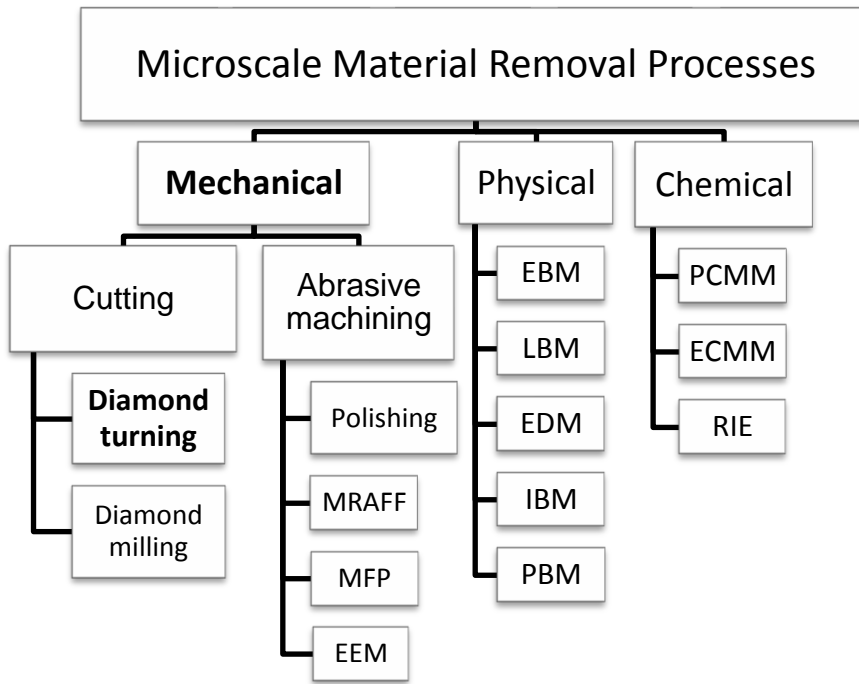
- advanced micro-machining processes to shape and size a component
- advanced micro-/nano-finishing processes (AMNFs) to fine finish a component to the required tolerances [8]

MNM processes can also be divided into three major categories based on whether they involve the addition of material, removal of material or no nominal change in the amount of material during the

process, the last with or without a melt stage. The first category involves deposition of material, and includes processes such as Ultrasonic laser deposition, Chemical vapour deposition, Rapid prototyping, LIGA and Electric discharge deposition. The second category of micro-machining involves the removal of material. This might be accomplished by mechanical, chemical or physical means. Finally, the category involving no gain or loss of material (i.e. micro-thermo forming and micro-injection moulding) is most suited to the class of materials exhibiting low critical temperature, such as polymers. Micro-thermo forming is achieved by thermally softening the part to conform to a mould; whereas micro-injection moulding involves the material inserted into a heated barrel, mixed, and forced into a mould cavity.

The focus of this review is diamond-machining process, which falls into the category of material removal processes, and it is only this technology that is discussed in this review. As shown in figure 2, the material removal processes can be further classified into mechanical, physical, or chemical processes depending on the nature of the mechanism of the material removal. A review [9] capturing finest details of much of these non-conventional manufacturing processes could be a good source of information to begin simulation work on such processes. While physical and chemical machining processes are restricted to specific materials and applications, machining by mechanical means is considered to be almost universal in its applicability [10] to almost all the materials. Machining offers the following advantages [11]:

- it is an optimum way to produce a prototype in a batch.
- it has the least effect on the metallurgical properties of the finished component.
- it generates desirable surface contour and surface textures within an acceptable tolerance



MRAFF: magneto-rheological abrasive flow finishing; MFP: magnetic float polishing; EEM: elastic emission machining; EBM: electron beam machining; LBM: laser beam machining; EDM: electro discharge machining; IBM: ion beam machining; PBM: proton beam micro-machining; PCMM: photo chemical micro-machining; ECMM: electro chemical micro-machining; RIE: reactive ion etching.

Figure 2: Classification of various ultra-precision manufacturing processes

Although sometimes used synonymously, one major difference between the micro- and nano-machining is the size of the attainable chip thickness. For example, a minimum ratio of the chip thickness to the cutting edge radius in micro-machining has been estimated to be 0.293, whereas in nanometric cutting it could be as low as 0.1 [6]. Aside from this major difference, some other significant differences were highlighted by Brinksmeier during a talk at the Royal Society in 2011, and these are summarized in table I.

Table I: Differences between macro, micro and nano level machining processes [10]

|                                      | <b>Macro-Machining</b>                          | <b>Micro-machining</b>                          | <b>Nano-machining</b>                             |
|--------------------------------------|---|---|---|
| Size of machined area                | 1 to $10^5 \text{cm}^2$                         | 1 to $10^5 \text{mm}^2$                         | 1 to $10^5 \mu\text{m}^2$                         |
| Volume removal in one machining step | from $10^{-3}$ to $10^2 \text{cm}^3$            | from $10^{-3}$ to $10^2 \text{mm}^3$            | from $10^{-3}$ to $10^2 \mu\text{m}^3$            |
| Material removal rate                | from $10^{-5}$ to $1 \text{cm}^3 \text{s}^{-1}$ | from $10^{-5}$ to $1 \text{mm}^3 \text{s}^{-1}$ | from $10^{-5}$ to $1 \mu\text{m}^3 \text{s}^{-1}$ |
| Relative figure error                | from $10^{-5}$ to $10^{-3}$                     | from $10^{-7}$ to $10^{-5}$                     | from $10^{-5}$ to $10^{-3}$                       |
| Surface roughness                    | up to 10 micron                                 | up to 0.1 micron                                | 0.1 to 10 nm                                      |

The chip formation mechanism, the distribution of cutting forces, the role of material microstructure and crystal anisotropy, and the elastic recovery of the machined surface, all result in the transition of the scale of machining from the macro to the nano level. The foremost of these is the mechanism of chip formation which shifts from continuous to discrete as the scale descends. The effect of the cutting edge radius is non-trivial in nanometric cutting as there exists an upper bound edge radius beyond which there occurs an undesirable ductile-brittle transition (DBT) [12].

While some ultra precision products are increasing in size (the size of a finished silicon wafer reached 300 mm in the year 2000), the size of many other precision components (such as fuel injectors and bearings) have been significantly reduced to meet the functional requirements and to reduce manufacturing and product costs. The need for tight dimensional tolerances and miniaturization for such products is driven by the global mission to reduce emissions and increase the efficiency of IC-engines. This is just one example of how environmental and sustainability issues are increasingly driving ultra precision technologies. Other examples can be found in optical devices and computer chips, where the required tolerances are approaching the atomic length scale, thus requiring significant ultra precision manufacturing research in the fabrication of silicon. Due to its abundance and its capability to form better oxides, silicon dominated the electronic consumer market for much of the 20th century [13]. Traditional machining methods to fabricate silicon rely on lapping and polishing. In addition to being labour and time intensive, these processes are not particularly successful for manufacturing complex shapes, such as aspheric, diffractive, and “hybrid” components when judged in terms of quality and cost effectiveness. This review is therefore aimed at discussing the possible improvements in manufacturing of silicon using diamond machining technology and the role that MD simulation has been playing in advancing the current state of knowledge in this field.

## **2. Diamond machining**

### *2.1 Introduction*

Single point diamond turning (SPDT) is one of the most efficient ultra precision material removal

processes. It is capable of removing material at the scale of a few atomic layers to produce optical quality machined surfaces using a single point diamond-cutting tool. SPDT provides machining form accuracy and machined surface finish that are among the best ranges obtained via a multitude of processes such as lapping and polishing [4]. Experiments have shown that samples of silicon machined using SPDT exhibit a surface quality corresponding to that achieved by optical polishing. For example, an average surface roughness  $R_a = 0.6$  nm and Peak to valley i.e.  $R_{max} = 6$  nm [14], which is better than that obtained through grinding, i.e.  $R_a = 7$  nm and  $64 \text{ nm} < R_{max} < 148$  nm [15]. Furthermore, SPDT offers a flexibility of generated form, improved step-definition, deterministic form accuracy, and economy of fabrication time, that makes it the preferred ultra precision manufacturing process to fabricate silicon wafers. Indeed, SPDT has remained one of the greatest advancements in the field of ultra precision manufacturing and is at the pinnacle of the ultra high precision turning process [4]. Currently, with Fast Tool Servo or fly cutting techniques, SPDT can be used to machine freeform (both axisymmetric and non- axisymmetric) machined surfaces.

In its early stages of development, SPDT was limited to the machining of soft and ductile materials, such as aluminium and copper. However, advances in optical and defence systems required precision manufacturing of materials commonly used by the optical, semiconductor and optoelectronics industries, such as silicon, silicon carbide, and gallium arsenide. These materials are capable of transmitting light over a variety of wavelengths making them a superior choice to soft materials concerning optical applications. This requirement drove an expansion of SPDT technology to the machining of hard and brittle materials like silicon. However, machining of silicon, such as slicing, cutting and grinding produces damages such as dislocations, microfractures, scratches and micro-cracks which makes silicon a difficult-to-machine material [16]. Early attempts to understand the ductile behaviour of such brittle materials through interrupted cutting tests are well documented [17-18]. The key discovery from these experiments is that with careful selection of the process parameters, brittle materials can be machined in the “ductile-regime” where chip removal takes place by virtue of plastic deformation rather than by brittle

fracture. The seminal approach to quantify the machining parameters using an analytical mathematical model to make the SPDT operation more deterministic was developed by Scattergood *et al.* [19], who attempted to optimize the feed rate and highlighted the importance of a parameter called critical chip thickness [20]. Although the accuracy of the estimated values of maximum feed rate obtained from this model was later realized to be dependent on the machining conditions [21], this model is still widely used to demonstrate the brittle-ductile transition. More recently, the ductile behaviour of brittle materials has been attributed to high-pressure phase transformation (HPPT) [22]. Most of the literature on contact loading of silicon (both nanometric cutting and nanoindentation), have reported HPPT to be the primary mechanism governing the plasticity of silicon that causes brittle-ductile transition except Mylvaganam *et al.* [23] who from their MD simulation studies observed nanotwinning (associated with Si-I to bct-5 phase transformation) along the  $\langle 110 \rangle$  direction that stops at Shockley partial dislocation especially at cutting depths over 1 nm. Their simulation results suggest that aside from HPPT, silicon also undergoes Shockley partial dislocation on scratching when the cutting load is above  $0.7 \mu\text{N}$  (which results in plastic response of silicon).

The general view on ductile-regime machining of silicon is that HPPT causes structural transformations and associated volume changes in the cutting chips of silicon. These transformations were not accounted in earlier analytical models (which could contribute up to 25% of the prediction error) [21]. There are still many challenges associated with the ultra precision ductile-regime manufacturing of silicon (see Figure 3) since it involves a complex interplay of a number of processes at the atomic scale. These include the following:

- wear of cutting tool
- elastic recovery of the machined surface
- influence of process variables
- tool geometry

- state of local stresses (which drive the high pressure phase transformation in the cutting zone)
- movement of dislocations and cracks in the sub-surface
- microstructure of the work piece and the cutting tool
- crystal anisotropy of the workpiece and the cutting tool

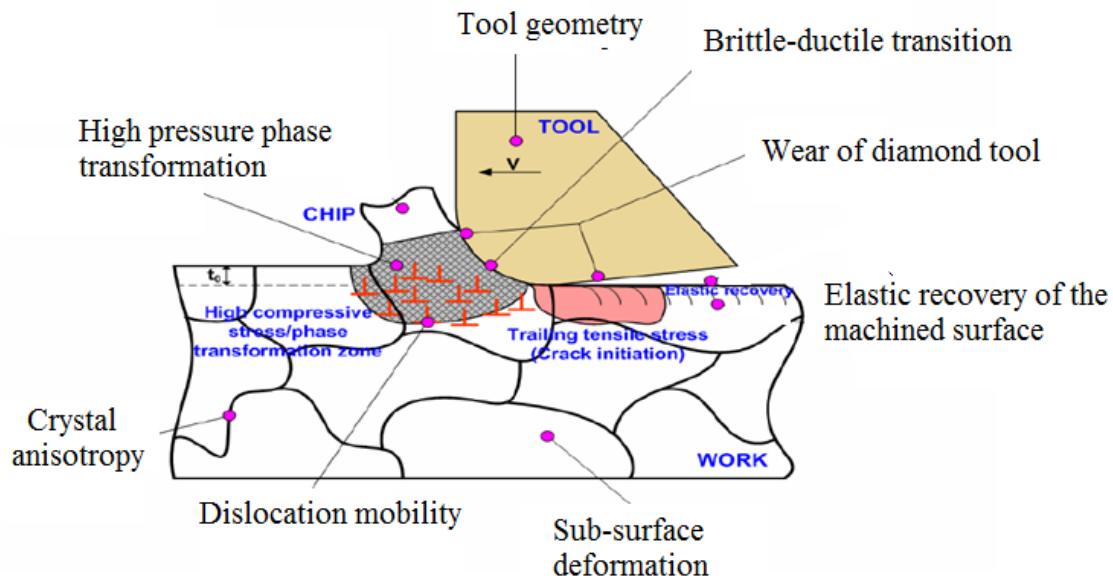


Figure 3: Various complexities inherent in nanometric cutting of hard brittle materials [24]

A common consequence of the failure to control these processes is the undesirable ductile-brittle transition, which results in a poor quality of machined surface and shorter tool life. While the chip formation mechanism and high-pressure phase transformation of silicon has been explored, still an overall phenomenological understanding of the complex interplay of all aspects that effect tool wear and its dynamic influence on the machined surface is not quite complete. To that end, this review aims to provide an atomistic understanding of the high-pressure solid-state physics of cutting chips. Specifically, it focuses on the influence of the microstructure and crystal structure of the tool and workpiece, sub-surface crystal deformation layer depth and on the phenomena involved in the wear mechanism of diamond tools. The next section explores how these problems are addressed in the MD simulation and also explains the phenomena of the brittle-ductile transition involved in the

manufacturing of silicon or other nominal brittle materials.

## 2.2 *Diamond machining of brittle materials*

Unlike most metals, brittle materials exhibit very low fracture toughness. As such, they usually fracture with little or no plastic deformation, thus making them difficult to machine using conventional machining processes. However, it is possible to machine such brittle materials at a very fine scale of several micro or nanometres using appropriate machining parameters. The execution of such a machining process, where the aim is to generate the chips through plastic deformation rather than fracture, is known as “ductile-regime machining”. The possibility of machining brittle materials in the ductile-regime was first acknowledged by King and Tabor [25] in 1954, as a result of observations on frictional wear of rock salt. They observed that although some cracks and surface fragmentation occurred during heavy abrasive wear, there was some plastic deformation involved. Later, Bridgman et al. [26] showed that a brittle material, such as glass, exhibited ductility under high hydrostatic pressure. Subsequently, Lawn and Wilshaw [27] observed the same ductile behaviour of glass during nano-indentation testing, and identified the elastic-plastic transition. Lawn and Marshall [28] used indentation testing and proposed an empirical relationships between the indentation load ( $P$ ), crack length ( $c$ ), fracture toughness ( $K_c$ ) and hardness ( $H$ ) of the substrate as follows:

$$P = \lambda_0 \left[ \frac{K_c^4}{H^3} \right] \quad (1)$$

$$c = \mu_0 \left[ \frac{K_c^2}{H^2} \right], \quad (2)$$

where  $\lambda_0$  and  $\mu_0$  are geometrical constants dependent on the indenter shape,  $P$  is the indentation load,  $c$  is the observed crack length,  $K_c$  is the fracture toughness (resistance to fracture) of the substrate material and  $H$  is its hardness (a measure of its resistance to the plastic flow). The fracture toughness ( $K_c$ ) of diamond cubic crystal structured materials, such as in silicon and 3C-SiC, has

been suggested to follow the below relationship [29]:

$$K_c^2 = \frac{4GEa_0}{72(1-2\nu)} \quad (3)$$

where  $a_0$  is a constant,  $G$  and  $E$  are the shear and Yang's Elastic modulus, and  $\nu$  is Poisson's ratio.

Subsequent research on ductile-regime machining led to the identification of the so called critical indent size (CIS) [30] which is expressed as:

$$CIS = \mu \left[ \frac{K_c}{H} \right]^2, \quad \text{where } \mu \propto E/H \quad (4)$$

In the late 1990s, Blake and Scattergood [19] suggested that a critical chip thickness ( $t_c$ ) separates the regime of plastic deformation from brittle fracture material removal. Accordingly, they proposed a new machining model to explain the ductile-regime machining of brittle materials (shown in figure 4) which has also been verified experimentally (as shown in figure 5).

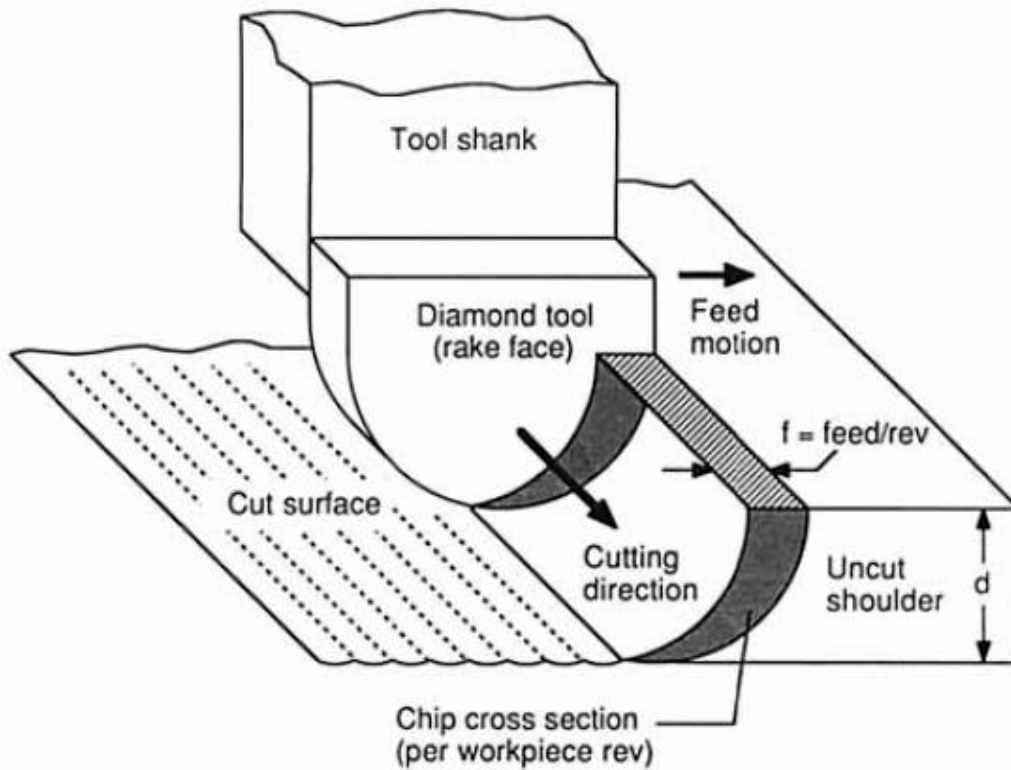


Figure 4: Ductile-regime machining model using a round nose cutting tool [19]

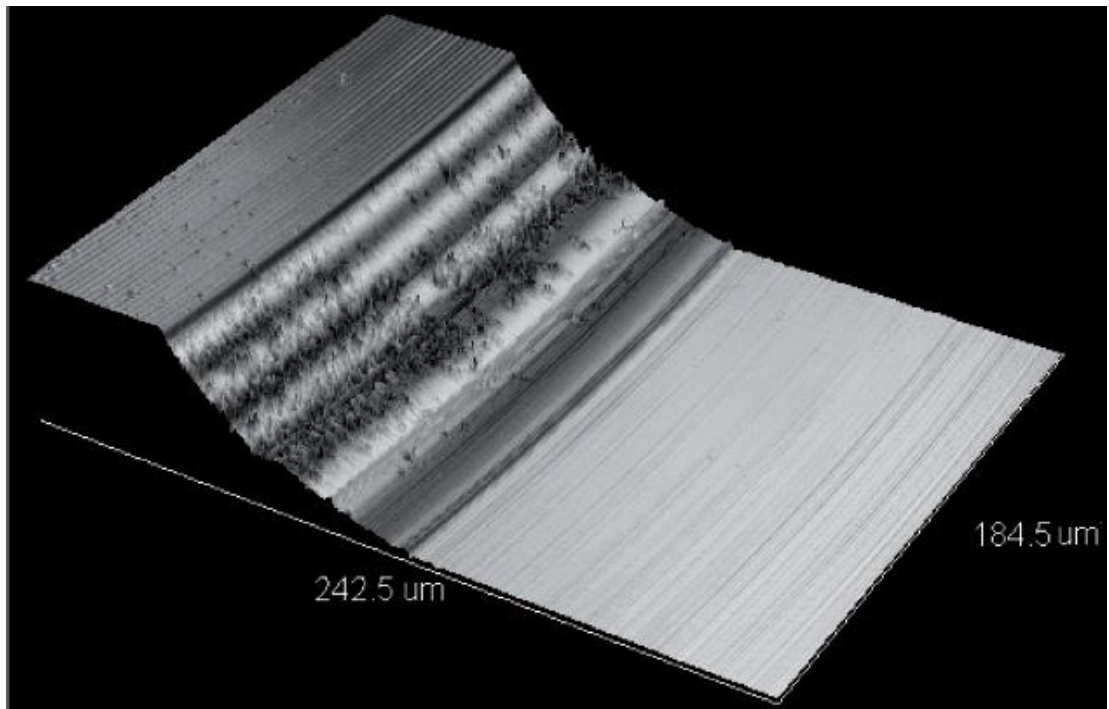
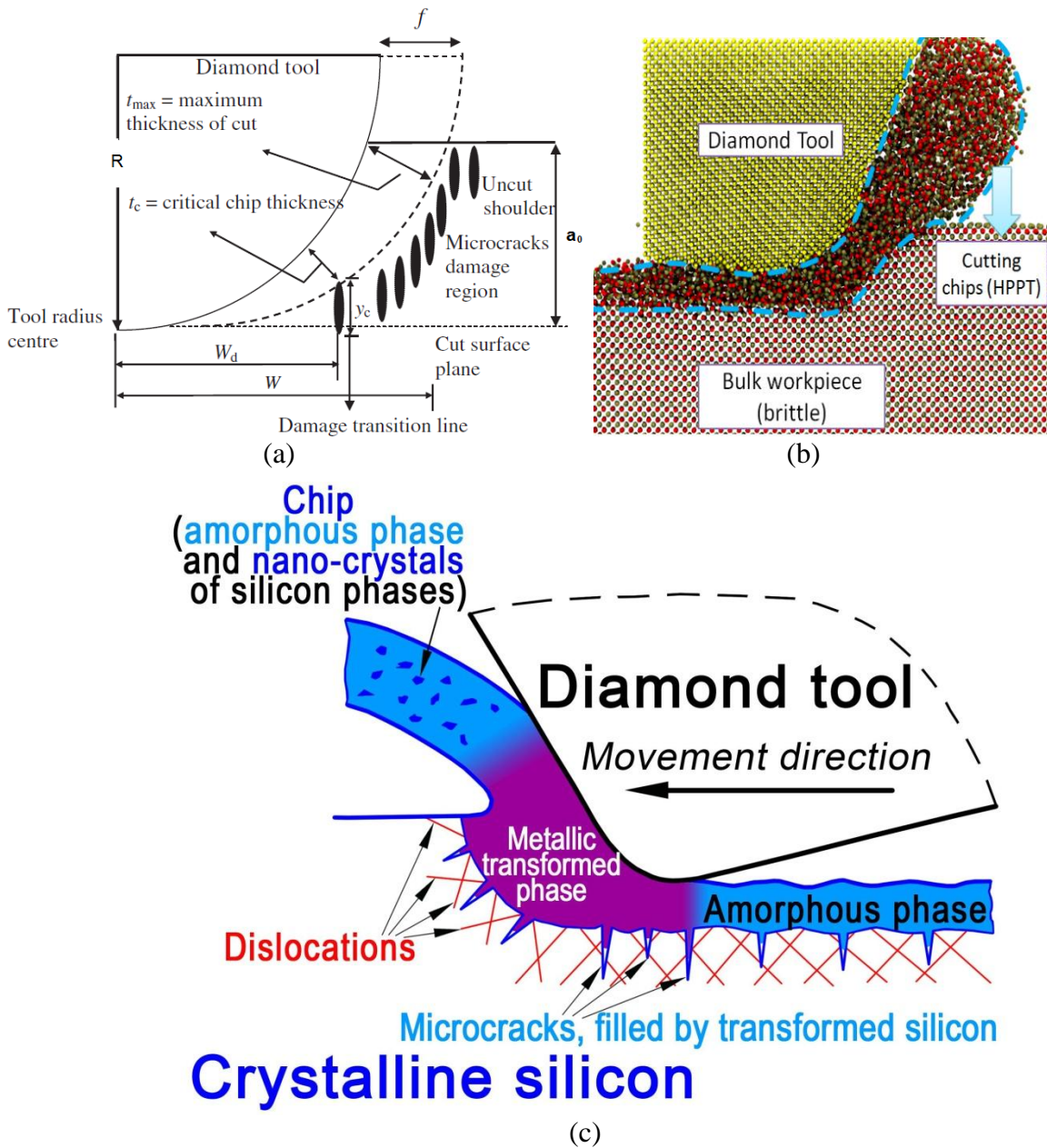


Figure 5: Three dimensional image of the uncut shoulder showing an occurrence of the brittle-ductile transition in silicon [31]



W: Width of cut,  $W_d$ : ductile width of the chip,  $f$ : feed rate,  $R$ : tool nose radius and  $y_c$ : critical damage depth,  $a_0$ : Depth of cut

Figure 6: Ductile-regime machining (a) analytical model (2D representation of the 3D condition showing nose radius of the tool [17, 20] (b) MD model (2D model showing cutting edge radius) (c) Schematic of ductile cutting of silicon with the formation of cracks and its self-healing mechanism [32]

A schematic view of the cross-section of brittle-ductile transition proposed during the 1990s is shown in figure 6a which has been compared with a MD simulation result (figure 6b) and with another schematic model proposed recently (figure 6c) [32]. It is important to note that none of the previously proposed schematic models consider the formation of an amorphous layer around and especially in front of the cutting edge radius of the tool tip that tends to recover back by a small

extent on release of instantaneous pressure exerted by the cutting tool (as evident from figure 6b and figure 6c). Furthermore, TEM imaging has revealed that it is the plastic phase of silicon (Si-II) that fills up the unavoidably formed microcracks, microfractures and spallings underneath the amorphous layer (figure 6c) of silicon during its machining. This phenomenon is referred to as 'crack self healing mechanism' [32].

The classical model shown in figure 6a illustrates the horizontal distance between the critical chip thickness and the tool nose centre  $W_d$  (sometimes called  $Z_{eff}$ ), which is considered as an important parameter in the diamond machining process. For an SPDT operation, undesirable fracture damage is assumed to initiate at the critical chip thickness ( $d_c$ ), which propagates up to a depth,  $y_c$ . The critical crack length ( $y_c$ ) varies along the nose radius according to the feed rate of the tool. As shown schematically in figure 7, the crack does not penetrate below the subsurface damage at smaller feed rates and hence does not affect the final machined surface. However, as feed increases,  $y_c$  moves toward the machined surface and thus cracks begin to propagate into the final cut surface (i.e. the machined surface begins to show undesirable brittle fractures).

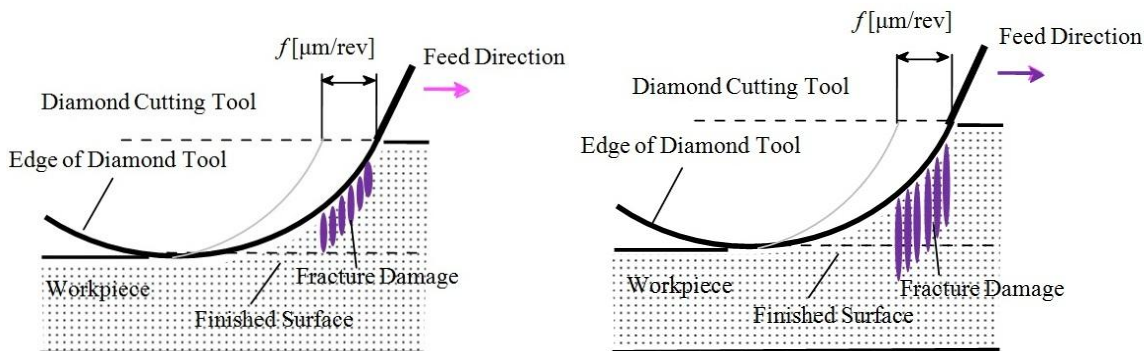


Figure 7: Schematic for diamond turning at (a) low feed rate and (b) high feed rate

As long as the fracture damage does not penetrate to the final machined surface, ductile-regime machining is achievable. Notably, the fractured material in the remaining region of the uncut shoulder is carried away by the tool in the succeeding passes and is therefore of no concern. This phenomenon seems to indicate that materials exhibiting short critical crack lengths are more amenable to SPDT. Additionally, the critical chip thickness  $d_c$  represents the condition for any

fracture initiation, whereas  $y_c$  is an indicator of the average depth of fracture propagation. Both these parameters are interdependent, and interact in a non-linear fashion which depends primarily on the state of the stress in the cutting zone.

### 2.3 Theoretical models of brittle-ductile transition

Griffith's criterion suggests that the propagation of brittle fracture happens when the released elastic energy concentrated in the region of the crack tip overcomes the minimum energy associated with the appearance of a free surface [33]. Of interest is the fact that the hardness of silicon around radial microcracks is lower than the hardness of pristine silicon. Bifano et al. [18] suggested that, at smaller feed rates the energy required to propagate a crack is greater than the energy required for plastic yielding. As such, plastic deformation becomes the dominant mechanism of chip formation during ductile-regime machining. The energy required for plastic deformation is directly proportional to the volume of the material removed, whereas the energy for brittle fracture is directly proportional to the cracked surface area. Hence, the process of machining brittle materials can be treated in terms of minimum energy [21]. Thus, the BDT can be determined as the condition at which it will take more specific cutting energy to execute ductile-regime machining than it takes to execute brittle-fracture dominated machining. In a model using this approach [34], the consumption of energy involved during the machining of brittle materials was described as a function of the properties of the workpiece material, tool geometry and process parameters. *Ibid.* categorised brittle mode cutting and ductile mode cutting on the basis of the specific cutting energy. They found that the former expend lower energy while the latter involves more consumption of energy because plowing between the tool flank face and the workpiece during elastic recovery is more pronounced during ductile-regime machining. They related specific cutting energy to undeformed chip thickness and obtained the upper bound of the critical undeformed chip thickness of silicon as 220 nm.

Earlier, Nakasuji *et al.* [35] had proposed a model of the brittle-ductile transition by considering the forces giving rise to slippage and cleavage as shown schematically in figure 8.

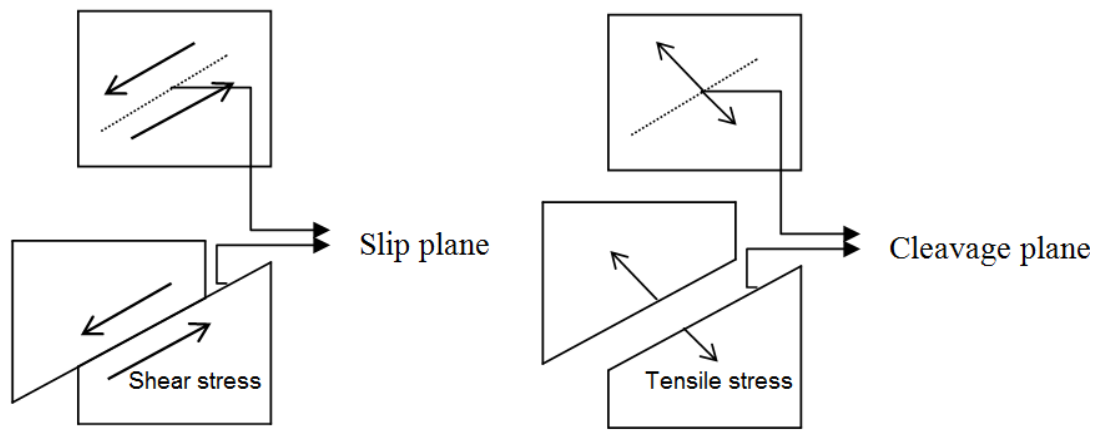


Figure 8: Slip and cleavage mechanisms of chip removal [35-36]

They suggested that plastic deformation occurs in front of the cutting edge when the resolved shear stress exceeds a certain critical value in the direction of the shear plane. However, cleavage will take place if the resolved tensile stress exceeds a certain critical value in the direction normal to the cleavage plane. Furthermore, they highlighted the importance of the size effect i.e. they claimed that the critical value of stress for plastic deformation and cleavage are also governed by the density of lattice defects and dislocations present in the real-world work material. With smaller uncut chip thicknesses, the size of the resulting critical stress field is small enough to avoid cleavage initiated at the defects. With larger uncut chip thicknesses, however, the larger critical stress field allows for sufficient nuclei for crack propagation, which originates from the defects within the material, as shown schematically in figure 9.

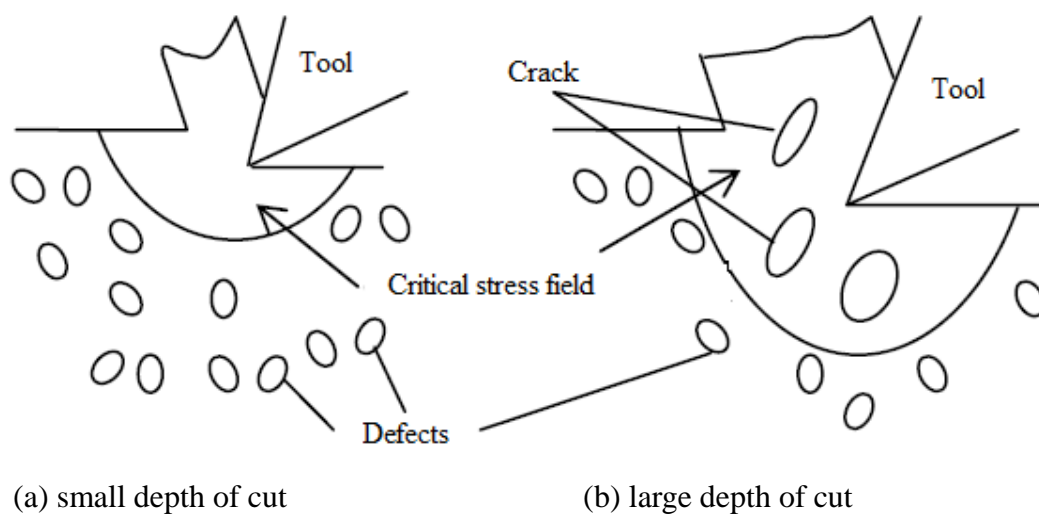


Figure 9: Schematic representation of size effect for small-scale chip removal [35]

Conversely, the theory of plasticity suggests that the magnitude of hydrostatic stress determines the extent of plastic deformation prior to fracture, which in turn, determines the material's ductility. Therefore, when the tool edge radius in the cutting region generates sufficient hydrostatic pressure, plastic deformation is more likely to occur than crack generation, even at a lower temperature. The above proposition is considered to be the classical theory of the brittle to ductile transition in diamond turning. Indeed it has been cited [37] as a main reason for the requirement of the cutting edge radius in the diamond cutting tools rather than sharp-edged tools as shown in figure 10.

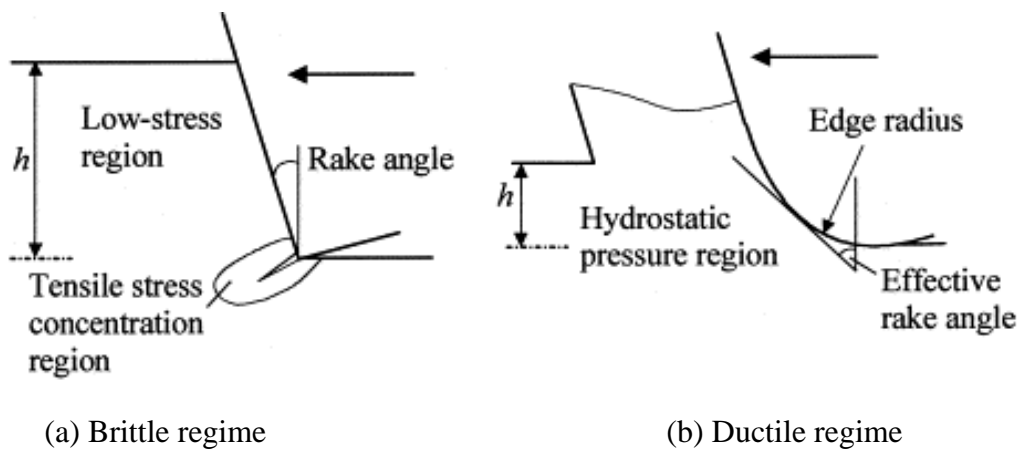


Figure 10: Schematic illustration of the influence of the edge radius on SPDT [37]

Providing an edge radius on the cutting tool causes two particularly significant phenomena:

- Edge roundness decreases the stress concentration and produces a hydrostatic stress field in the cutting region.
- The effective rake angle caused by the small radius becomes large and negative and, as a result, material in front of the cutting edge is pushed downward and compressive stresses (a hydrostatic stress field) become dominant.

For semiconductors, a strong correlation was found between nano-indentation hardness and metallization pressure [38-39]. The metallization pressure (Herzfeld-Mott transition [40]) is the value under which brittle semiconducting materials becomes metallic (i.e. the band gap vanishes

because of the closure of the valence-conduction band gap due to the overlap of wave functions and hence the delocalization of the valence electrons). This process is facilitated by a high pressure phase transformation (HPPT) which has been demonstrated to be an outcome of the shear strain rather than simple hydrostatic strain (i.e. predominance of bond-bending over bond-stretching) [41]. Gilman [38-40] suggested that it is a change in the bond angle rather than a change in bond length that appears to cause the metallization of semiconductors, as observed during polishing of diamond as well [42]. Gilman explained that in a diamond cubic lattice, bond length could only bring about a change in volume, not necessarily shape; whereas a change in bond angle can change both shape and volume. Topologically, the diamond cubic structure (Si-I) is quite similar to the  $\beta$ -tin structure (Si-II) form of silicon. It is shown schematically in figure 11 that compressing the Si-I structure on the tetragonal axis by 50% will result in the transformation of the Si-I structure to the Si-II structure. Conversely, stretching of the Si-II structure by 200% will provide the Si-I lattice structure of silicon.

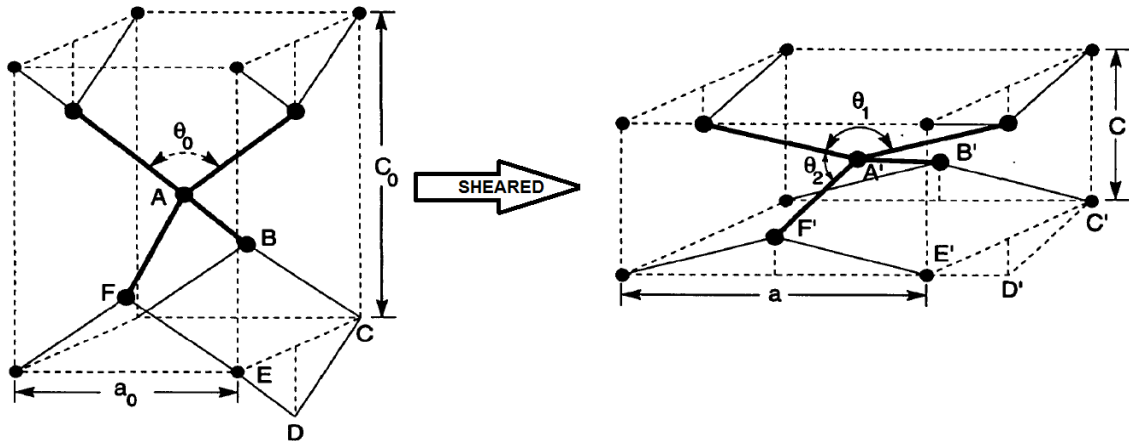


Figure 11: Shear transformation of Si-I (brittle) silicon to Si-II (ductile) silicon [40]

#### 2.4 Influence of machining variables on brittle-ductile transition

Extant literature suggests that the cutting forces or the specific cutting energy of ultra precision machining is size dependent. When the scale of cutting decreases (undeformed chip thickness, depth of cut, size of the cutting tip etc.), the specific cutting energy tends to be higher. In the past, this size effect has been postulated to arise out of any, or a combination of the following three

reasons:

(i) The energy required to cut a single grain (in single crystal material) requires breaking of atomic bonds which is relatively higher in comparison to the energy required to dislodge cluster of grains (during cutting of polycrystalline substrate).

(ii) Nanometric cutting causes two forces acting on the cutting tool namely, shearing force and elastic recovery force. With the reduction in the scale of machining, the shearing force reduces proportionately whereas the elastic recovery force is believed to remain unchanged. Consequently, the specific cutting energy at low cut depths tends to be higher due to the relatively higher elastic recovery force.

(iii) At nanoscale, the experimental shear strength of the material approaches near theoretical in the absence of defects, flaws, vacancies and cracks whereas at macro-scale the presence of a high density of these defects facilitates easy shearing of the material.

A tool with a very sharp edge may wear out quickly because of stress concentration; hence a finite edge radius is always preferable. Arefin et al. [43] highlighted the importance of the tool cutting edge radius and the maximum un-deformed chip thickness of the workpiece. Based on their experimental work on silicon and a molecular dynamics simulation model [44], they suggested that the following condition must be satisfied in order to obtain ductile-regime machining on silicon:

$$807 \text{ nm} > \text{Cutting edge radius} > \text{Maximum undeformed chip thickness}$$

They claimed that as the tool cutting edge radius increases, the shear stress in the workpiece material around the cutting edge decreases to a lower level. At this point, the shear stress becomes insufficient to sustain dislocation emission in the chip formation zone, and then crack propagation dominates [12]. Consequently, the chip formation mode changes from ductile to brittle, which impacts the tool's life adversely. Additionally, when the uncut chip thickness is less than the tool cutting edge radius, the thrust force increases more rapidly than the tangential cutting forces [45]. This has however been contradicted by several experimental studies which show that the

undeformed chip thickness has been observed to be larger than the cutting edge radius [16]. Hence, this direction needs more research to establish a sound correlation between cutting edge radius and undeformed chip thickness. We suggest that such an investigation must be based on 3D SPDT models rather than 2D or semi 2D models (incorporating crystal anisotropy (tool and workpiece), tool wear, influence of coolant, high pressure phase transformation of silicon, crack healing mechanism, elastic recovery, feed rate, cutting speed and depth of cut etc.).

Leung *et al.* [46] examined the influence of the depth of cut during the nanometric cutting of silicon. Using varying depths of cut, they observed a sharp transition of material removal from ductile deformation to brittle fracture. Based on further experimental work, they were able to plot a relation between the depth of cut and feed rate to distinguish brittle regime machining from ductile regime machining. Accordingly, they proposed a schematic diagram highlighting the regime map as shown in figure 12.

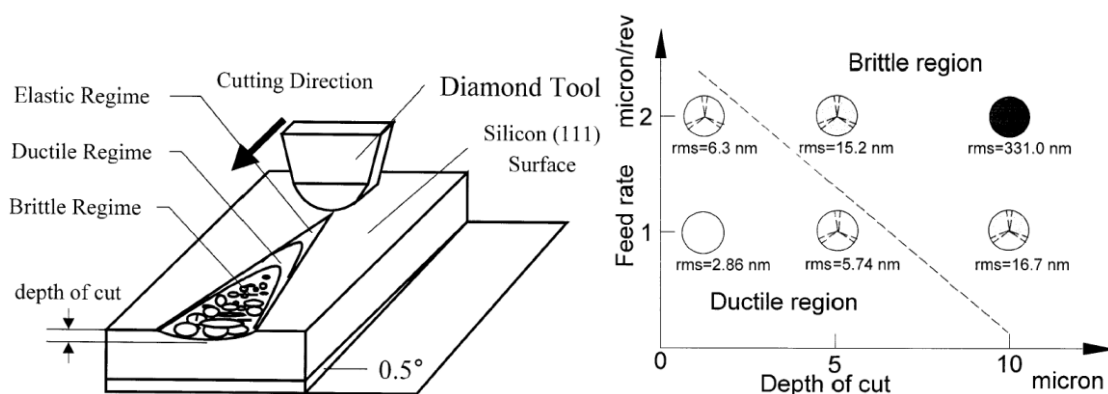


Figure 12: Influence of depth of cut and feed rate on brittle-ductile transition [46]

Figure 12 provides critical information about the influence of the depth of cut in altering the machining regime and also highlights how a combination of the feed rate and depth of cut together influences the attainable measure of the achievable root mean square (rms) value of the machined surface roughness on a machined component. Thus, it is not just a single machining parameter but the interaction of several parameters that are responsible for the ductile-brittle transition. This makes the machining process more complex. The equations relating the instantaneous rake angle

and shear angles as a function of cutting edge radius and undeformed chip thickness are expressed elsewhere [34].

## 2.5 Influence of crystal anisotropy

### 2.5.1 Anisotropy of silicon workpiece

Following crystallographic convention, this review will use ( ) and < > notations to represent crystallographic plane orientations (direction of plane normal) and crystallographic directions (such as cutting and slip) respectively. Under normal conditions, natural silicon prefers a diamond cubic lattice structure with the (111) planes acting as both slip planes and cleavage planes. The Burgers vector of the diamond cubic lattice can be calculated as:  $b_{(111)} = 1/2a$ ,  $b_{(110)} = 1/\sqrt{2}a$  and  $b_{(100)} = a$  where  $a$  is the lattice parameter of silicon. The angle between the (111) plane and the (100) plane in a diamond cubic lattice is  $54.74^\circ$  while the angle between the (110) plane and the (111) plane is  $35.26^\circ$ . Recent work by Wang et al. [29] on the influence of the crystal anisotropy of silicon during its ductile-regime machining showed the (110) crystal orientation to support more dislocation movement than the (111) orientation. However, they recalled the findings of Marsh et al. [47] in which cleavage fracture occurs in a direction parallel to the (111) crystal plane and perpendicular to the (110) plane. Compared to other combinations for the same machining parameters, Wang et al. [29] obtained the best machined surface roughness of  $R_a=9.22$  nm on silicon while cutting along the  $\langle \bar{1}10 \rangle$  direction on the (111) orientation. This result was consistent with the earlier work of Shibata et al. [48] where a Schmidt-type slip orientation factor was proposed and the  $\langle \bar{1}10 \rangle$  direction was recognized as the preferred cutting direction for silicon either on the (100) or on the (111) planes. It must be noted here that while the (100) orientation permits a larger critical undeformed chip thickness, it is the (111) orientation that provides a superior experimentally observed machined surface roughness during SPDT of silicon. One of the most convenient ways of measuring the critical un-deformed chip thickness of any material is through a fly cutting experiment in which the depth of tool engagement varies around the circumference of the tool path.

An example test result provided by Connor et al. [49] is shown in figure 13:

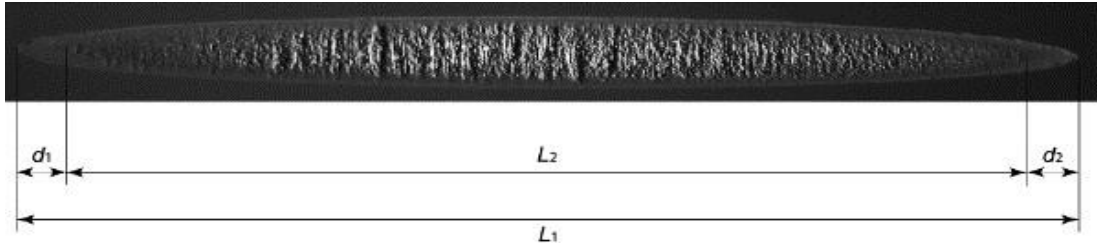


Figure 13: Scratch made on a silicon workpiece using fly cutting [49]

Using the parameters shown in figure 13, the critical undeformed chip thickness,  $t_c$ , can be calculated as follows:

$$t_c = \frac{2(L_1 d_1 + L_1 d_2 - d_1 d_2) - d_1^2 - d_2^2}{8R} \quad (5)$$

R is the fly-cutter radius.

These diamond fly-cutting experiments, performed using a cutting speed of up to 5.6 m/s, showed that the critical chip thickness during ductile-regime machining of silicon is at a maximum of 120 nm on the (100) planes and a minimum of 40 nm on the (110) planes [49]. The value of maximum critical chip thickness is reasonably consistent with the value obtained by applying a simple mathematical formula to the optimized machining parameters suggested by Born and Goodman [50]. In quantitative (but not qualitative) contrast to the above, Jasinevicius et al. [31] recently reported a maximum critical un-deformed chip thickness of 285 nm on the (100) planes and a minimum of 115 nm on the (110) surface of silicon during SPDT with a  $-5^\circ$  rake angle tool at a feed rate of 2.5  $\mu\text{m}/\text{rev}$  and a depth of cut of 5  $\mu\text{m}$ .

Ichida [51] recognized that an increase in the cutting velocity during ductile-regime machining of silicon enhances the upper bound of the critical chip thickness. Yan et al. [37] provided the quantitative illustration of critical un-deformed chip thickness with crystallographic direction (shown in figure 14) and proposed that, in order to obtain homogeneous ductile crystal surfaces the un-deformed chip thickness ( $d_c$ ) must be kept below the critical chip thickness for all

crystallographic orientations.

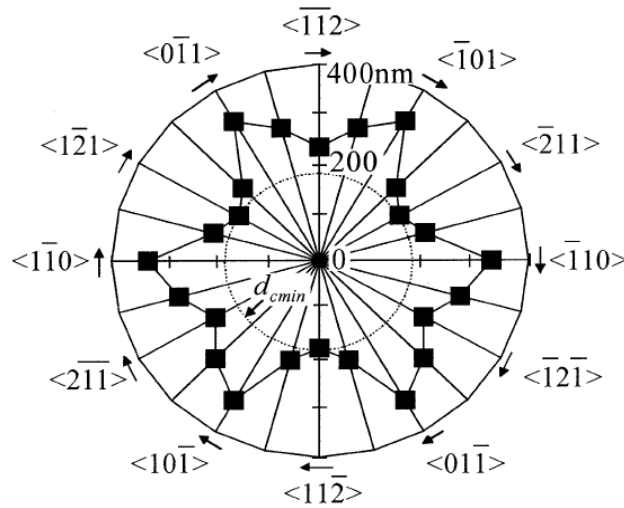


Figure 14: Crystallographic direction dependence of minimum un-deformed chip thickness in silicon [37]

### 2.5.2 Anisotropy of Diamond tools

Diamond tool manufacturers usually select the crystallographic orientations of the tools based on the convenience of the polishing process. The three most commonly used planes of a diamond crystal are highlighted in figure 15. These are octahedron (111), cube (100) and dodecahedron (110).

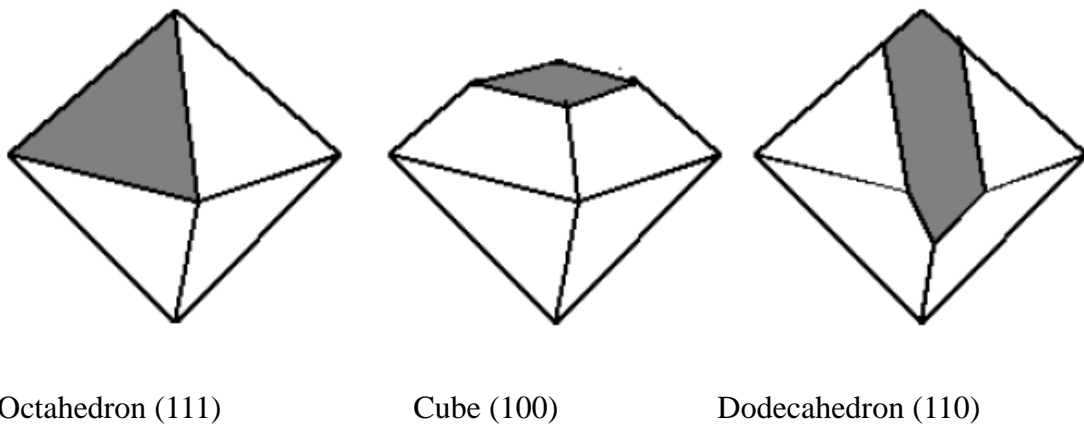


Figure 15: Schematic showing (111), (100) and (110) planes of diamond

The (110) or (100) crystallographic planes are often chosen as the tool rake face with the axis of the tool and the tool shank parallel to  $\langle 110 \rangle$  direction. However, it is possible that the optimum

orientation for a particular tool may be a few degrees away from these crystallographic planes and directions. The crystallographic plane (110) is often used as the rake face and flank face of the diamond tools because it is the easiest to shape by abrasion. In order to obtain the best performance, the flank and rake face must be polished as smoothly as possible to minimize friction and to ensure that the cutting edge remains smooth [52].

As early as 1975, Bex [53] demonstrated that diamond tools with a flank face oriented on the (100) plane had a wear rate of almost one-sixth of those oriented on the (110) plane when used for machining Al-Si alloy. This observation was further supported by Casey et al. [54] based on tool wear experiments on LM13 (Al-12%Si), where tools with (100) rake face showed a tool life that was 7 times higher compared to that of other orientations. In the same experiments, *ibid.* further showed that the tool wear rate was independent of the cutting speed and that the intermittency of cutting did not affect tool wear. Hurt et al. [55] investigated the effect of crystallographic orientation on the wear characteristics of diamond tools during the machining of oxygen-free high conductivity copper and gold. They found that diamond tools with cubic orientation exhibited higher wear resistance than those with a dodecahedral orientation.

Additionally, cleavage fracture in a direction along the (111) crystal plane was responsible for the deterioration of the cutting edge of the tool for the dodecahedral orientation. Ikawa et al. [56] estimated the fracture strength of the cutting edge of diamond tools using a three-dimensional FEM model with crystallographic orientations (100), (110) and (111) as the rake faces. Based on the tangential stresses on a rake face, they suggested that the (100) crystallographic plane is a more suitable rake face for chip resistance. On the assumption that the friction between the diamond tool and the work material effects shear deformation, tool wear and machined surface quality, Yuan et al. [57] first observed the frictional characteristics between diamonds with (100), (110) and (111) crystallographic planes, and an aluminium alloy, copper, brass and cast iron. They compared two diamond tools: one with (100) as the rake and flank faces, and the other with (110) as the rake and flank faces. They carried out ultra-precision machining trials and found that the diamond tool with

(100) as the rake and the flank faces possessed higher wear resistance and provided better machined surface quality than the (110) oriented tool. All of the above studies suggest that the cubic orientation of the cutting tool provides a superior performance to the dodecahedral orientation in machining metallic workpieces.

The research work on the tool wear characteristics and the effect of diamond crystal orientation reviewed above is mostly based on the traditional cutting of nonferrous metals/alloys such as aluminium, brass and copper, where a diamond tool can last a cutting distance of up to a few hundred kilometres. For the machining of brittle materials, two independent papers have provided experimental evidence suggesting that the dodecahedral orientation can sometimes be better than the cubic orientation [58]. Although this contradicts the theoretical findings [55, 59], it seems that for a  $0^\circ$  rake angle tool, the dodecahedral orientation offers superior wear resistance to the cubic orientation. However, evaluation of the relative wear resistance of the two orientations becomes significantly more complex when the rake angle is negative. Although there are several possible explanations for the above contradiction, it has been recognized of late that the best orientation of the diamond tool must be determined by considering how the cutting tool is to be used [58].

## *2.6 Influence of cutting tool geometry*

It has been demonstrated that material removal at extremely fine depths of cut for certain atomic layers involves a high coefficient of friction that is dependent on the rake angle and is independent of the thrust force of the cutting tool [60]. When the uncut chip thickness approaches the size of the cutting edge radius during SPDT, the rake angle of the cutting tool appears to determine both the direction and the magnitude of the resultant cutting force. Lucca et al. [61] demonstrated this phenomenon in SPDT trials on OFHC copper, where the cutting tool rake angle dictated the direction of the resultant force vector for smaller uncut chip thicknesses. In fact, the use of a negative rake angle tool for SPDT operations has become somewhat of a conventional practice for the machining of brittle materials [62-63]. A schematic comparison of the cutting process using negative and positive rake angle tools is shown in figure 16.

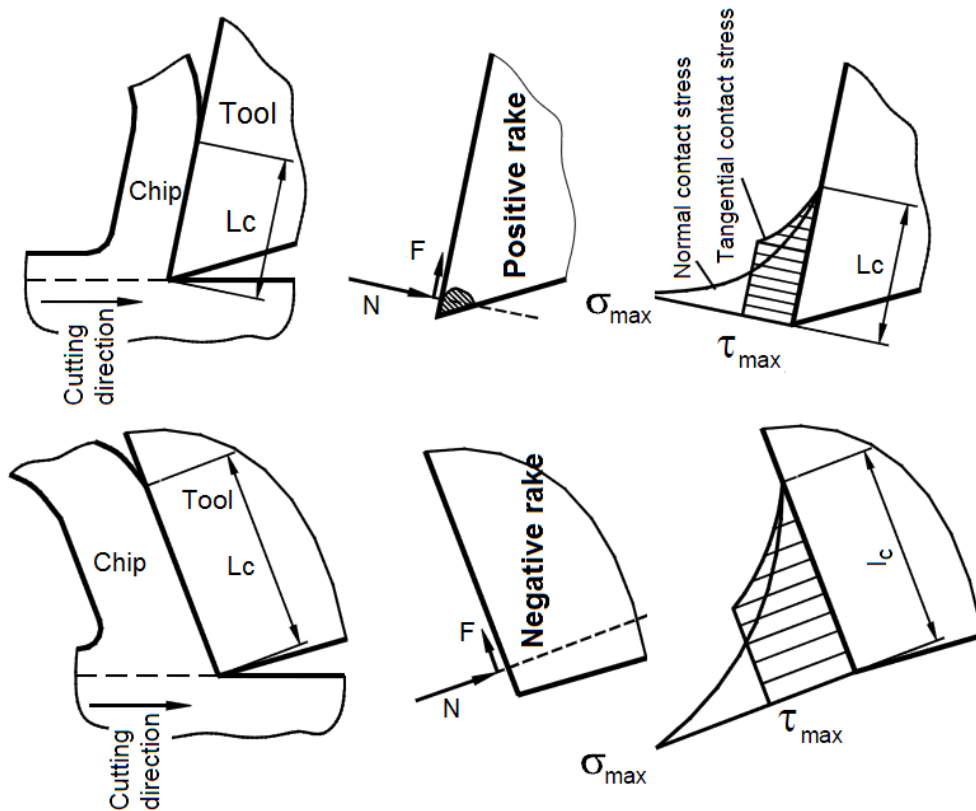


Figure 16: Difference in the force vector and stress distribution due to positive and negative rake angles [64] where  $l_c$  is length of contact between cutting tool and chip

It can be seen from figure 16 that the tangential force  $F$  acts along the wedge of the cutting tool so that the normal force acts onto the wedge face. Along these directions, the shear stress and compressive stress on the cutting tool vary during the course of machining. When positive rake angles are used, the normal force exerts a bending stress on the cutting tip of the tool under which diamond, being extremely brittle, might eventually chip off. When a negative rake-angled cutting tool is used, this bending effect does not occur because it is replaced by compression on the cutting tool. Additionally, a negative rake angle cutting tool is thought to exert a hydrostatic stress state in the workpiece, which inhibits crack propagation and leads to a ductile response from brittle materials during their nanometric cutting [12, 35]. Nakasuji et al. [35] noted that the effect of rake angle in cutting as analogous to that of the apex angle of an indenter: low angles of approach result in relatively small hydrostatic stress fields which, in turn, enable ductile regime machining. Negative rakes of approximately  $-25^\circ$  to  $-45^\circ$  degrees with clearance angles of approximately  $8^\circ$  to

12° are recommended for improved tool life [65]. The reason for such a selection is that a high clearance angle reduces rubbing while a corresponding increase in rake angle provides mechanical strength to the wedge of the cutting tool [66]. It was also noted that a 0° rake angle (clearance angle of 8°) provided superior performance than a +5° or -5° rake angle for machining electro-less nickel plate die material [67]. However, this was due to the fact that when the depth of cut is smaller than the edge radius, an effective rake angle is presented by the cutting tool [68]. In such cases, a 0° rake angle tool already presents some negative rake which made it to perform better than -25° or -30° rake angle tools. For hard steels, the critical value of the rake angle (the dividing line between efficient and inefficient material removal) is 0° [69]. Table II summarizes the work of many researchers who investigated the effect of the cutting tool rake and clearance angle during machining of brittle materials, primarily silicon.

Table II: Influence of rake angle on the outcome of the SPDT of brittle materials

| <b>Work material and citation</b> | <b>Rake Angle</b> | <b>Clearance angle</b> | <b>Total included angle of the tool</b> | <b>Remarks/Observations</b>   |
|-----------------------------------|-------------------|------------------------|---|---|
| Germanium [20]                    | -30°              | 6°                     | 114°                                    | Better machining conditions (large feed rate) was obtained for a -30° rake tool than a -10° and 0° rake angle tool.   |
| Silicon [29]                      | -40°              | 5°                     | 125°                                    | Enabled better plastic deformation of the workpiece than that of a (-25°) rake angle tool.  |
| Silicon [48]                      | -40°              | 10°                    | 120°                                    | A -40° rake angle tool provided a better ductile finished surface than a negative -20° angle rake tool.   |
| Silicon [70] and SiC [71]         | -45°              | 5°                     | 130°                                    | With an adjustable arrangement for varying rake angle, a -45° rake angle tool was found to provide better response of the workpiece for ductile-regime machining.               |
| Silicon [72]                      | -25°              | 10°                    | 105°                                    | Performed better than -15° and -45° rake angle tool; however, inferior quality of gem was suspected to be the reason for poor performance of the diamond tool having -45° rake. |
| Silicon [46]                      | -25°              | 10°                    | 105°                                    | Provided a better machined surface finished in comparison to a -15° and 0° rake angle tool.   |
| Silicon [68]                      | -30°              | 7°                     | 113°                                    | A rake angle between 0° and 60° was tested by keeping other parameters unchanged  |

|              |                                 |               |               |   |
|--------------|---------------------------------|---------------|---------------|---|
|              |                                 |               |               | and a 30° rake was found superior by LLNL.  |
| Silicon [73] | 0°                              | Not specified | Not specified | An effective rake angle is presented by the tool when the depth of cut is smaller than the edge radius. In this condition, a 0° rake angle tool already presented some negative rake and was found to provide better finish than a -25° or -30° rake angle tool. However, a 0° rake angle tool permits reduced critical chip thickness and hence low material removal rate (MRR). |
| Silicon [74] | Varying tool rake and clearance |               | 84°           | Both tool rake angle and clearance angles were varied from -15° to -45° and from 21° to 51° respectively. A (-30°) rake angle tool permitted higher critical chip thickness while (-45°) angle tool enabled to reduce the micro-cracks.   |

Although it is evident from table II that the rake angle and the clearance angle have a significant influence on the critical un-deformed chip thickness and the sub-surface lattice deformation layer depth, there is no systematic answer or model available that can be used to determine the best tool geometry for tool longevity. Komanduri et al. [75] used MD to simulate a wide range of rake angles to observe the mechanism of chip formation during the nanometric cutting of silicon. They compared the chip formation process in extrusion, particularly for large negative rake angle tools, where the space available to accommodate departing chips decreases causing an increase in chip side flow. From their simulation results, they were able to explain that an increase in the negative rake angle results in a significant increase in the extent of sub-surface deformation. Furthermore, rake angle calculation can be used to relate cutting edge radius as shown in figure 17.

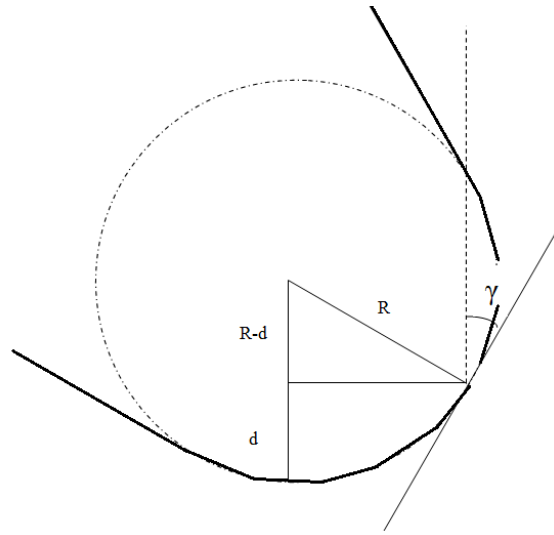


Figure 17: Schematic diagram showing effective rake angle [76]

$$\sin \gamma = \frac{R-d}{R} = 1 - \frac{d}{R} \quad (6)$$

where  $R$  is the tool nose radius,  $d$  is the depth of cut and  $\gamma$  is the effective rake angle.

### 3. Molecular dynamics simulation of SPDT

Molecular dynamics (MD) simulation is a combination of three disparate techniques: molecular modelling, computer simulation and statistical mechanics. MD is a scientific algorithm through which an assemblage of atoms and/or molecules is given prescribed intermolecular interactions for a specified period of time to yield a trajectory of their movement. The idea that classical Newtonian mechanics with a known potential and initial state of a system can effectively predict molecular motion is essentially an eighteenth century concept [77], when Laplace quoted,

Given for one instance an intelligence which could comprehend all the forces by which nature is animated and respective situations of the beings that compose it intelligence sufficiently vast to submit these data for analysis it would embrace in the same formula the movements of the greatest bodies of the universe and those of the lightest atoms.

The implementation of MD simulation was first developed through the pioneering work of Alder and Wainwright in the late 1950s [78] in their study of the interactions of hard spheres. The principle of molecular dynamics was based on the notion that Newton's second law of motion is

valid even at the atomic level.

Machining in general and SPDT in particular are difficult processes to be monitored in real-time owing particularly to the problems of high heat flux and the danger of cutting chips flying towards the operator. Also, once a material is cut, the process cannot be reversed; thus it is impossible to examine the machining experiments in infinitesimal time steps. On the other hand, MD simulation provides flexibility to study machining processes with a high degree of reversibility and safety. While MD offers many advantages, it is somewhat restricted by the size of the simulation and the time to perform that simulation. Recently, methods such as homogenisation in time [79-80], model reduction techniques [81], movable cellular automaton [82], discrete element method [83] and coupling of FEM with MD simulation [84] are being explored to overcome the limitations of MD. However, while these methods have solved the problem of size scale, they have not succeeded in mitigating the problem of time scale. In fact, particularly for simulators, the analogy of the “Law of Constancy of Pain” is that while computing power has grown over time, the amount of wall-clock time available on large computing platforms has not [51]. While, MD is still a productive phenomenological tool for understanding discrete processes such as the effect of the crystal structure of the material (cutting tool and the workpiece), high-pressure phase transformation, wear of cutting tools, and tribochemistry involved during the process, an appropriate MD simulation, requires understanding the importance of potential energy function which must include aspects of HPPT to simulate both ductile and brittle phase machining. In view of the aforementioned comments, a summary of the key advantages and current limitations of MD simulation in the context of machining studies is presented in table III.

Table III: Advantages and limitations of molecular dynamics simulation

| S.No. | Advantages   | Limitations  |
|-------|--|--|
| 1.    | MD algorithm enables consideration of a more fundamental unit of matter (i.e. the atom) and hence material properties are described naturally by their interaction potentials. Influence of crystal anisotropy, tribochemistry of the process and basic mechanisms | MD cannot predict the attainable experimental measure of machined surface roughness which is a prime requirement governing the choice of a material in an industrial application. Even if a theoretical value is |

|    |  |   |
|----|--|---|
|    | underlying a wear process can thus be suitably studied through MD. Furthermore, MD permits an investigation of theoretical approachable limits.  | estimated, it will always remain an ideal limit that can only be attained under an ideal set of machining conditions.   |
| 2. | MD permits online monitoring of the machining processes with good quality temporal and spatial resolution in a reversible manner. Any time step can simply be reversed through a computer program to analyze it at any given time.   | Time to finish one simulation is a major challenge associated with performing a simulation with a realistic cutting speed and large specimen size.  |
| 3. | MD simulation avoids the use of expensive equipment and apparatus, which are key requirements in order to perform nanometric cutting experiments. Moreover, material once consumed will be required to reorder, whereas MD can perform any number of trials with a number of varying parameters. | Size of the workpiece and tool material cannot be varied to a larger (experimental) scale because of the current memory limitations associated with handling a large data file size.                                |
| 4. | MD simulation offers repeatability of the process. The type of work material, cutting tool material, and environmental conditions can all be kept intact and maintained at a pre-determined value.   | Ongoing work on the development of potential functions is still restricted to using a variety of coolants during a simulation, which is often a prerequisite for a real experiment.                                 |
| 5. | MD simulation provides flexibility to perform the simulation at any place. A computer system is mobile whereas an ultra precision machine tool (exhibiting high stiffness) demands a static foundation and the experiment is thus static.  | Only an advanced researcher can perform an appropriate MD simulation as it requires an accurate understanding of various disciplines. A machining trial can be performed using relatively less trained technicians. |

### 3.1. Simulation based studies

Yan et al. [85] simulated SPDT of silicon using the finite element method (FEM) and demonstrated two important phenomena as follows:

- increase in the cutting edge radius causes a decrease in the cut chip thickness and a corresponding increase in the thrust force
- lowering the cutting edge radius (below 200 nm) shifts the high temperature zone from the tool rake face to the tool flank face resulting in the transition of the wear pattern from crater to flank wear

Similarly, Patten and Jacob [86] simulated SPDT of single crystal 6H-SiC by employing a Drucker-Prager (pressure sensitive) yield criterion in a commercial FEM software. They found that the

cutting forces agreed with those experimentally measured only under ductile-regime machining conditions and not under brittle-regime. This limitation was attributed to the criterion used for yielding which does not include a fracture criterion or, by implication, a brittle material removal mechanism.

While FEM is a useful tool for gaining some insights into the cutting pressure under ductile-regime conditions and the effect of cutting edge radius, yet some of the important mechanisms, such as high pressure phase transformation, influence of the crystal anisotropy, and cutting direction and mechanism of tool wear cannot be thoroughly studied using standard FEM simulations. Consequently, Aly *et al.* [87] proposed a hybrid scheme of extracting the mechanical properties of silicon (yield stress, ultimate stress and Young's modulus) from the tensile test simulation using MD and fed these properties to the FEM simulation model of micromachining of silicon to predict the cutting forces. While such hybrid approaches hold promise, they are difficult to implement since significant expertise is needed to execute such schemes.

MD simulation was adapted for ultra precision machining at LLNL, USA during the late 1980s [88]. Belak, Shimada and Ikawa [89] pioneered the concept of MD in the framework of nanometric cutting followed by Voter *et al.* [90]. Since then, Shimada and Ikawa [91], Rentsch *et al.* [92], Komanduri *et al.* [62], and Cai *et al.* [44] have contributed significantly to this arena and set a foundation for the study of nanometric cutting processes using MD simulation. In their seminal study, Belak *et al.* [93] reported the amorphisation of silicon chips and indicated the possibility of molten silicon under the influence of heat generated during the cutting processes. They also observed that the simulated silicon atoms cling quite tightly to the rake and flank faces of the cutting tool. Ikawa *et al.* [89] explored the limits of thickness of cut attainable during the process of diamond turning. By combining their simulation work with the experiments, they successfully obtained 1 nm size of cut chip thickness on copper and demonstrated the feasibility of nanometric size chip removal through SPDT. By converting an atomistic model into the equivalent continuum model, Inamura *et al.* [36] observed a high compression rather than a concentrated shear stress in

the primary shear zone. They used Prandtl-Reuss equations to suggest that the deformation of the workpiece in the primary shear zone could be accounted for by shear plastic deformation resulting from levels above the yield shear stress. Nozaki et al. [94] used the Stillinger-Weber potential energy function to compare the performance of machining silicon on different planes to that of machining metals. They found that, unlike metal, the plastic deformation in silicon is highly confined, and results in the brittle nature of silicon. The machined surface was found to be smoother with increasing depth of cut. Shimada et al. [95] examined the brittle-ductile transition phenomenon in silicon using MD simulation. Underneath, and in the vicinity of, the cutting tool (included angle  $90^\circ$ ), they observed the movement of voids. They also found that elastic and thermal shock waves are generated and propagate in the substrate. However, when the depth of cut was in the nanometre range, they found that the potential energy was too low for the shock wave to supply the necessary energy to initiate a crack or to propagate a pre-existing crack. Komanduri et al. [96] found that dislocations were absent in their simulations and consequently suggested that inelastic deformation via amorphous phase transformation is an energetically more favourable mechanism than plastic deformation involving the generation and propagation of dislocations. Komanduri et al. [96] also suggested that a decrease in the  $w/d$  ratio (i.e. the ratio of width of cut to depth of cut) caused an exponential increase in the side flow of silicon. Based on the simulation results, they suggested that a reduced width of cut will result in a reduced deformed layer depth on the machined surface of amorphous silicon. Additionally, some surface damage on the machined surface of silicon was found to be inherent in the nanometric cutting process irrespective of the depth of cut, width of cut and rake angle used. Based on these observations, they suggested that the difficulty in the SPDT of silicon is not attributable to high cutting forces or specific cutting energy, but to the problems of tool wear and subsurface deformation underneath the cutting tool. Another reviews highlights some additional considerations in this regard [97-98].

### 3.2. *Potential energy function*

MD simulation requires a constitutive description of the terms for which particles in a simulation

interact. This interaction is governed by a potential energy function that roughly accounts for quantum interactions between electron shells and represents the physical properties of the atoms being simulated, such as its elastic constants and lattice parameters. Potentials used in chemistry are generally called “force fields,” while those used in materials physics are called “analytical potentials.” Most force fields in chemistry are empirical and consist of a summation of forces associated with chemical bonds, bond angles, dihedrals, non-bonding forces associated with van derWaals forces and electrostatic forces. Balamane et al. [99] presented a comprehensive review of the potential energy functions that have been used to simulate silicon. While newly developed formalisms provide greater accuracy, they are sometimes computationally very expensive as shown in table IV and figure 18.

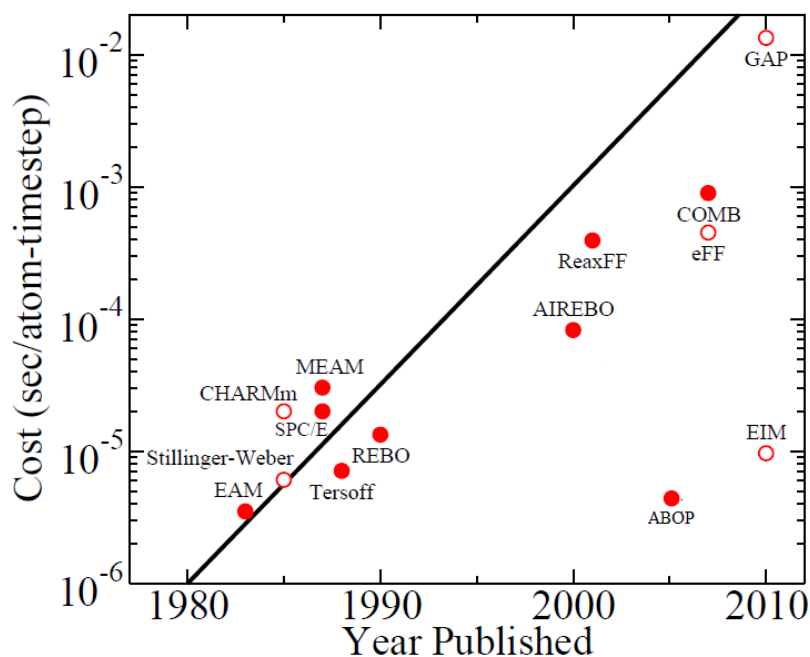


Figure 18: Single CPU cost in seconds/atom/time step for various potential functions (The black line represents a doubling in computational cost every two years, akin to Moore’s Law for hardware complexity [100])

Table IV: List of potential functions with respect to the time of introduction

| S.No. | Year | Name of the potential function       | Materials suited |
|-------|------|--------------------------------------|------------------|
| 1     | 1984 | EAM: embedded-atom method [101]      | Cu               |
| 2     | 1985 | Stillinger-Weber potential [102-103] | Si               |

|    |                                      |  |   |
|----|--------------------------------------|--|---|
| 3  | 1987                                 | SPC: simple point charge [104]   | H <sub>2</sub> O  |
| 4  | 1988<br>1988<br>1989<br>1990<br>1994 | BOP: bond-order potential <ul style="list-style-type: none"> <li>• Tersoff-1 variant for silicon [105]</li> <li>• Tersoff-2 for better elastic properties of silicon [106]</li> <li>• Tersoff-3 for Si, C and germanium [107-108]</li> <li>• Tersoff-4 for silicon and carbon [109]</li> <li>• Tersoff-5 for amorphous silicon carbide [110]</li> <li>• Refinements in Tersoff potential function [111-113]</li> <li>• EDIP [114-115]</li> </ul> | Si<br>Si<br>Si, Ge and C<br>Si and C<br>SiC<br>Si and C<br>Si and C |
| 5  | 1989                                 | MEAM: modified embedded-atom method [116] <sup>*</sup>   | <u>Universal</u>  |
| 6  | 1990                                 | REBO: reactive empirical bond order [117]  | Carbon  |
| 7  | 2000                                 | AIREBO: adaptive intermolecular reactive empirical bond order [118] (4 body potential function)  | Hydrocarbons and Carbon   |
| 8  | 2001                                 | ReaxFF: reactive force field [119] (Capable of bond breaking and bond-formation during the simulation)   | <u>Universal</u>  |
| 9  | 2005                                 | ABOP: analytical bond order potential [120] (3 body potential function)  | Si and C  |
| 10 | 2007                                 | COMB: charge optimized many-body [121]   | SiO <sub>2</sub> , Cu, Ti   |
| 11 | 2008                                 | EIM: Embedded-ion method [122]   | Ionic e.g. NaCl   |
| 12 | 2010                                 | GAP: Gaussian approximation potential [123]  | Universal   |
| 13 | 1998-2001                            | Other important potential functions relevant in contact loading problems [124-126]   | Si, B and N   |
| 14 | 2013                                 | Screened potential functions [127-128] <sup>†</sup>  | Range of materials  |

Table V: Morse potential function for some metallic elements [60]

| Element    | Crystal structure | Lattice constant (Å) | D (eV) | a (Å <sup>-1</sup> ) | r <sub>0</sub> (Å) |
|------------|-------------------|----------------------|--------|----------------------|--------------------|
| Lead       | FCC               | 4.95                 | 0.2348 | 1.1836               | 3.733              |
| Silver     | FCC               | 4.09                 | 0.3323 | 1.369                | 3.115              |
| Nickel     | FCC               | 3.52                 | 0.4205 | 1.4199               | 2.78               |
| Iron       | BCC               | 2.87                 | 0.4174 | 1.3885               | 2.845              |
| Chromium   | BCC               | 2.89                 | 0.4414 | 1.5721               | 2.754              |
| Molybdenum | BCC               | 3.14                 | 0.8032 | 1.5079               | 2.976              |
| Tungsten   | BCC               | 3.165                | 0.9906 | 1.4116               | 3.032              |

Chemistry force fields commonly employ preset bonding arrangements (exceptions include *ab initio* dynamics and ReaxFF) and are thus unable to simulate the processes of chemical bond-breaking and chemical reactions. The Morse potential function is an example of a pair potential that

<sup>\*</sup> Latest modifications (2NN MEAM) are available through [https://cmse.postech.ac.kr/home\\_2nnmeam](https://cmse.postech.ac.kr/home_2nnmeam)

<sup>†</sup> Details available from <https://github.com/pastewka/atomistica>

was frequently used in early research work and is used for simulations even now. Morse potential parameters for some typical metallic materials are shown in table V. Nanometric cutting of aluminium or copper using a diamond tool may be conducted using the Morse parameters, as shown in table VI.

Table VI: Morse potential parameters for nanometric cutting of metals [129]

| Element | D (eV) | a ( $\text{\AA}^{-1}$ ) | $r_0$ ( $\text{\AA}$ ) |
|---------|--------|-------------------------|------------------------|
| Cu-Cu   | 0.342  | 1.3588                  | 2.866                  |
| Al-Al   | 0.2703 | 1.1646                  | 3.253                  |
| C-C     | 3.68   | 2.2                     | 1.54                   |
| Cu-C    | 0.087  | 1.7                     | 2.05                   |
| Al-C    | 0.28   | 2.78                    | 2.2                    |

A major limitation of Morse potential (or any other pair potential) is its inability to reproduce the Cauchy pressure of a material. This was one of the motivations for introducing EAM potential in 1984. Unlike Morse potential functions, many of the potentials used in physics, such as those based on bond order formalism, may describe both bond breaking and bond formation (e.g. Tersoff is a three-body potential function, while the AIREBO function is a four-body potential function). The Tersoff formalism or, more appropriately, the ‘‘Tersoff-Abell’’ formalism is the most widely used bond order potential formalism and has become the basis for a sizable number of potential functions. Tersoff based his potential on an idea presented by Abell a few years earlier on bond order potential (BOP), which has environmental dependence and no absolute minimum at the tetrahedral angle. Initially, Tersoff proposed two variants for pure Si in which Si(B) sufficiently describes the surface properties of silicon while Si(C) sufficiently describes the elastic properties [105-106] of silicon.

Tersoff functions gained wide popularity in the 1990s for MD simulations. However, one key drawback of this potential function is that it describes the graphite-to-diamond transformation rather poorly. However, it has been noted that simply increasing the parameter  $S$  in the potential to  $2.46 \text{ \AA}$  improves this aspect [130]. Tersoff functions are also known to poorly predict the melting point of

silicon, which was later refined by an adjustment of three parameters of this potential [111]. To overcome another limitation of the poor description of the dimer properties of silicon by Tersoff, another potential function has been proposed that is an analytical bond order potential (ABOP) of almost the same formalism [120]. Overall, Morse potential functions limit the exploration of interaction within atoms of the workpiece and the cutting tool, while Tersoff potential functions have limitations in accurately describe the thermal aspects of silicon which might limit the study of some machining processes related to high temperature applications. This is a potential area for future research. Another drawback of Tersoff in its original formulation is the way next nearest neighbor atoms are determined, namely *via* a narrow distant-dependent cutoff. This artificial abrupt change in energy-distance relation cause the forces required for bond breaking to be severely overestimated leading to ductile behaviour in silicon. Consequently, the potential functions proposed by Tersoff and Erhart et al. i.e. BOP and ABOP to describe the interaction in silicon and carbon, fails in reproducing the density-temperature relation of silicon however another potential reproduces close results with experiments [113]. This suggests that both BOP and ABOP potential function are not fully reliable to obtain the phase diagram of silicon. In an attempt to address this problem, a recent effort has been made by decoupling the condition for a nearest-neighbor relationship from the range of the potential [128]. Subsequent refinements have led to a formalism, which is developed by using the screening functions to increase the range of these potentials [127]. By changing the cut-off procedure of all the bond order potential functions, screening function has been reported to reproduce an improved description of amorphous phases and brittle behavior of silicon, diamond and silicon carbide.

Overall, a potential energy function is an important consideration for a realistic MD simulation. There are some shortcomings of the currently used potential functions. For example, the ductile-brittle transition during nanometric cutting of silicon and silicon carbide cannot be described well by the Tersoff potential energy function (that has been a heavily used potential function). Similarly, the mechanism of cleavage on certain crystal orientations of brittle materials is yet another aspect

that cannot inherently be captured by all the potential energy functions [131-132]. Indeed, in absence of crystal orientation information, this was perhaps misinterpreted as ductile-brittle transition in a previously published study [12]. An important consideration for simulating nanometric cutting of silicon is that the surface bonds or the nascent surface of silicon will be reactive and will tend to bond together with the surface of the diamond tool cutting tool during its approach. In order to avoid such an artefact, it is a good practice to saturate the surface bonds by using hydrogen or any other similar material before the start of the simulation. Finally, MD considers the environment as vacuum, however experimental environment is known to play a key role in influencing the machining outcome.

### *3.3. MD simulation of nanometric cutting*

In what follows, steps involved in an MD simulation are described briefly. The description is generalized and may be adapted to any software platform.

#### *3.3.1. Boundary conditions and ensemble*

A schematic diagram of the nanometric cutting simulation model that has been suggested to be appropriate for a nanometric cutting simulation [133] is shown in figure 19. In this model, the nanocrystalline workpiece and the cutting tool are modelled as deformable bodies in order to permit tribological interactions between them. The model used negative tool rake angle, as this is generally recommended for machining hard, brittle materials [62-63].

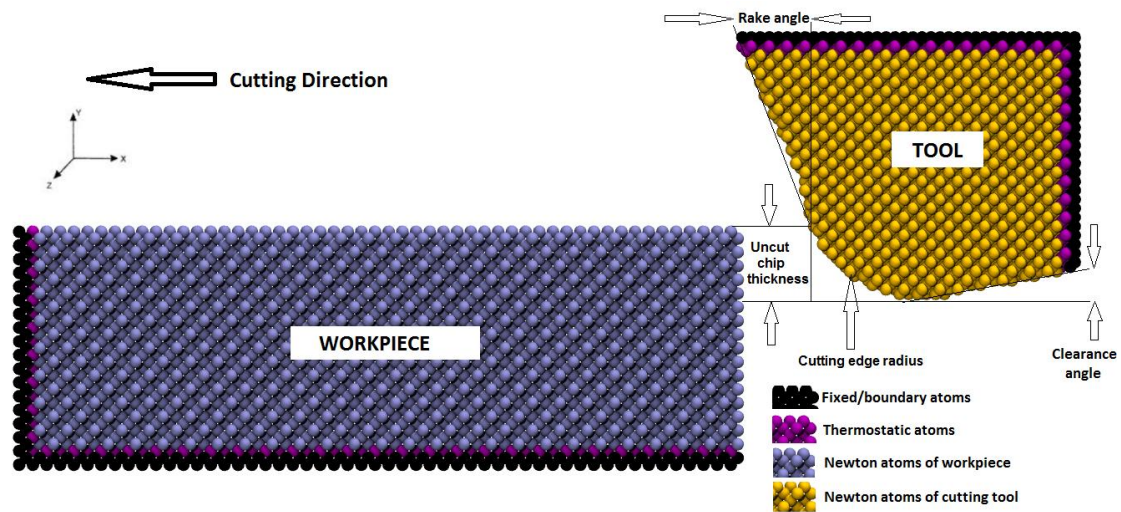


Figure 19: Schematic of MD simulation model

In this simulation model, the atoms of the cutting tool and the workpiece are allocated into one of three different zones: Newton atoms, thermostatic atoms and boundary atoms. The boundary atoms are assumed to remain unaffected and fixed in their initial lattice positions during the simulation, serving to reduce the boundary effects and to maintain the symmetry of the lattice. In conventional machining operations, the energy from plastic deformation in the primary shear zone and friction at the tool-chip interface generate heat, which is carried away by chips, lubricant and by conduction into the tool and workpiece. The nanometric cutting model is, however, extremely small and is not capable of dissipating the heat itself. The velocity of the thermostatic atoms is therefore re-scaled to a desired temperature (300K) at each step of the computation to dissipate the artificial heat. It may be noted here that a thermostat layer so close to the cutting zone strongly exaggerates the cooling since it forces that zone to have room temperature. In reality, the thermostat area is at a macroscopic distance. Such a problem can be handled by either increasing the size of the simulation model both in the X and in the Y direction or by using the multiscale simulation method.

MD simulations are usually implemented considering a system of N particles in a cubic box of length L. Since N is typically in the range of 100 to 10000 (very far from the thermodynamic limits), it is necessary to use a periodic boundary condition (PBC) to avoid surface effects. An important consideration for performing a simulation is to first determine the equilibration lattice

parameter[134]. This could be achieved by averaging the lattice constant from the NPT dynamics ran on a small volume of a material at the desired temperature and pressure for few femtoseconds. Note that nanometric cutting of silicon using a diamond tool involves the use of two different lattice constants i.e. silicon (0.5432 nm) and diamond (0.356 nm). Care must be taken to choose the periodic cell dimensions in such a way that these two lattice constants are in an integer proportion, e.g.  $L_z = n_1 \times a_1 = n_2 \times a_2$  where  $L_z$  is the box size (in the z direction),  $n_1$  and  $n_2$  are integers and  $a_1$  and  $a_2$  are the two lattice constants. It is generally difficult to find an exact solution to this equation, but for a large enough system,  $n_1$  and  $n_2$  can be approximated reasonably well. Similarly, a change in crystal orientation also requires an adjustment in the dimension of periodic boundary. For example, a workpiece may be positioned on the (111) orientation by specifying the basis vectors in the x direction as (-2 1 1), in the y direction as (1 1 1), and in the z direction as (0 1 -1). An alternative orientation specification could be (-1 1 0), (1 1 1) and (1 1 -2). In both cases, the z orientation varies and hence the simulation box size in the z direction should accordingly be adjusted to accommodate the cutting tool and the workpiece. Once the geometry of a model is ready, the velocities to the atoms can be assigned using the Maxwell-Boltzmann distribution. Followed by an energy minimization, the velocities of all the atoms can be set to a desired temperature. This step is followed by the process of equilibration, wherein, the aim is to achieve a desired temperature until a steady state is achieved. The amount of time required for equilibration depends on the system being investigated as well as the initial configuration of the system. Newton atoms are then allowed to follow Newtonian dynamics (LAMMPS NVE dynamics), while atoms in an intermediate thin boundary layer were subjected to a thermostat (LAMMPS NVT dynamics) to dissipate the extra heat generated in the finite simulation volume. This consideration of boundary conditions ensures that the process of deformation is not affected by any artificial dynamics.

### 3.3.2. *Identification of phase transformation in brittle materials*

Phase transformation of brittle materials is of particular interest to the field of nanometric cutting because it makes possible the obtainment of a ductile response from brittle materials [135]. An

understanding of high pressure phase transformation is necessary so that the deviatoric stress conditions can be controlled in order to drive phase transformation in brittle materials to execute the ductile-regime machining. From the MD simulation point of view, it is challenging to assign a definite phase to the material and a combination of several methods is sometimes needed to understand and analyse the material's phase under a given set of conditions. A state-of-the-art review by Stukowski [136] covers the relevance, importance and application of these methods, as well as description of several new methods, such as Voronoi analysis and Neighbour distance analysis. Some of these methods are briefly discussed below with an emphasis on their applications as part of an MD simulation of nanometric cutting.

#### *3.3.3.1. Coordination number*

Cheong *et al.* [137] have shown that Si-I to Si-II phase transformation in silicon is associated with changes in the inter-atomic distance of the atoms of silicon from a uniform 2.35 Å to 2.43 Å for four nearest neighbour atoms and to 2.58 Å for two second nearest neighbour atoms. Early research established that this change in inter-atomic distance is associated with a change in the coordination number of silicon from 4 to 6 [96] which means that the number of nearest neighbour atoms in pure silicon changes from 4 to 6, signifying ductile-regime machining. However, Gilman [40] noted that the coordination number of Beta-silicon (Si-II) cannot be exactly 6 because there is always a difference of 5.6% between consecutive nearest neighbour atoms. Since this anomaly has persisted for a decade, it is advisable to confirm the HPPT state of the material by applying other alternative methods as well in addition to the measure of the coordination number.

#### *3.3.3.2. Radial distribution function*

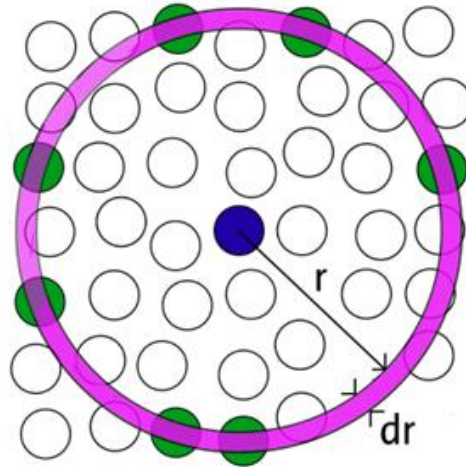


Figure 20: Schematic diagram of radial distribution function [134]

The radial distribution functions, also called “pair distribution functions” or “pair correlation functions,” are the primary link between macroscopic thermodynamic properties and intermolecular interactions. Figure 20 shows the scheme of the radial distribution function. As illustrated in figure 20, the blue coloured atom is the central atom from which neighbour distance is measured; green coloured atoms are the atoms that count as the first neighbour distance atoms and white coloured atoms are the remaining atoms in the system. If the atoms in a space are distributed homogeneously, then the RDF,  $g(r)$ , gives the probability of finding the centre of an atom in a shell  $dr$  at a distance  $r$  from the centre of an atom chosen as a reference point. RDF can thus be used as a tool to monitor the changes in the inter-atomic bond length of the materials during, upon, and after the contact loading process, which can be used to gain useful insights from the process.

### 3.3.3.3. Angular distribution function or bond angle analysis

A classic example of the use of an angular distribution function is for distinguishing between FCC and HCP crystal structures. These structures can be differentiated using bond angle distribution functions, but it is a tedious process using a coordination number alone (both have a coordination number of 12). During the nanometric cutting of brittle materials, HPPT can lead to a change in the bond angle to up to 37%, in comparison to the corresponding change in bond length, which can be up to 4% only. Therefore, an angular distribution function could be thought of as a more robust and

more sensitive measurement than the RDF. An advanced algorithm named “Interactive structure analysis of amorphous and crystalline systems” allows for the use of this feature. Alternatively, this could also be accomplished by performing an Ackland analysis [138] within OVITO.

#### 3.3.3.4. *Centro-symmetry parameter*

Dislocations play a crucial role in governing the plastic response of brittle materials. The thermal vibration of atoms at finite temperatures makes it difficult to observe dislocations in environments with changing temperatures. As such, the commonly used methods for tracing such dislocations and other lattice defects are coordination number, slip vector, and centro-symmetry parameter (CSP). Although CSP was originally developed for BCC and FCC lattice structures, it can also be applied to a diamond cubic lattice by considering the diamond cubic lattice as two identical FCC lattices [139-140]. CSP was proposed as the most effective method for measuring dislocations since it is robust to the thermal vibration of atoms [141]. A CSP can be computed using the following formula:

$$CSP = \sum_{i=1}^{N/2} \left| \vec{R}_i + \vec{R}_{i+\frac{N}{2}} \right|^2 \quad (7)$$

$N$  nearest neighbours of each atom are identified and  $R_i$  and  $R_{i+N/2}$  are vectors from the central atom to a particular pair of nearest neighbours. Thus, the number of possible neighbour pairs can be given

by  $\frac{N \times (N-1)}{2}$  [142].

### 3.3.3. Calculation of cutting forces

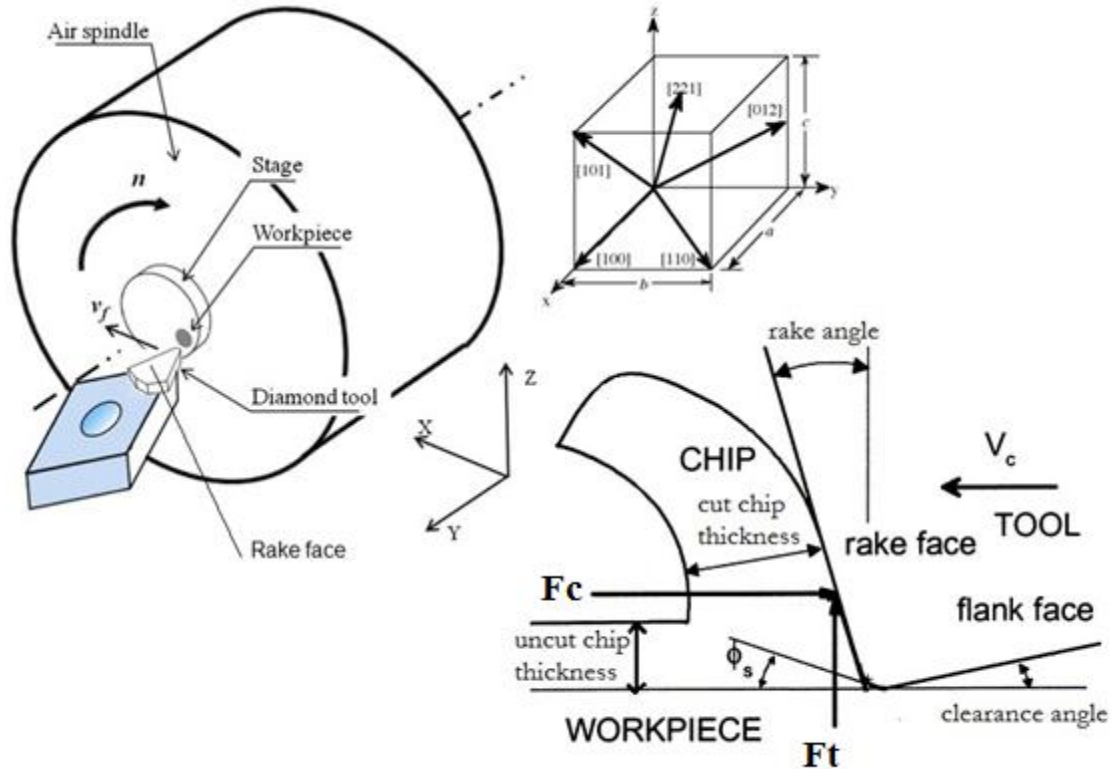


Figure 21: Schematic diagram of chip formation during SPDT [143]

Figure 21 shows schematically the main parameters affecting the process of the nanometric cutting of anisotropic brittle materials, including a schematic representation of the crystal orientation [144-147]. As shown in the bottom panel of figure 21, two coplanar forces (namely, the tangential cutting force ( $F_c$ ) and the thrust force ( $F_t$ )) acting on a cutting tool fundamentally govern the cutting action of the tool. The third component,  $F_z$  acts in the direction orthogonal to the X and Y planes and mainly influences surface error, as it tends to push the tool away from the workpiece. The tangential force causes displacements in the direction of cut chip thickness and its variation therefore relates to chatter. These are the reasons why cutting force measurement is an important indicator of tool wear [148]. From the MD simulation perspective, the calculation of the cutting forces using a diatomic pair potential, such as Morse or Lennard Jones function is relatively simpler because the interaction energy will include a pair component which is defined as the pairwise energy between all pairs of atoms where one atom in the pair is in the first group (workpiece) and the other is in the second group (cutting tool). These pair interactions can directly be used to compute the cutting forces. For a

many-body potential function, such as EAM, Tersoff, ABOP and AIREBO, in addition to the pair-potential, there are other terms that make them computationally expensive. Accounting for these extra terms needs additional computations in addition to those in the pair-wise interactions. Earlier Cai *et al.* [44] have reported that ductile mode cutting is achieved when the thrust force acting on the cutting tool is larger than the cutting force. While this was found to be true in several experimental studies, this is not the case observed during several nanoscale friction based simulation studies where cutting forces were found dominant over thrust forces [5, 149]. It is therefore yet another important area for future research.

### 3.3.4. Calculation of machining stresses

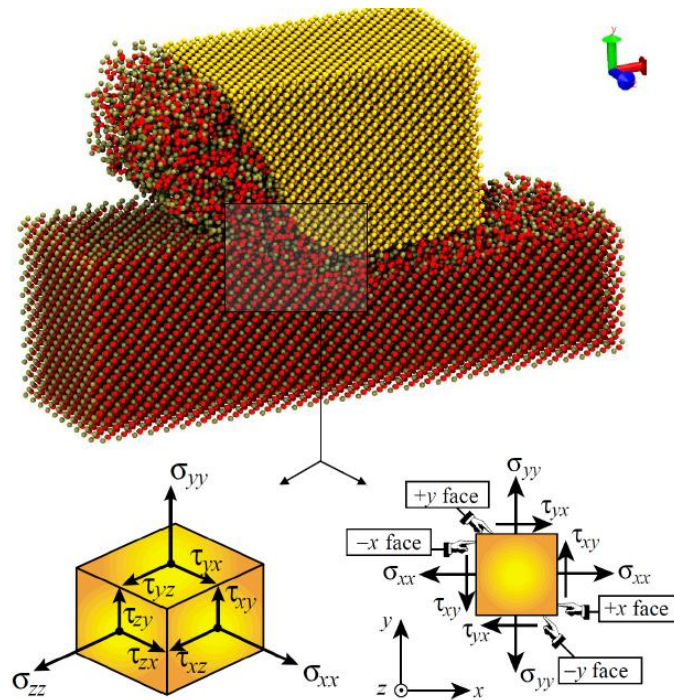


Figure 22: Stresses in the cutting zone

The state of stress acting in the machining zone is shown schematically in figure 22 for both 2-D and 3-D stress systems. The instantaneous values of the stress calculated from the MD simulation should always be time averaged. One fundamental problem with the computation of atomic stress is that the volume of an atom does not remain fixed during deformation. To mitigate this problem, the best method is to plot the stresses on the fly by considering an elemental atomic volume in the

cutting zone. The total stresses acting on that element could be computed and divided by the pre-calculated total volume of that element to obtain the physical stress tensor. When a stress tensor from the simulation is available, the following equations can readily be used to obtain the Tresca stress, von Mises stress, Octahedral shear stress and hydrostatic stress.

$$\text{Stress tensor} = \begin{bmatrix} \sigma_{xx} & \tau_{xy} & \tau_{xz} \\ \tau_{xy} & \sigma_{yy} & \tau_{yz} \\ \tau_{xz} & \tau_{yz} & \sigma_{zz} \end{bmatrix} \quad (8)$$

Invariants:

$$I_1 = \sigma_{xx} + \sigma_{yy} + \sigma_{zz} \quad (9)$$

$$I_2 = \sigma_{xx}\sigma_{yy} + \sigma_{yy}\sigma_{zz} + \sigma_{zz}\sigma_{xx} - \tau_{xy}^2 - \tau_{xz}^2 - \tau_{yz}^2 \quad (10)$$

$$I_3 = \sigma_{xx}\sigma_{yy}\sigma_{zz} + 2(\tau_{xy}\tau_{yz}\tau_{xz}) - \tau_{xz}^2\sigma_{yy} - \tau_{yz}^2\sigma_{xx} - \tau_{xy}^2\sigma_{zz} \quad (11)$$

$$A_1 = -I_1; \quad A_2 = I_2 \quad A_3 = -I_3 \quad (12)$$

$$Q = \frac{3A_2 - A_1^2}{9} \quad (13)$$

$$R = \frac{9A_1A_2 - 27A_3 - 2A_1^3}{54} \quad (14)$$

$$D = Q^3 + R^2 \quad (15)$$

If  $D < 0$  then as follows: else the condition is 2D stress

$$\theta = \cos^{-1} \left( \frac{R}{\sqrt{-Q^3}} \right) \quad (16)$$

$$R_1 = 2\sqrt{-Q} \times \cos\left(\frac{\theta}{3}\right) - \frac{A_1}{3} \quad (17)$$

$$R_2 = 2\sqrt{-Q} \times \cos\left(\frac{\theta + 4\pi}{3}\right) - \frac{A_1}{3} \quad (18)$$

$$R_3 = 2\sqrt{-Q} \times \cos\left(\frac{\theta + 2\pi}{3}\right) - \frac{A_1}{3} \quad (19)$$

$$\sigma_1 = \max(R_1, R_2, R_3) \quad \text{and} \quad \sigma_3 = \min(R_1, R_2, R_3) \quad (20)$$

$$\sigma_{\text{tresca}} = \frac{\sigma_1 - \sigma_3}{2} \quad (21)$$

$$\sigma_{\text{von Mises}} = \sqrt{\frac{(\sigma_{xx} - \sigma_{yy})^2 + (\sigma_{yy} - \sigma_{zz})^2 + (\sigma_{zz} - \sigma_{xx})^2 + 6(\tau_{xy}^2 + \tau_{yz}^2 + \tau_{zx}^2)}{2}} \quad (22)$$

$$\sigma_{\text{octahedral}} = \frac{\sqrt{(\sigma_{xx} - \sigma_{yy})^2 + (\sigma_{yy} - \sigma_{zz})^2 + (\sigma_{zz} - \sigma_{xx})^2 + 6(\tau_{xy}^2 + \tau_{yz}^2 + \tau_{zx}^2)}}{3} = \frac{\sqrt{2}}{3} \sigma_{\text{von Mises}} \quad (23)$$

$$\sigma_{\text{hydrostatic}} = \frac{\sigma_{xx} + \sigma_{yy} + \sigma_{zz}}{3} \quad (24)$$

In an earlier study, Cai *et al.* [44] used MD simulation to simulate the cutting of silicon (using Tersoff function for describing the silicon workpiece and Morse function for cross interactions between the rigid diamond tool and the workpiece) and reported that when the tool cutting edge radius increases, the shear stress in the workpiece material around the cutting edge decreases and crack propagation becomes dominating, leading to a transition from ductile to brittle in the chip formation mode. While the authors in the above study have not clarified as to how the stresses were computed by them in the MD framework in terms of averaging (spatial or temporal), a noticeable thing in their work is that they used Tersoff potential function which is a short ranged potential function and lacks the robustness in describing the brittle behaviour of silicon. Furthermore, they discarded the role of crystal anisotropy in the study and also did not consider the fact that the stress state in the cutting zone is normally deviatoric and the plane-stress consideration will make the results erroneous so in order to assert whether the compression or shear are compensated by each other it will be a worthier future work to compare the total deviatoric stress in the cutting zone (von Mises stress or Tresca Stress) as a function of undeformed chip thickness or cutting edge radius.

### 3.3.5. Calculation of machining temperature

Due to the nature of the statistical mechanics by which an ensemble is defined, the instantaneous thermodynamic values for the atoms differ from the bulk property of the substrate. This phenomenon is called as “fluctuation”. Temperature is an ensemble property, and measurement of the temperature is not straightforward. The suitability of any method used to measure the temperature in atomic simulations depends primarily on how many atoms are being analysed and how fast the released energy is dissipated by the surroundings. The velocity of the atoms is used to compute the average temperature of the atoms. This is done with regard to the relationship between kinetic energy and temperature:

$$\frac{1}{2} \sum_i m_i v_i^2 = \frac{3}{2} N k_b T \quad (25)$$

where  $N$  is the number of atoms,  $v_i$  represents the velocity of  $i^{th}$  atom,  $k_b$  is the Boltzmann constant ( $1.3806503 \times 10^{-23}$  J/K) and  $T$  represents the atomistic temperature. During the process of nanometric cutting, the instantaneous fluctuations in kinetic energy per atom could be very high, so these are averaged temporally and/or spatially over few time steps and reassigned to each atom at every  $N^{th}$  step to be converted into equivalent temperature. The movement of the tool will also contribute to the kinetic energy, and so the component of tool displacement should be subtracted beforehand from the above calculations.

Overall, MD simulation of nanometric cutting starts with the development of the geometry of the material, and description of the interactions of the atoms with the material using a suitable potential energy function. This is followed by equilibration of the model and simulation in an appropriate ensemble. After the simulation is over, atomic trajectories can be used for post processing of the results (with or without time averaging depending on the quantity).

## 4. Properties of machined surface and ductility of silicon

High pressure phase transformation (HPPT) is known to induce the Herzfeld-Mott transition, which causes the metallization of brittle materials during their nanometric cutting. This research area is

now emerging as a new field of knowledge and is being referred to as High Pressure Surface Science [150]. It is envisaged that the semiconductor to metal transition via HPPT occurs in the athermic region and therefore the hardness obtained from the nanoindentation does not reflect the yield stress but corresponds to the critical pressure of the phase transition [16, 98]. Experimental studies on this topic include veritable resolution using in-situ and ex-situ imaging, quasistatic nanoindentation [151], acoustic emission detection [152], Scanning spreading resistance microscopy [153], high temperature studies [154], monitoring of electrical resistance [155], X-ray diffraction [156], Raman scattering [135], laser micro-Raman spectroscopy [157] and transmission electron microscopy [158-159]. Many simulation studies also provided support to the experimental studies. These simulation studies involves use of molecular dynamics simulation [134, 140], finite element simulation [160-161] and multiscale simulation using Quasicontinuum method [162-163]. In what follows, the phenomenon of HPPT and the properties of the machined surface are discussed.

#### 4.1. *HPPT of silicon*

At ambient pressure, crystalline Si-I (brittle) structure contains four nearest neighbours at an equal distance of 2.35 Å. Upon hydrostatic loading of 10-12 GPa or from 8.5 GPa under non-hydrostatic condition, Si-I transforms to Si-II phase (metallic and ductile) which contains four nearest neighbours at a distance of 2.42 Å and two other neighbours at 2.585 Å (lattice parameter  $a = 4.684$  Å and  $c = 2.585$  Å) [137]. Further increase of pressure in the range of 13-16 GPa, results in the formation of Si-XI (Imma silicon) phase of silicon. Further phases at high pressure formed as a result of transformation recognized to date are Si-V, Si-VI, Si-VII and Si-X [164].

The reverse transformation depends on the mode of unloading/release of the pressure. For example, upon slow unloading, a crystalline phase of Si-XII and Si-III may persist interspersed with an amorphous region. The Si-XII phase has four nearest neighbours within a distance of 2.39 Å and also another at a distance of 3.23 Å or 3.36 Å at 2 GPa while Si-III has four nearest neighbours within a distance of 2.37 Å and another unique atom at a distance of 3.41 Å at 2 GPa. The main

difference between these two phases is that while Si-XII is known to be a narrow band gap semiconductor that can be electrically doped with boron and phosphorus at room temperature to make electronic devices, Si-III is postulated to be a semi-metal [165]. Si-III can first transform to a six coordinated Si-XIII phase which could transform further to either Si-IV or to amorphous-Si [153]. On the other hand, a rapid unloading causes the transformation of Si-II to tetragonal Si-IX or tetragonal Si-VII phase of silicon. All these phases ultimately stabilize to form amorphous Si (a-Si). Also, a non-hydrostatic pressure could directly transform Si-I to a stable bct-5 (five coordinated) phase of silicon. The bct5-Si crystalline structure contains one neighbour at a distance of 2.31 Å and four other neighbours at 2.44 Å. This cycle is schematically represented in figure 23. Thus, it is the corresponding change in volume from Si-II (more dense and low volume) to a-Si (more structural volume) which causes expansion and the consequent elastic recovery of the machined surface after the tool passes the cutting area. However, the extent of this elastic recovery reduces with an increasing E/H ratio of the materials involved [166].

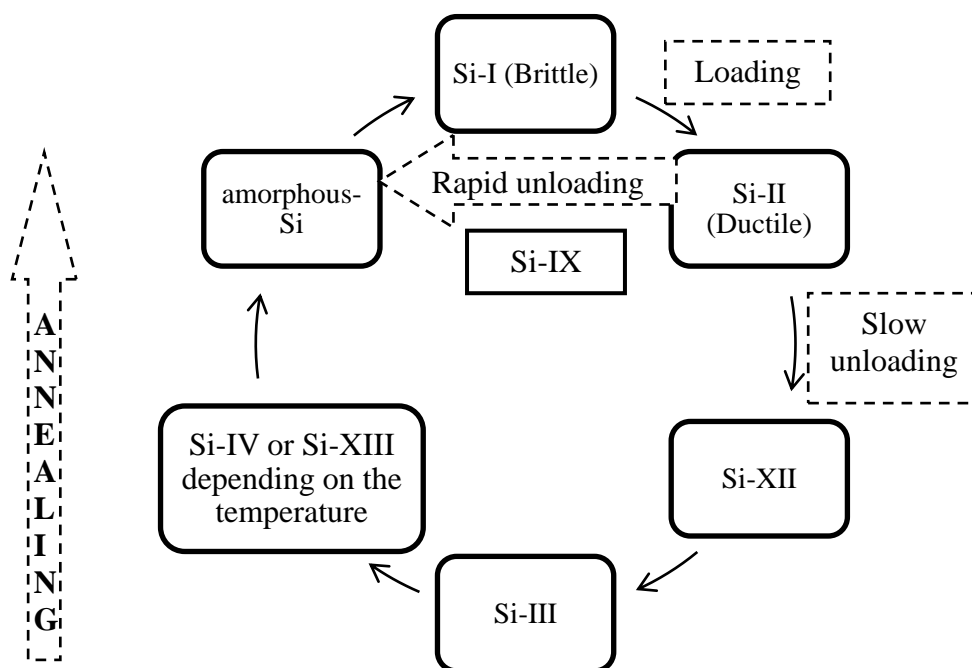


Figure 23: Phase transformations in silicon during its contact loading [16]

The various phases involved in the response of silicon during its cutting in the ductile regime are summarized in table VII [167]. Ample deviatoric stress underneath the cutting tool leads to the

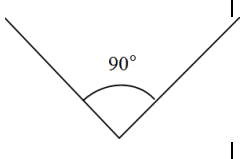
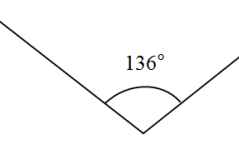
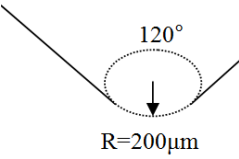
metallization of silicon and the metallic phase of silicon can be deformed plastically akin to a metal machining process [168]. Back transformations from Si-II phase are accompanied by an increase in volume of ~10% and contribute to the elastic recovery of the machined surface after the cutting tool passes. Interestingly, while bulk silicon experiences HPPT, which is responsible for its ductility, this is not the case with its nanoparticles. In contrast to bulk silicon, plasticity in silicon nanoparticles has been attributed to dislocation driven plasticity [169-170] rather than to HPPT.

Table VII: HPPT of silicon during its contact loading – adapted [151, 159, 167]

| Phase of Silicon        | Lattice structure   | Pressure (GPa)                       | Lattice parameter (Å)         | Raman band (cm <sup>-1</sup> )    | Relative volume |
|-------------------------|---|--------------------------------------|-------------------------------|-----------------------------------|-----------------|
| Pristine Si-I (brittle) | Diamond cubic   | 0-12.5                               | a =5.42                       | 521                               | 1               |
| Si-II (Metallic)        | (Beta-tin)  | 9-16                                 | a=4.69<br>c=2.578             | 137,375                           | 0.78            |
| Si-XII                  | R8, Rhombohedral  | 12-2                                 | a=5.609<br>γ=110.07           | 184, 350, 375, 397, 435, 445, 485 | 0.9             |
| Si-III                  | bc8 (BCC)   | 2.1 – 0 (ambient)                    | a=6.64                        | 166, 384, 415, 433, 465           | 0.92            |
| Si-IV                   | Hexagonal diamond   | Martensitic transformation from Si-I | a=3.8<br>c=6.629              | 510                               | ~0.98           |
| Si-IX                   | St12, tetragonal  | Upon rapid decompression from Si-II  | Information not available yet |                                   | ~0.88           |
| Si-XIII                 | New martensitic phase, Raman peaks at 200, 330, 475 and 497 |                                      |                               |                                   |                 |
| a-Si                    | Raman bands at : TA-160, LA-300, TO-390, LO-470             |                                      |                               |                                   |                 |

The geometry of the diamond tool also effects the transformations. For example, Gogotsi et al. [171] used a nano-scratching test to demonstrate the influence of geometry of the indenter in driving the various phases during contact loading of silicon on the (111) crystal orientation. The outcome of their results is shown in table VIII.

Table VIII: Comparison of the ductile response of silicon with different tools [171]

| Category         | Conical tool  | Pyramidal tool<br>(Vicker indenter)   | Spherical tool<br>(Rockwell indenter)   |
|------------------|---|---|---|
| Shape            |  |  |  |
| Rake angle       | -45°  | -68°  | Variable from about -60° to -90°  |
| Material removal | Yes   | Yes   | No  |
| Si Phases        | Si-III, Si-XII,<br>Si-IV<br>and a-Si  | Si-III, Si-XII, Si-IV<br>and a-Si   | Si-III, Si-XII and<br>a-Si  |
| Maximum stress   | Near the edge   | Near the edge   | In the middle   |

The timescales and the conditions of temperature and pressure effecting HPPT in silicon have been detailed recently [172]. An excerpt for a ready glance from that work is demonstrated in figure 24 which shows the evolution of the machining temperature and von Mises stress during nanometric cutting of silicon (Red line shows Si-I to Si-II transformation as the cutting tool reaches the cutting zone and the blue line shows Si-II to a-Si transition as the cutting tool passes the cutting zone). It was found that the peak temperature in the cutting zone of silicon was 1378 K while the peak von Mises stress in silicon was 13 GPa. Noticeably, these two peak events did not occur simultaneously (i.e. until peak loading, temperature lagged the peak stress and during unloading while the tool moved, stress lagged the temperature). Therefore, the peak temperature at peak stress was only up to 800K; whereas peak stress at peak temperature was only about 3-4 GPa. Fitting of local conditions of stress and temperature obtained from the simulation on the phase diagram of silicon confirmed that during machining of single crystal silicon, there occurs a Si-I to Si-II transformation (rather than the melting of silicon) and as the cutting tool passes by, the Si-II phase transforms to low density a-Si (LDA). The former event takes place in 40 picoseconds while the later takes place in about 20 picoseconds. Note that nanoindentation and nanometric cutting (despite few differences) are similar in many aspects [173] and hence the mechanism of brittle-ductile transition

was actually understood from the nanoindentation experiments which suggests that brittleness is an indentation size effect [34]. Figure 25 highlights that irrespective of the indentation speed, silicon transforms to high pressure metallic phase rather than melting as was previously thought [93].

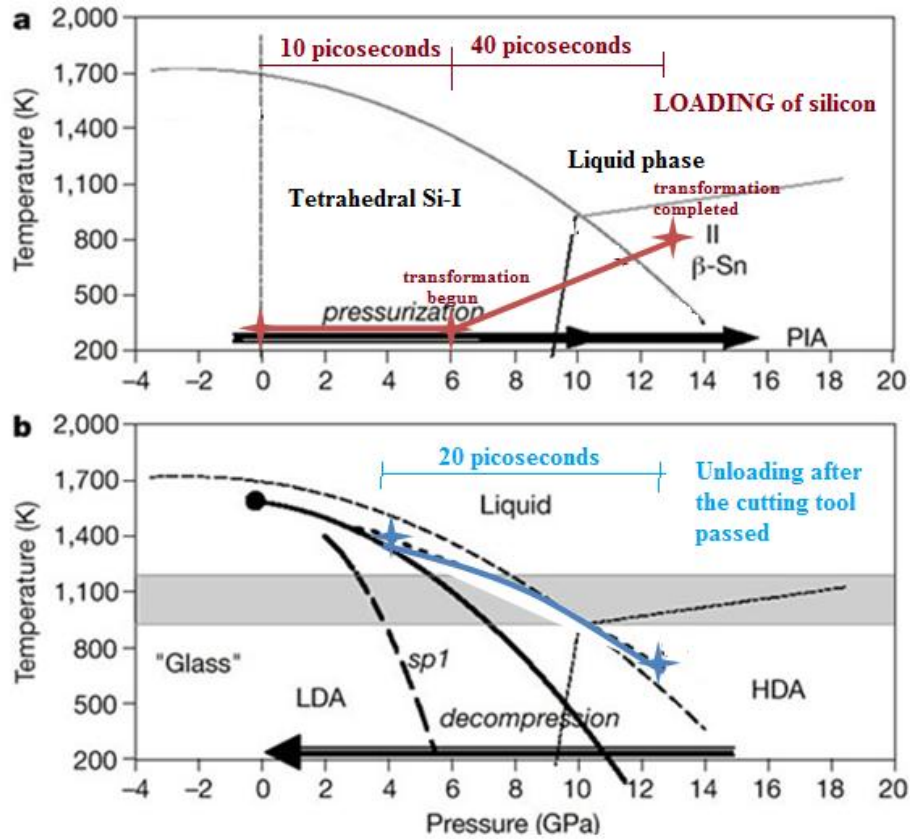


Figure 24: Variation in the stress and temperature of silicon obtained from the MD simulation of nanometric cutting of silicon fitted to the experimentally obtained phase diagram of silicon [174]. Red line during cutting/loading indicates metallization of silicon while blue line during unloading indicates amorphisation of silicon

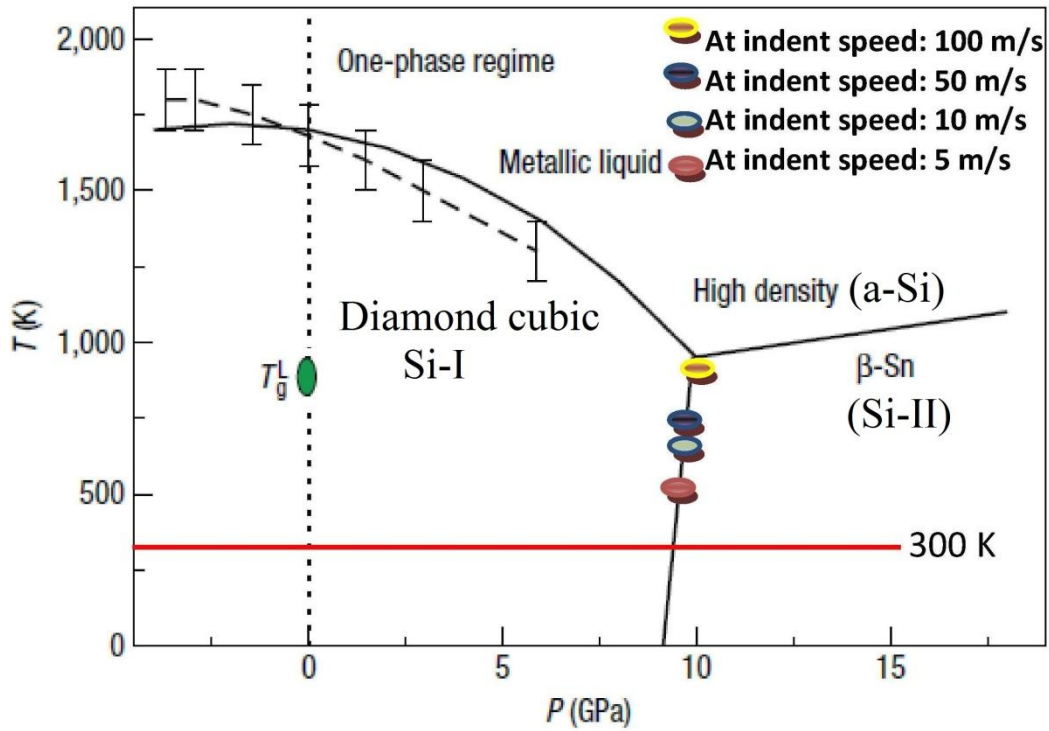


Figure 25: Variation in the peak stress and peak temperature in the indentation zone of silicon fitted to the experimentally obtained phase diagram of silicon reflecting Si-I to Si-II phase transformation as a function of indentation speed. The dashed line, with error bars represent the uncertainty in the melting point determination using Stillinger-Weber potential function while  $T_g^L$  indicates the LDA polymorph transition and its details can be had from its respective reference [173].

A study on the nanoindentation of single crystal silicon at different cutting speeds was recently carried out by the authors [173]. They find that irrespective of whether the material is single crystal or polycrystal, it will still undergo metallization, albeit, its degree and extent may differ (due to the presence of grain boundaries). This study also delineates that it is the deviatoric stress that drives HPPT in silicon rather than temperature. Another interesting finding of interest is that the hardness of the surface of diamond turned silicon was found to be lower than that of pristine silicon [175] which was attributed to the presence of a-Si on the machined surface of silicon.

#### 4.2. Residual stress on the machined surface of silicon

A few studies have focused on the extent of residual stress induced in the machined component by the SPDT process. The pioneering experimental work of Jasinevicius *et al.* [157] used Micro-Raman spectroscopy to investigate the extent of residual stresses on the (100) oriented silicon wafer machined by a  $-25^\circ$  rake angle diamond tool at varying feed rates and depth of cut. Using the

formulation below:

$$\varpi = \varpi_0 + 0.52L \quad (26)$$

where  $\varpi$  is the experimental peak obtained using Raman spectroscopy,  $\varpi_0$  is the theoretical characteristic peak of silicon ( $521.6 \text{ cm}^{-1}$ ) and  $L$  is the residual stress measured in an area in Kilobar, their results suggest that the extent of the tensile residual stress on the machined surface increases with the decrease in either depth of cut or the feed rate. See table IX for details.

Table IX: Variation in the residual stress on the machined silicon surface probed by using Raman spectroscopy as a function of depth of cut while the feed rate was kept fixed [157]

| Fixed feed rate ( $\mu\text{m}/\text{rev}$ ) | Varying depth of cut ( $\mu\text{m}$ ) | Residual stress (MPa) |
|--|--|-----------------------|
| 1  | 0.1                                    | +221.59               |
| 1  | 1                                      | +103.8                |
| 1  | 5                                      | +77                   |
| 1  | 10                                     | 0                     |

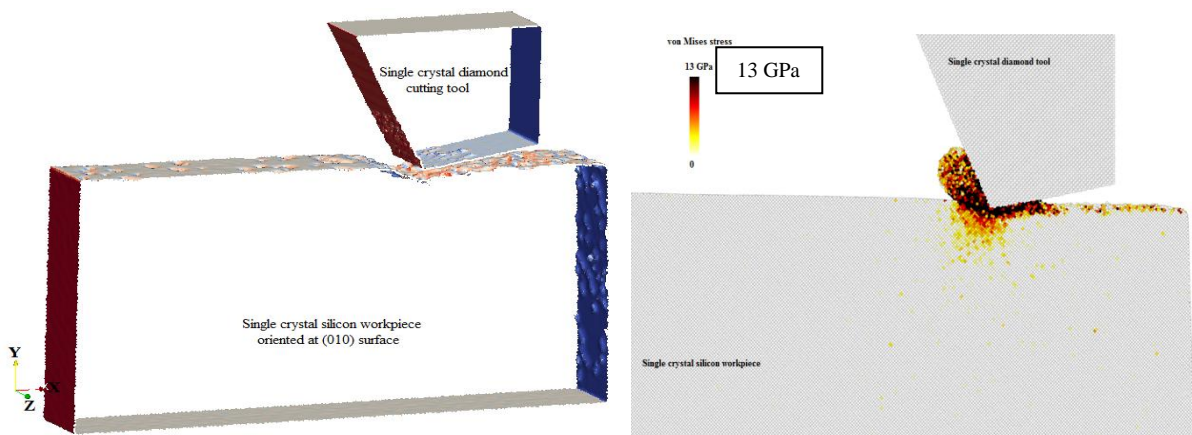
They used TEM to explain that the formation of microcracks in the sub-surface at higher depth of cuts or at higher feed rates is the reason why the residual stress gets relieved and its extent lowers. Residual stress on the machined silicon substrate has also been obtained using MD simulation [176] which showed that an increase in the negative rake of the tool tends to produce a deeper layer of amorphous silicon after machining. Hence, investigation of residual stresses on the machined surface of silicon as a function of cutting parameters is still a promising area of research.

#### 4.3. Influence of the crystal structure on HPPT

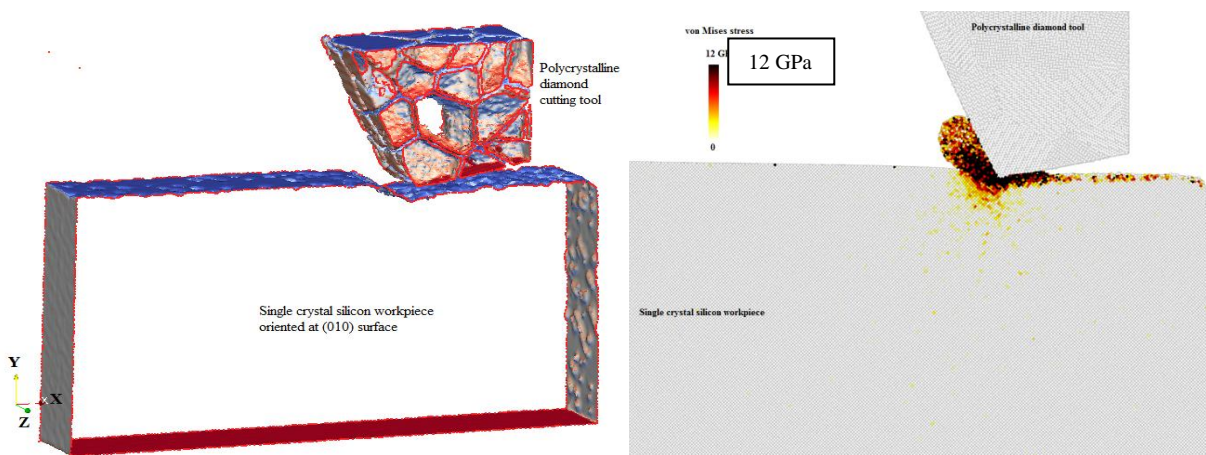
In the above section, it was shown that there is a rich body of literature on nanometric cutting of single crystal silicon. However, the use of polycrystalline silicon substrate (which is widely used in many real world applications such as solar panel, thin transistors, and VLSI manufacturing) or a polycrystalline diamond cutting tool (which is used in many automotive and aerospace applications for high-speed machining) is relatively unexplored. The unique feature of a polycrystalline material is the microstructure of a crystallite that consists of a set of topological entities with different

dimensionality, such as the three-dimensional grain cell (GC), two-dimensional grain boundary (GB), one-dimensional triple junction (TJ), and zero-dimensional vertex point (VP) [177]. On account of these features, the nanomechanical response of a polycrystalline material is different from that of a single crystal material and hence an understanding of these aspects is crucial for a better understanding of machining of a polycrystalline material. Sumitomo *et al.* [178] carried out nanoindentation and nanoscratching trials on multilayer thin film solar panels of a-Si. Their experiments reveal that material removal below a critical depth is dominated by plastic mechanisms and this critical depth depends on the indenter geometry and material properties. Two conditions that were found to promote the ductile-regime (crack free) machining were (i) high scratch speed and (ii) lower included angle of the tip. Recently, Goel *et al.* [172] carried out MD simulations involving a polycrystalline silicon workpiece and a polycrystalline diamond cutting tool. Figure 26 present their MD simulation results comparing the machining performance in three simulated cases: (i) cutting a single crystal silicon substrate with a single crystal diamond cutting tool (ii) cutting a single crystal silicon substrate with a polycrystalline diamond cutting tool and (iii) cutting a polycrystalline silicon substrate using a single crystal diamond cutting tool. From the snapshots shown in figure 26, significant differences are visible in the chip morphology and in the grain structure of the substrate. Diamond atoms have a different atomic volume than silicon, thus stresses in the tool were not computed and shown here. It may be seen from figure 26a that cutting single crystal silicon with a single crystal cutting tool showed the magnitude of von Mises stresses in the cutting zone to be highest (13 GPa). The magnitude of this stress dropped to 12 GPa when using a polycrystalline cutting tool to cut a single crystal substrate (as can be seen from figure 26b) and become minimum (10.5 GPa (figure 26c)) when cutting a polycrystalline substrate using a single crystal cutting tool. The stress state in all of the cases and the indicative magnitude are consistent with the reported values required to cause HPPT of silicon from its stable diamond cubic structure to Si-II metallic structure. Metallic phase transformation in all the cases was achieved. However, figure 26c showed that atoms at the grain boundaries carry a very large magnitude of internal stress.

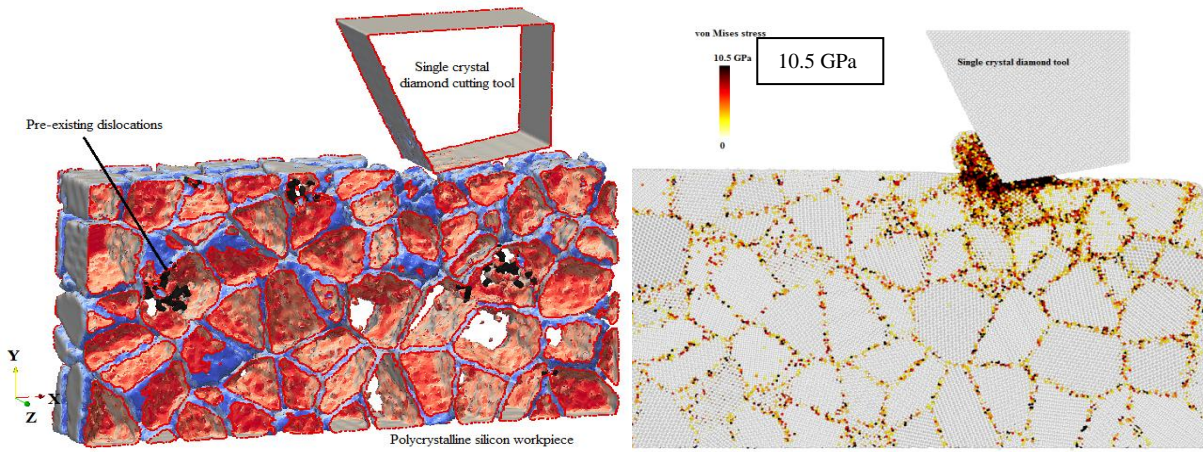
The magnitude of this stress at the grain boundary is either equal to or higher in magnitude than that induced by the cutting tool in the cutting zone. Such a high magnitude of stress at the interface of the grains in the cutting zone results in yielding of the material at the grain boundaries. This makes it easier to initiate the slip of one grain over the other. These simulations reveal that cutting a polycrystalline material (unlike cutting a single crystal silicon substrate) is influenced by the movement of grains over each other in tandem with the HPPT mechanism simultaneously. Furthermore, a polycrystalline silicon workpiece, unlike single crystal silicon workpiece did not showed crack propagation (dislocations) underneath the machined surface and requires the least specific cutting energy and machining temperature in the cutting zone both on the workpiece and the single crystal cutting tool, whereas a polycrystalline cutting tool consumes the most specific cutting energy and shows a very high temperature on the tool cutting edge.



(a) Cutting of a single crystal workpiece with a single crystal cutting tool



(b) Cutting of a single crystal workpiece with a polycrystalline cutting tool



(c) Cutting of a polycrystalline workpiece with a single crystal cutting tool

Figure 26: Output of the MD simulation showing snapshots of nanometric cutting of silicon and von Mises stress distribution. The geometric boundaries of workpiece and cutting tool and the respective grains are shown, while the geometric boundaries of the disordered phases are not visible in these visualizations [172].

## 5. Wear of diamond cutting tools during machining of silicon

Currently, silicon is considered amenable to SPDT even though it is a difficult-to-machine material. However, it is extremely tough to machine a silicon wafer of diameter over 100 mm with consistent form accuracy. A major reason underlying this limitation is heavy tool wear, in particular, the flank wear of the diamond cutting tool.

In general, natural diamond exhibits significant variation in its physical, mechanical and chemical properties. Industrial characterization of diamond is usually based on the colour of the gem; a more quantitative assessment is possible using more sophisticated optical characterization but this is time consuming and costly. There are two broad classifications of diamond, the main features of which are shown in table X.

Table X: Classification of diamonds [83]

|                | Type I                                 |                    | Type II<br>(Extremely good heat conductors) |  |
|----------------|--|--------------------|---|--|
|                | I <sub>a</sub>                         | I <sub>b</sub>     | II <sub>a</sub>                             | II <sub>b</sub>                          |
| Nitrogen (ppm) | ~200-2400                              | ~40                | ~8-40                                       | ~5-40                                    |
| Boron (ppm)    | None                                   | None               | None  | ~0.5                                     |
| Remarks        | Nitrogen exists in small geometrically | Nitrogen exists as | Chemically pure with very little            | Little nitrogen but contains substantial |

|  |                  |                                |          |                  |
|--|------------------|--------------------------------|----------|------------------|
|  | clustered groups | isolated<br>substitution atoms | nitrogen | boron impurities |
|--|------------------|--------------------------------|----------|------------------|

Unlike type II diamonds, type I diamonds have low dislocation density and a high density of platelets [101]. The presence of these platelets hinders the movement of dislocations in type I diamond making it even more difficult to cause plastic deformation. It has been demonstrated that type Ib diamond exhibits good repeatability of the tool life under identical test conditions whereas type IIb diamond is the most wear resistant of all categories of diamond. In a recent study, Wang *et al.* [148] used wavelet transform method to decompose the cutting force signals for real-time tool condition monitoring with a notion that a good understanding of the wear mechanism is an essential step for identifying the measures needed to suppress wear and to enhance the usefulness of tool life. Wang *et al.* [179] cited Kronenberg to relate the temperature on the cutting tool with the workpiece properties and the cutting variables. This pioneering study did not consider the dynamic changes in the temperature with the cutting time. However, this effort led to implementation of cryogenic cooling as a measure to suppress the tool wear as an initial step. In a recent effort [180], a surface roughness conservation law incorporating the size effect arising out of the cutting edge radius has been proposed and was validated on a copper workpiece. A significant quantity of research has been done on the characterization of tool wear from SPDT through observations and measurements of the worn tools. An important consideration in the study of wear of diamond cutting tools is that at constant spindle rotation speed, the surface cutting speed varies from maximum on the outside of the workpiece to zero at the centre. Thus, the differences in wear behaviour due to different cutting speeds have to be accounted for [10, 181]. Previous characterizations of tool wear used qualitative descriptors such as normal wear, chipping, setting problems (not related to diamond tools), line effects, chip dragging and fracture [182]. Paul *et al.* [183] presented a review dedicated to the wear of diamond tools during SPDT operations. With only a few exceptions, they proposed a hypothesis in which rapid chemical wear of the diamond tools was attributed to the presence of unpaired *d-shell* electrons in the substrate. They explained that the wear of diamond might be a consequence of

any, or a combination of the following mechanisms:

- adhesion and formation of a built up edge
- abrasion, micro-chipping, fracture and fatigue
- tribo-thermal wear
- tribo-chemical wear

Another, similar classification of the wear of cutting tools in general includes the following mechanisms [184]:

- diffusion wear: influenced by the chemical affinity between the workpiece and the cutting tool
- abrasive wear: influenced by the hardness of the workpiece and the cutting tool
- oxidation wear: influenced by the affinity of the cutting tool to oxygen
- fatigue wear (static or dynamic): influenced by the thermo-mechanical effect and its duration
- adhesion wear: occurs at relatively low machining temperature when there is a strong intermolecular attraction between the atoms of the cutting tool and the workpiece

Wong [182] used 150 single crystal diamond tools and classified tool wear into six categories: normal wear, chipping, setting problems, line effects, chip dragging and fracture by inclusions in the work material. He noticed that diamond tools with shorter tool lives exhibited broader infrared absorption at  $1365\text{ cm}^{-1}$ . Based on this observation, he postulated that the presence of the nitrate bond (N-O) in diamond tools induces unfavourable internal strains within the crystal lattice, which may shorten the tool life. Jasinevicius et al. [185] conducted an experiment in which they machined a single crystal silicon wafer with a worn diamond tool. Their results indicate that worn tools can generate high stress levels with an increase in penetration depth. If the compressive stresses are high enough and the tensile stresses are low enough, the onset of the phase transformation and plastic deformation takes place prior to cracking. Li et al. [186] noted that diamond tool wear starts with the appearance of nanoscale grooves on the tool flank. These grooves form secondary cutting edges which tend to change the cutting mode from ductile to brittle fracture. Khurshudov et al. [187]

conducted a nanoscratching experiment on a silicon wafer using a diamond AFM tip to measure the wear rate. They suggested that the diffusion rate of carbon from diamond into silicon was quite high, and that this explained the high wear rate during the interaction of diamond and silicon. In addition, tool geometry, crystal orientation and the quality of the diamond gem have all been found to influence tool wear significantly [49, 72, 188-189]. Additionally, natural mono-crystalline diamonds always contain a range of defects such as cracks, inclusions, lattice defects (including twins and dislocations) and impurities (including metal atoms, hydrogen, nitrogen or oxygen) [58]. In tandem with these studies, a few molecular dynamics studies followed to investigate the wear of the cutting tools. A brief summary of past tool wear studies performed using MD simulation and their conclusion is presented in table XI.

Table XI: MD studies on tool wear during SPDT

| Potential function for tool-workpiece interaction | Material | Author, Year and country            | Tool consideration               | Conclusion of the study concerning cause of tool wear  |
|---|----------|-------------------------------------|----------------------------------|--|
| LJ  | Silicon  | J. Belak, 1990, USA [88, 93]        | Deformable                       | SiC asperity was observed during SPDT of silicon   |
| Morse   | Copper   | K.Maekawa, 1995, Japan [190]        | Deformable                       | Interdiffusion and readhesion  |
| Tersoff   | Silicon  | R.Komanduri, 1998, USA [62, 96]     | Rigid                            | -  |
| MEAM  | Silicon  | X.Luo, 2003, UK [191]               | Deformable                       | Thermo-chemical mechanism  |
| Morse   | Silicon  | M.B. Cai, 2007, Singapore [192-193] | Deformable                       | Formation of dynamic hard particles  |
| MEAM  | Iron     | R. Narulkar, 2008, USA [194]        | Deformable                       | Graphitization of diamond  |
| Morse   | Silicon  | Z. Wang, 2010, China [195]          | Deformable                       | No mechanism has been described  |
| Not clearly described                             | Diamond  | Fung et al. [196]                   | Elevated temperature compression | Fracture along the (111) shuffle plane, partial dislocation at elevated temperature and $sp^3$ to $sp^2$ disorder in the colder areas was reported |

As table X shows, there is a debate on the mechanism of the wear of diamond tool obtained from

these studies. While Cheng et al. [191] identified a thermo-chemical mechanism as governing wear, Maekawa et al. [190] suggested inter-diffusion and re-adhesion. A theory in which formation of “dynamic hard particles” causes tool wear has also been proposed [192-193], but it lacks experimental evidence. Thus, the MD simulations performed earlier did not revealed a convincing mechanism of tool wear during SPDT of silicon. This is plausible due to the fact that most of the MD simulations to date used a Morse potential function to describe the tool-workpiece interactions [190, 192, 195]. An exception to this is the study conducted by Komanduri et al. [96] who used a Tersoff potential function but assumed the tool to be a rigid body. Thus, tool wear could not be studied. Contrarily, in the investigation of Fung et al. [196], it is not clear as to which potential function (ABOP or the Tersoff) has been used to study the elevated temperature deformation of diamond. Recent investigations suggest the role of tribochemistry being dominating in causing the tool wear during SPDT of silicon [134, 140]. Using a radial distribution function, it has been demonstrated that the wear of diamond cutting tool is initiated by the chemical activity between silicon and carbon. The close contact between the workpiece and tool results in a locally high temperature, and in the actual machining environment, it is supplemented by the presence of ambient oxygen as well. The highly reactive, freshly generated dangling bonds of silicon tend to combine with the atmospheric oxygen to form silicon dioxide as the free energy is negative at all temperatures [197]. However, the reaction mechanism thereafter may be through a single-phase solid state reaction or through a multiphase reaction, as shown in table XII.

Table XII: Reaction mechanism for formation of silicon carbide

| Process                      | Chemical Reaction   | Free energy change for the reaction               |
|------------------------------|---|---|
| <b>Single Phase Reaction</b> |   |   |
| Formation of Silicon carbide | $\text{Si (s,l,g)} + \text{C} \rightarrow \text{SiC}$ [198]               | $\Delta G_T^O = 499820 - 149T \text{ J / mol}$    |
| <b>Multiphase Reaction</b>   |   |   |
| Formation of Silicon Dioxide | $\text{Si} + \text{O}_2 \rightarrow \text{SiO}_2$ [198]                   | Free energy change in negative in all cases [197] |
| Formation of Silicon oxide   | $\text{SiO}_2 + \text{C} \rightarrow \text{SiO} + \text{CO}$ [198]        | $\Delta G_T^O = 670402 - 327T \text{ J / mol}$    |
| Formation of                 | $\text{SiO} + 3\text{CO} \rightarrow \text{SiC} + 2\text{CO}_2$ [199-200] |   |

|                 |  |  |
|-----------------|--|--|
| Silicon carbide | or   |  |
|                 | $\text{SiO (g) + C (s) } \rightarrow \text{Si (g) + CO (g) [198]}$ |  |
|                 | $\text{Si (g) + C (s) } \rightarrow \text{SiC (S) [198]}$          |  |

Figure 27 shows the decrease in hot hardness of several tool materials and also shows the free energy change for the chemical reaction leading to the formation of SiC via two routes as a function of process temperature. Figure 27 indicates that the free energy change is positive in either case, thus the reaction will not be spontaneous. Also, the solid state single phase reaction between silicon and carbon is thermodynamically more favourable to a temperature of 959 K. Beyond a temperature of 959 K, the silicon dioxide path is energetically the more favourable route towards the formation of silicon carbide, which implies that the presence of oxygen at a temperature above 959 K will accelerate the formation of silicon carbide. The authors also showed that the maximum cutting temperature (figure 28) during the SPDT process does not surpass 959 K [140] even when high cutting speeds of about 100 m/s was used in the simulation.

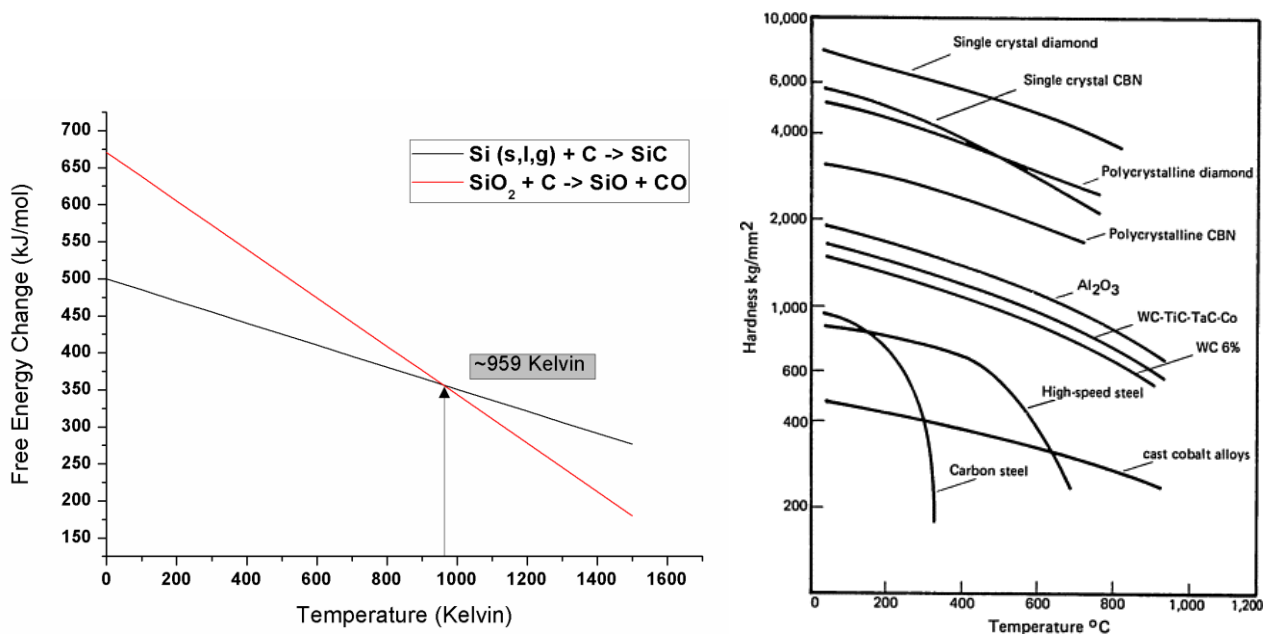


Figure 27: Gibb's free energy change for the formation of SiC [134] and typical hot hardness characteristics of some hard (cutting tool) materials [11]

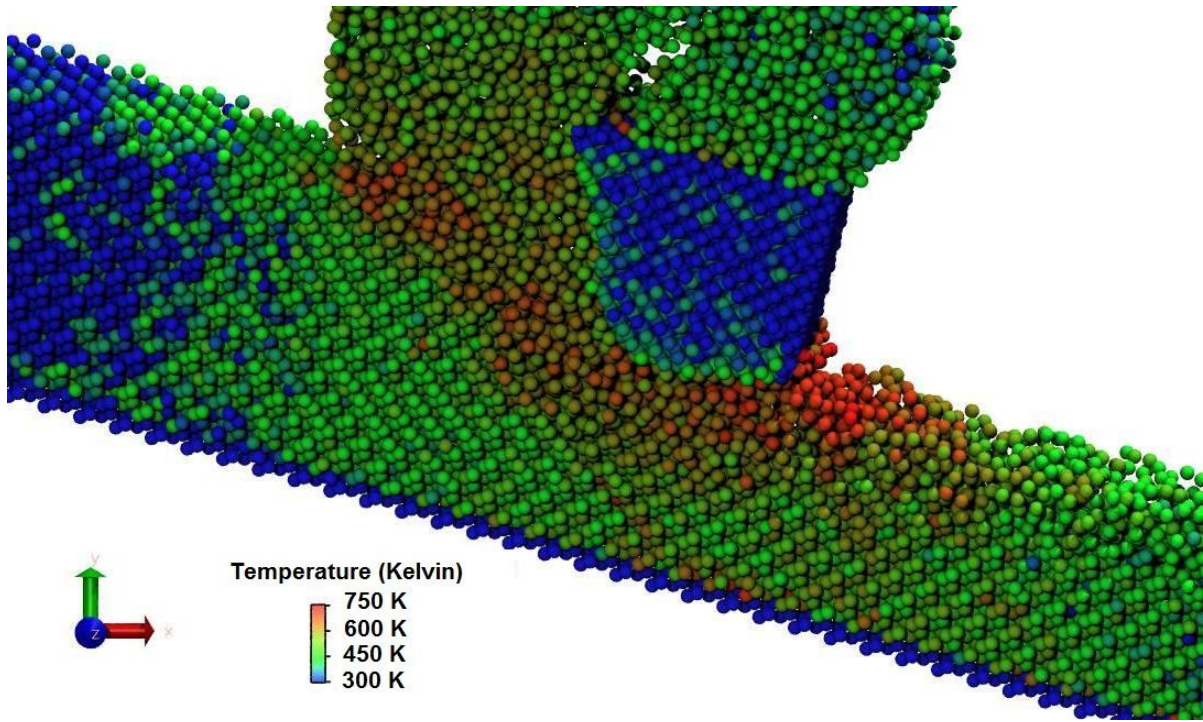


Figure 28: Temperature distribution on atoms during SPDT of silicon [140]

Furthermore, figure 28 also shows that the maximum temperature on the cutting edge of the tool tip was only about 380 K. On the other hand, the maximum temperature in the workpiece was observed at the primary shear zone and on the finished surface approaching 750 K at a (high) cutting speed of 100 m/s. Considering the fact that the local temperature was well below 959 K, even at such a high cutting speed, the authors asserted that the formation of silicon carbide will proceed via a single phase solid state chemical reaction between dangling bonds or nascent surfaces of silicon and carbon. This finding is aligned with that of Pastewka et al. [145], who asserted that wear of diamond during its polishing (in a similar way) is governed by the tribochemistry of carbon. *Ibid.* conducted MD simulation of polishing of a diamond crystallite with another diamond crystallite at a sliding speed of 20 m/s, and concluded that tribochemistry plays a significant role in governing the wear rate of diamond, as shown in figure 29.

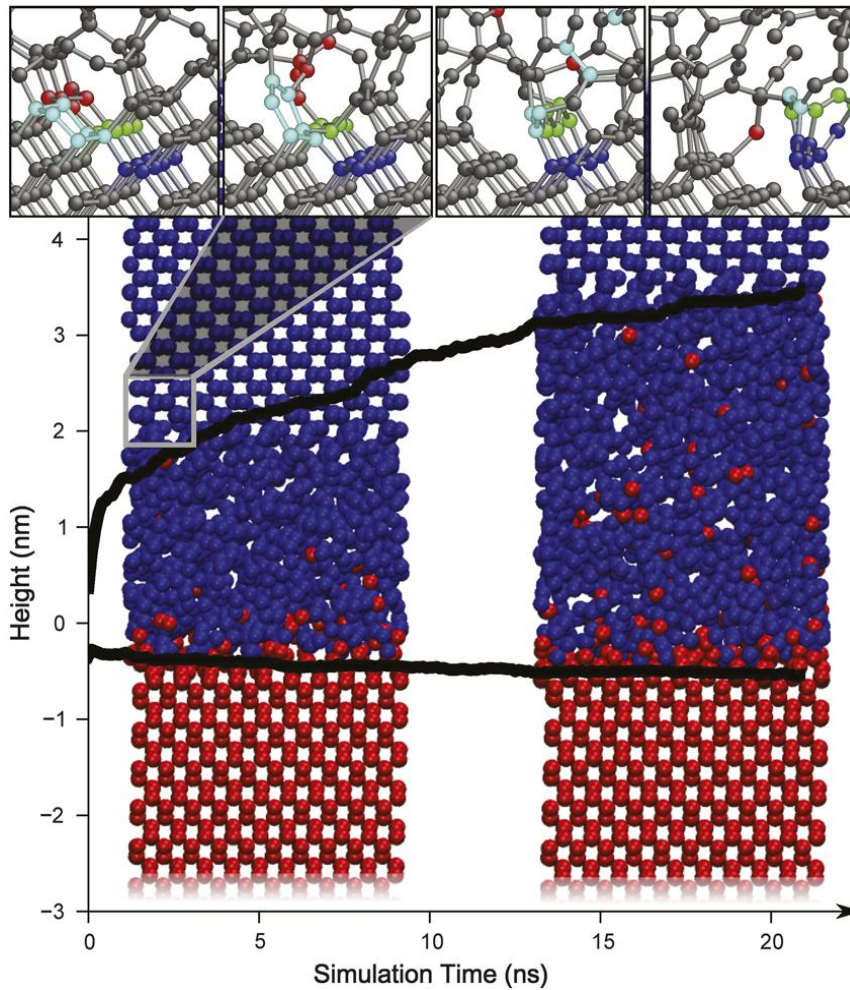


Figure 29: Sliding of diamond over another diamond at 20 m/s [201]

Various colours used in figure 29 indicate whether the atom was initially bound to the top or bottom crystallite of the diamond, while the upper black line shows the evolution of an amorphous interface of carbon atoms during the polishing process. Correlating these two processes, the authors proposed that similar to a diamond polishing process, a layer of “pilot” atoms that move around on the ordered phase repeatedly attracts the crystalline surface atoms [145]. Since the amorphization of the “pilot” atoms changes over time, the plucking forces also change. A surface atom is lifted into the amorphous phase when the pulling force becomes larger than the cohesive force holding the carbon atom into the diamond crystallite. This layer is subsequently removed by the ambient oxygen [202]. This phenomenon is similar to the plucking of surface atoms from the diamond tool to form a thin film of SiC on silicon during machining. Jasinevicius et al. [31] reported the formation of an amorphous layer to a depth of 340 nm on the machined surface of silicon. They found that the

micro-hardness of the diamond-turned silicon was lower than that of the pristine silicon, which was attributed to the presence of the amorphous layer. Mechanical machining on silicon generally introduces a barrier layer, known as a Beilby layer (tribomaterial), which exhibits a different refractive index from that of the substrate [15], as shown schematically in figure 30. Thus, SiC can either be formed in the cutting chips or as a thin film on the surface of the diamond tool. In either of these cases, it will result in the formation of vacant sites on the diamond tool, which were earlier identified as groove wear [186]. Furthermore, the freshly formed SiC film will scrape off during continuous frictional and abrasive contact during SPDT of silicon.

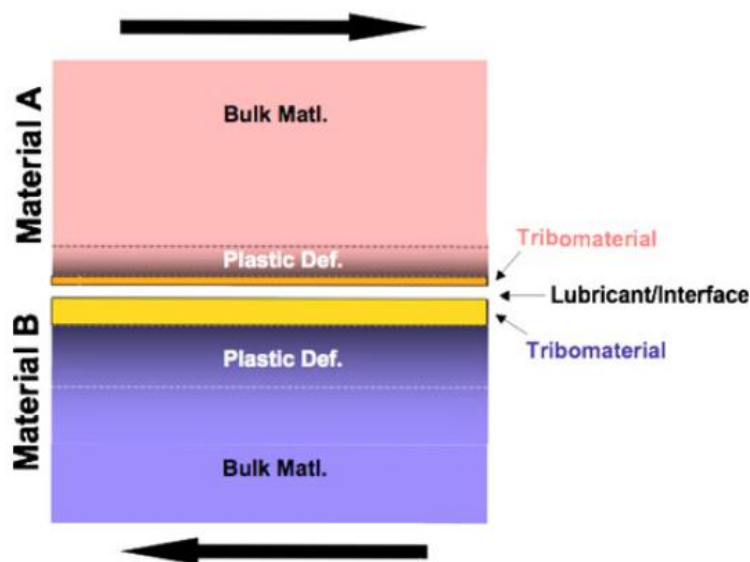


Figure 30: Schematic of a simple system consisting of a harder material ‘A’ sliding on a softer material ‘B’. Near the sliding interface, a Beilby layer of tribomaterial develops [203]

During a nano-scale ductile cutting of brittle materials, the undeformed chip thickness varies from zero at the centre of the tool tip to a maximum value at the top of the uncut shoulder. Thus, a “zero-cutting zone” exists within which no chips are produced. In this zone, the tool acts more like a roller than a cutter and continuously slides on and burnishes the machined surface. A schematic diagram of this is shown in figure 31 [146].

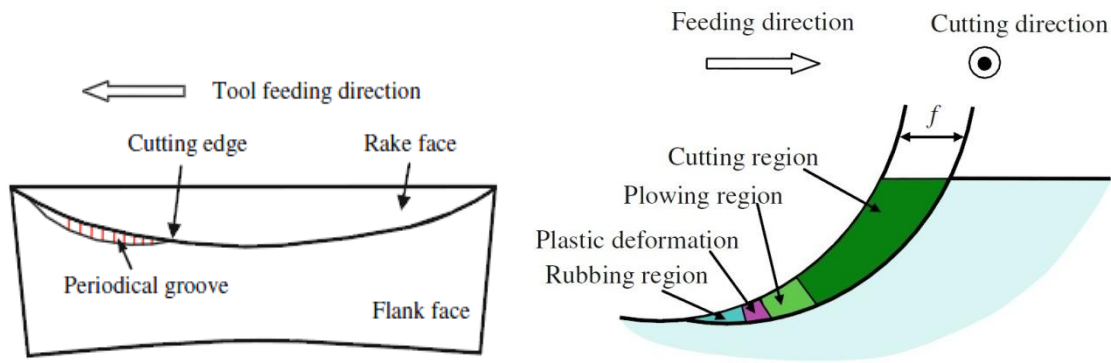
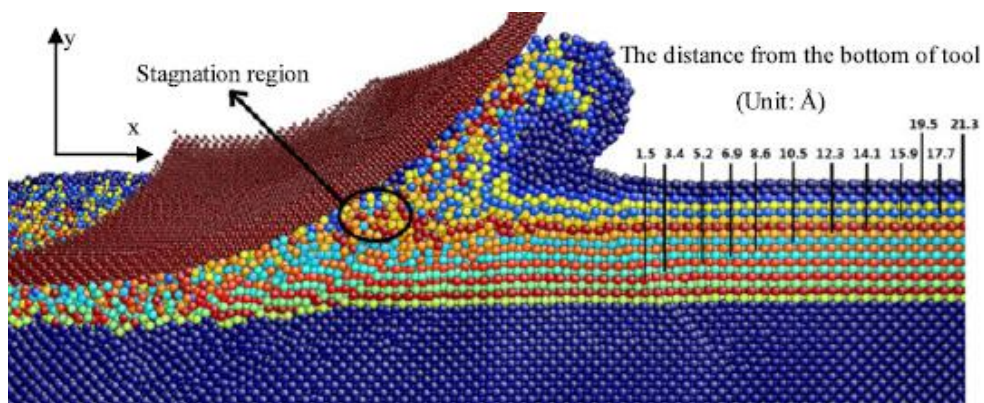
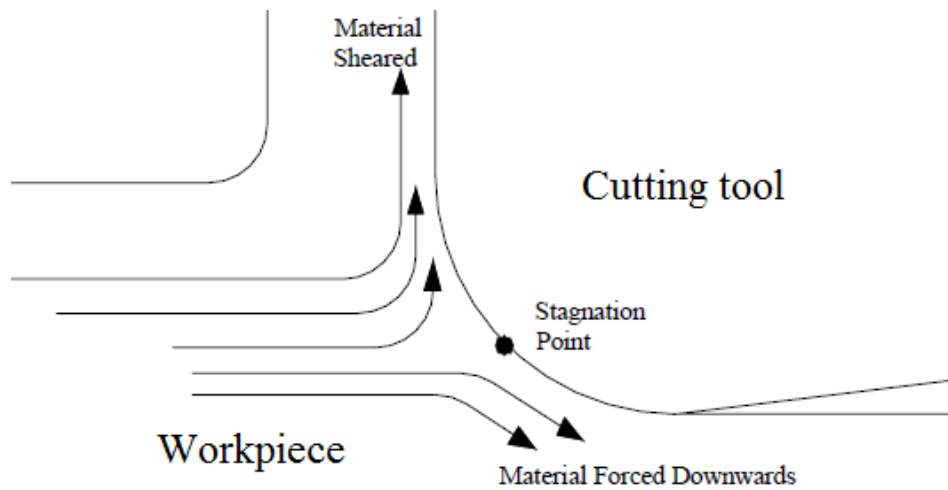


Figure 31: Schematic of the groove wear [204]

Figure 31 shows that the cutting edge of the tool continues to recede, and the flank wear region becomes predominant. This may be represented and understood as a kind of stagnation, as shown in figure 32, showing a point on the cutting edge radius where the tangential velocity of the workpiece becomes zero [205]. Notably, below the stagnation point, the material is compressed downwards in the wake of the tool. Above the stagnation point, shear of the material is more pronounced than compression. Consequently, the sheared material is carried away as cutting chips. This supplement the findings of Woon *et al.* [206] who adapted an arbitrary Lagrangian-Eulerian FEM approach to simulate micromachining of AISI 1045 steel over a wide range of undeformed chip thickness (2 to 20 microns). Their findings suggest that irrespective of the magnitude of the simulated undeformed chip thickness, the stagnation phenomenon is insensitive.



(a) MD model [76]



(b) Schematic model

Figure 32: Stagnation point on the cutting tool during SPDT

Flank wear causes a reduction in the clearance angle, which gives rise to an increased friction resistance. This is the reason for a relatively high temperature at the tool flank compared with the rake face – a phenomenon that contrasts conventional machining where the tool rake face is at a higher temperature than the tool flank face. This occurs because of the large amount of energy released from the cutting chips and the consequent heat dissipated into the tool rake face. In contrast, during SPDT, the effect of frictional heat between the tool flank face and the finished surface of the workpiece is more than that on the tool rake face. Due to the high temperature on the flank face, the chemical kinetics between silicon and carbon atoms becomes more favourable at the flank face than at the rake face. Subsequently, abrasion due to continuous friction contact with the flank face further enhances the wear rate, making the ratio of rake wear to flank wear minimal. The plucking of surface atoms from the diamond tool and subsequent abrasion between a thin layer of SiC and the cutting tool gives rise to associated  $sp^3$ - $sp^2$  disorder on the diamond tool, and both were suggested to proceed in tandem [134, 140].

While the above reported MD simulations used a high cutting speed in contrast to the experimental operations which use very low cutting speeds, yet the outcome of the process (i.e. the formation of SiC and  $sp^2$  carbon) will remain unaltered because mechanochemistry of the process appears to be

the same in both the cases [207], although the process kinetics is still a subject for further research. Experimental studies (using X-Ray photoelectron spectroscopy) report a mixture of SiC and carbon like particles on a silicon wafer during the nanometric cutting process [15, 208] confirmed this MD simulation investigation. Overall, research on the mechanism of wear of diamond cutting tools in general is still a growing area which might help to realize several other phases of carbon.

## **6. Future Research Opportunities in MD simulation of nanometric cutting**

The review of current literature provides opportunities for new commercial, technological and scientific developments in the area of silicon manufacturing, some of which are outlined in the following.

### *6.1. Development of enhanced MD software*

Currently available MD packages are not dedicated to study nanoscale machining since MD requires a great deal of computational power. This is probably the main reason why commercialization of MD tools for the manufacturing of brittle materials has not happened yet. Commercial software designed to simulate engineering materials such as glass, quartz, tungsten carbide and boron carbide could be developed using the information provided in this review. Such a development could include the provision of much more flexibility in the size and shape of the workpiece and the cutting tool. The software could be made user-friendly, which would permit the simulation of other important cutting tool materials, such as steel, CBN, graphene and  $C_3N_4$  [209].

### *6.2. Development of Potential energy functions*

Although there have been many refinements in the development of bond order potential functions, a common limitation of all these potential functions is that they are short ranged and only represent ductile behaviour rather than the brittle behaviour of materials like silicon and diamond. Consequently, the study of mechanisms of fracture, wear, and plasticity is somewhat constrained by these potential functions. Pastewka et al. [201] highlight some important considerations needed to use a potential energy function to model the phenomena of fracture, wear or plasticity in materials such as silicon, carbon and silicon carbide. Despite a number of potential functions proposed to

describe carbon, there is still a need to have a robust potential function that can accurately describe all of the binary and tertiary phases of carbon at lower computational expense. This will help in an improved understanding of the tool wear.

One of the main drawbacks of MD simulation may be related to the short time and length scales. In other words, the short range bond order potentials do not provide or address the phenomenological understanding of the brittle-ductile transition observed during realistic machining experiments. The development of better potential functions is also lacking on the material front. Steel is perhaps the most important material in the infrastructure domain and is important even for engineering studies; however, despite recent developments [210-211], there is lack of a robust potential function to enable a simulation of nanometric cutting of steel, especially nitrided steels or of German silver (an alloy of copper-nickel-zinc). Furthermore, since diamond cannot anyways be used efficiently to cut soft iron or steel [194, 212-213], there is a need to develop a potential function of cubic boron nitride (CBN), which is a commercial material used to manufacture steel. Development of such potential functions will aid in the improvement of manufacturing processes.

### *6.3. Opportunities for improving diamond machining*

The literature reviewed above reaffirms that a diamond tool may undergo catastrophic wear during machining of hard, brittle materials such as silicon. This opens up the possibility for development of alternative methods that can improve the diamond machining process and thus help achieve more efficient manufacturing of silicon. Micro-laser assisted machining ( $\mu$ -LAM) [214] is one such process, where workpiece is preferentially heated and thermally softened at the tool-workpiece interface, using laser devices, in order to improve the machinability of the workpiece. While this approach has shown promise [215-216], certain limitations have impeded the commercial realization of  $\mu$ -LAM. Such limitations include the lack of direct control on laser power (which can cause premature degradation, accelerated dissolution-diffusion and adhesion wear of the tool tip).

Recently, a new method for the machining of hard material, known as the surface defect machining (SDM) method has been proposed in an attempt to reduce the cutting resistance of the workpiece

[217-218] but has only been tested on hard steels yet. This method has been acknowledged and appreciated by researchers in the field [219]. The central idea of the SDM method is to generate surface defects on top of the workpiece in the form of a series of holes prior to the execution of actual machining operation. Such defects can be generated by a secondary operation, such as laser ablation prior to the machining. The presence of these defects on the uncut chip thickness area reduces the bonding strength of the workpiece atoms, which consequently lowers the cutting resistance during machining. Other methods for improving the tribological response of the workpiece, such as making it more amenable to diamond machining, have also been suggested. These are summarized in Table XIII. Such improvements helped to increase tool life and improve the surface finish of the product.

Table XIII: Modified form of measures suggested for improved machinability[220]

| S.No.                                   | Theoretical approach   | Experimental realization  |
|---|--|---|
| <b>Modification of the Process</b>      |  |   |
| 1                                       | Reduction of chemical reaction rate between diamond cutting tool and workpiece | Cryogenic turning [221]   |
| 2                                       | Inhibition of chemical reactions   | Use of Inert Gas atmospheres [222]  |
| 3                                       | Reduction of contact time between tool and workpiece                           | Vibration assisted cutting [223-225]  |
| 4                                       | Lowering of temperature rise and chemical contact                              | Usage of appropriate coolant [226-227]  |
| 5                                       | Rotary Cutting   | Tool swinging method [228]  |
| 6                                       | Cutting point swivel machining   | Swivel motion of the tool [229]   |
| <b>Modification of the cutting tool</b> |  |   |
| 7                                       | Building a diffusion barrier on cutting tool                                   | Use of protective coatings [230]  |
| 8                                       | Modification of diamond lattice  | Ion implantation [10]   |
| 9                                       | By modifying the cutting tool geometry   | Use of straight nose cutting tools [37]<br>Providing nanogrooves on the cutting tool [231-232]. |
| 10                                      | Use of alternative cutting tool material                                       | Using CBN instead of diamond [233-234]  |
| <b>Workpiece modification</b>           |  |   |
| 11                                      | Surface layer modification of the workpiece prior to cutting                   | Ion implantation [235-236]  |
| 12                                      | Post-machining Laser recovery  | Nanosecond-pulsed laser irradiation recovery of the machined silicon surface [237]              |
| 13                                      | Thermal softening of the workpiece during the cutting process                  | $\mu$ -LAM ‡(Their novelty was that unlike other  |

‡ The developers of this method have formed their spin-out company (<http://www.microlamtechnologies.com/>)

|  |  |  |
|--|--|--|
|  |  | <p>techniques, they used the laser to supply external heat through a transparent diamond to the pressurized material).</p> |
|--|--|--|

Newer developments in this area are minimal. Suggestions related to machinability, using MD simulation is an area for further research. Liang *et al.* [238] used MD simulation to demonstrate the mechanism of elliptical vibration. This method is useful to machine materials that are chemically more affinitive towards diamond cutting tool. They found that tool displacement in the cutting direction has a more pronounced effect on the cutting forces rather than the thrust forces. Another effort was made by the inclusion of the focussed ion beam (FIB) machining method to understand and to manufacture the nanostructures on the cutting tools [239].

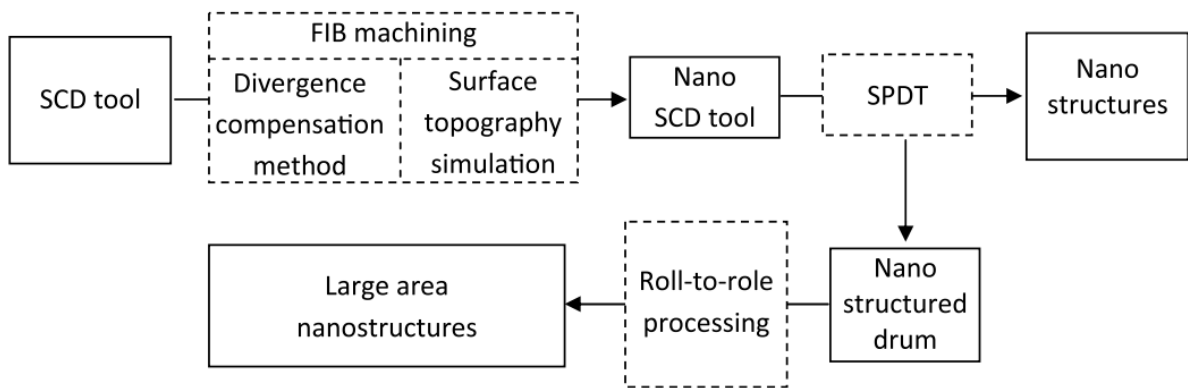


Figure 33: Block diagram of proposed nanofabrication of diamond cutting tools using FIB [239]

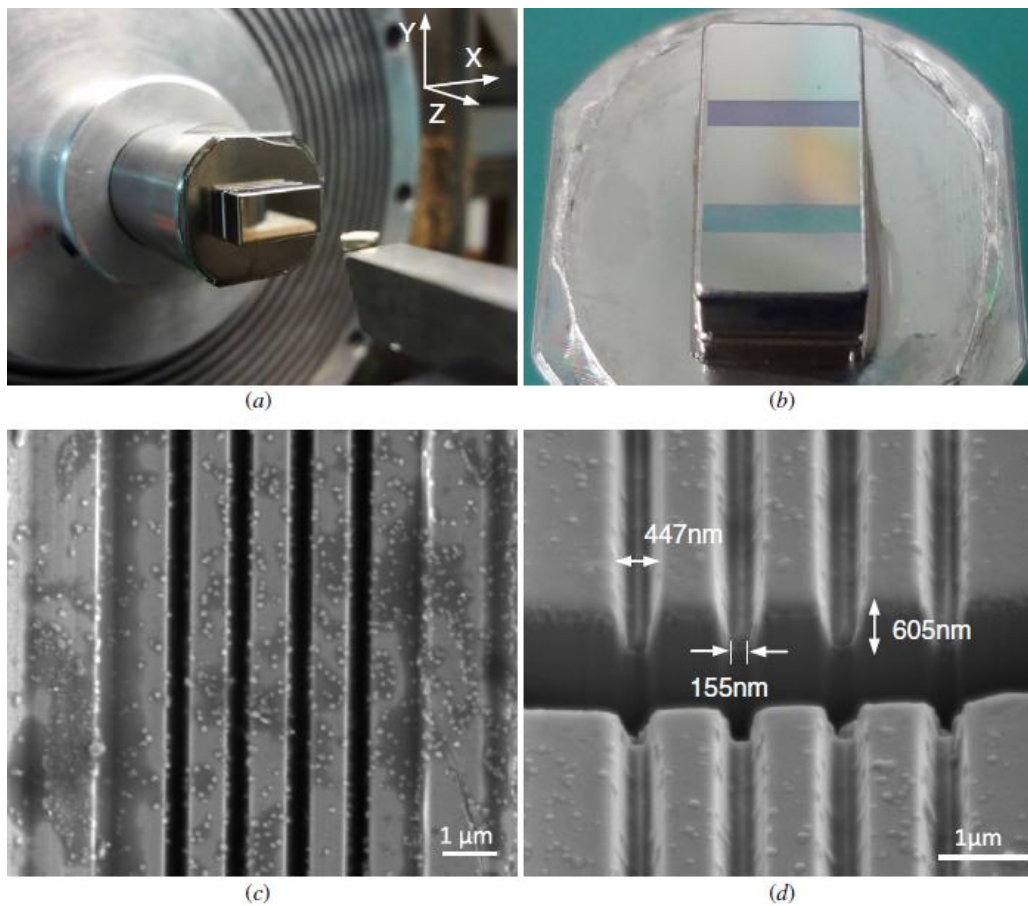


Figure 34: Nanograting array produced by FIB processed nanoscale single crystal diamond tools using diamond machining [239]

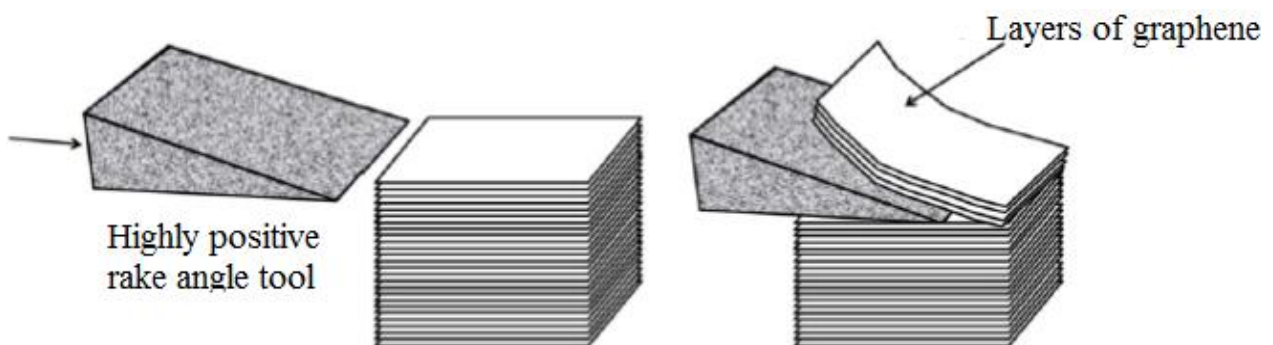


Figure 35: Schematic diagram of graphene production using diamond machining

The approach of using FIB in conjunction with diamond machining was directed at obtaining very fine textured nanogrooves on the substrate in fine precision of few microns (figure 33 and figure 34). This is an example of a complimentary evolution of simulation and experiments to improve the manufacturing processes. Another such example is a recently reported MD simulation study that revealed how diamond machining can be used to produce few-layer graphene by separation, folding

and shearing of the material (figure 35) using a highly positive rake angle diamond cutting tool [240]. These studies are preliminary in nature, and therefore more research is required. Over time, lack of a solid theoretical understanding has resulted in several anomalies and developments of misnomers. The convention for current flow from plus to minus instead of from minus to plus was a consequence of the fact that experiment preceded understanding. However, when that happened there were not many fundamental simulation tools available to the scientists as powerful as the molecular dynamics simulation [241-242] and thus such a situation can be avoided.

#### *6.4. Study of effect of coolants and coatings*

Danyluk and Reaves [243] compared the performance of water, absolute ethanol and acetone on the abrasion performance of the (100) orientation of silicon. They suggested that acetone across all of them performed superior in promoting ductility in silicon. In yet another experimental study on SPDT of silicon [72], water-based machining coolant (Fluid 'A') was found to prolong the tool life over oil-based machining coolant (Fluid 'B') by an extent of 300%. Thus, coolants can be seen to have a significant influence on the process of SPDT of silicon. The presence of a coolant certainly influences the tribo-chemistry of the diamond tool and studying its effect will help develop an understanding of the appropriate measures for the mitigation of tool wear. For example, a cryogenic environment is already known to improve tool life. A current investigation of these processes, conducted by Rentsch et al. [92], studied the influence of cutting fluid using MD simulation. They considered a hypothetical cutting fluid around a copper block, and modelled it using a Lennard-Jones interaction potential energy function. A snapshot from their work is shown in figure 36, where the effect of coolant on the chip generation process is demonstrated.

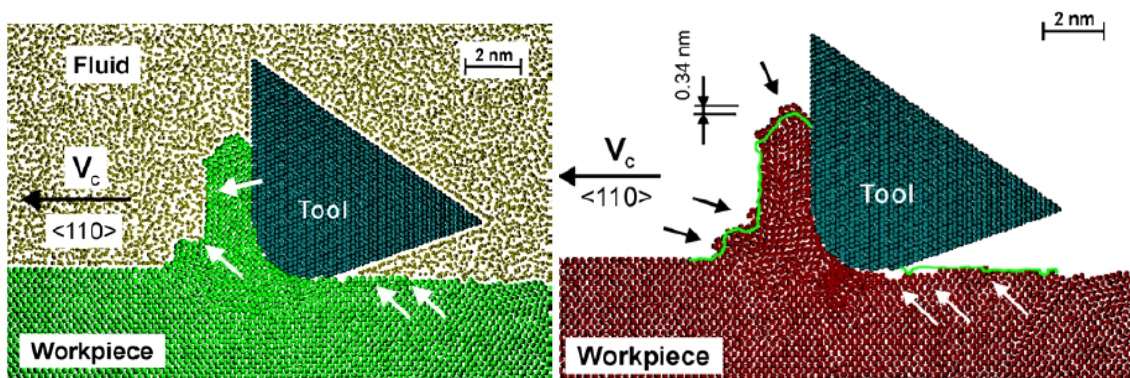


Figure 36: MD simulation of nanometric cutting of copper involving coolant [244]

The authors explained that the stress distribution in the workpiece remained unchanged irrespective of the cutting environment, while the temperature distribution in the machining zone changed, albeit, only in the area of local contact between the tool and workpiece. Future research on studying the nanometric cutting mechanisms using MD simulations may include the presence of oxygen, liquid nitrogen or water.

## 7. Concluding remarks

This review establishes that MD simulations have made and continue to make significant contributions to the understanding of several aspects of material science. These aspects are often complicated by the implementation of manufacturing technology itself. The quest to explore the manufacturing of brittle materials has led to the emergence of a new discipline of study, now known as high-pressure surface science. This discipline integrates disparate disciplines, such as chemistry, materials science, nanotechnology, physics and mechanical engineering. Brinksmeier and Preuss [10] noted that mechanical engineers previously relied on a knowledge of classical mechanics, electrostatics and thermodynamics. It became evident that all of the mechanical, chemical and electronic properties of matter are governed by the atomic motions and could be better understood through quantum mechanics, it was not absolute necessary for working engineers to understand quantum physics because they were not dealing with individual atoms but with clusters. Now with the emergence of ultra-precision machining methods, such as diamond machining, this course of study is changing. In particular, the advantage of modelling needs to come into practice to lead to

the proof of concept experimental trials. In the upcoming years, MD simulation is thus expected to contribute significantly to the field of diamond machining. Central to this success is the continuing effort to develop more accurate potential energy functions, which would help to better describe the nature of chemical bonding. These developments are adding newer horizons to obtain unprecedented accuracy from the MD simulations. It appears that similar to the descriptions of manufacturing accuracy, a potential energy function will soon be described by its tolerances or the margin by which it is accurate in predicting the outcome of an engineering event. Success was achieved as an outcome of the above developments by studying and mimicking simple materials; however, more work is required to study real-world materials. In particular, the realm of voids (volume), dislocations (point or line) and grain boundaries has yet to be modelled during construction of the geometry itself. This will help to enhance and reveal more than what is now known. The world of MD simulations is dependent on present day computers. This presents a limitation in that real-world scale simulation models are yet to be developed. The simulated length and timescales are far shorter than the experimental ones. Also, simulations of nanometric cutting are typically done in the speeds range of a few hundreds of m/sec against the experimental speed of typically about 1 m/sec. Consequently, MD simulations suffer from the spurious effects of high cutting speeds and the accuracy of the simulation results has yet to be fully explored. The development of user-friendly software could help facilitate molecular dynamics as an integral part of computer-aided design and manufacturing to tackle a range of machining problems from all perspectives, including materials science (phase of the material formed due to the sub-surface deformation layer), electronics and optics (properties of the finished machined surface due to the metallurgical transformation in comparison to the bulk material), and mechanical engineering (extent of residual stresses in the machined component).

Overall, this review provided key information concerning nanometric cutting of silicon, which is summarized as follows:

- I. MD simulations have shown that during nanomachining, silicon undergoes a Herzfeld-Mott

transition due to the high pressure phase transformation (HPPT) which leads to the transition of pristine Si-I (Brittle) silicon to Si-II (ductile) metallic form of silicon in the cutting zone typically in a span of approximately 50 picoseconds. The mechanism of HPPT of silicon is inevitable irrespective of the fact whether the cutting tool or the workpiece is a single crystal or a polycrystalline material. However, aside from HPPT, nanotwinning that stops at Shockley partial has also been reported to occur along the  $\langle 110 \rangle$  direction during machining of silicon.

- II. MD simulations have shown that the HPPT of silicon causes metallisation of silicon in the form of the Si-II phase, which is a metastable phase (approximately 22% reduction in atomic volume). This phase persists only when the cutting tool is able to retain sufficient amounts of stress. That is, while the cutting tool passes the machining area, the pressure developed by the cutting tool is released. Consequently, the Si-II phase transforms to an amorphous phase of silicon, which causes an expansion of the atomic volume. As a result, this causes elastic recovery of the finished machined surface. This suggests that a deterministic and finite precision surface finish can only be attained by controlling this contraction-expansion mechanism that happens due to the HPPT of silicon.
- III. MD simulations have shown that both silicon and diamond are highly anisotropic and this anisotropy is particularly important to control the machining process. While the use of a diamond in a cubic or a dodecahedral orientation is governed by a consideration of the geometry of the cutting tool, silicon provides a superior quality of the machined surface finish while being cut in the  $\langle 1-10 \rangle$  cutting direction on the (111) orientation. This is, therefore, the recommended crystal setup for manufacturing silicon.
- IV. Wear of a diamond tool has been one of the major impediments for consistent machining of silicon, especially for a sufficiently large piece for which replacing the tool midway through machining would induce many surface errors. MD simulations reveal that tribochemistry (formation of silicon carbide) through a solid state single phase reaction up to a cutting

temperature of 959 K in tandem with  $sp^3$ - $sp^2$  disorder of diamond is the basic wear mechanism of diamond tools against silicon during the SPDT process. This finding is consistent with the experimental results. Also, unlike conventional machining where tool rake wear is significantly higher than the flank wear, quite often a relatively high amount of tool flank wear is noticed in comparison to the tool rake wear during nanomachining of silicon. Recent MD simulations have shown that the increased frictional contact and abrasion between the tool flank face and the machined surface was the primary reason for higher temperatures at the flank face than that at the rake face. This promotes both the formation of SiC and abrasion, which explains observations of the relatively high flank wear compared to rake wear during SPDT of silicon.

#### **Acknowledgments:**

The first author acknowledges the funding support from the International Research Fellowship account of Queen's University, Belfast and an additional funding from an EPSRC research grant (Ref: EP/K018345/1). The authors would like to thank Dr. Alexander Stukowski (Darmstadt University of Technology, Germany) and Dr. Jining Sun (Heriot-Watt University) for their suggestions.

#### **References:**

1. Brinksmeier, E. and O. Riemer, *Measurement of optical surfaces generated by diamond turning*. International Journal of Machine Tools and Manufacture, 1998. **38**(5–6): p. 699-705.
2. Taniguchi, N. *On the basic concept of 'nano-technology'*. in *Proceedings of Production Engineering, Part -II, Japan Society of Precision Engineering*. 1974. Tokyo, Japan.
3. Taniguchi, N., *Current Status in, and Future Trends of, Ultraprecision Machining and Ultrafine Materials Processing*. CIRP Annals - Manufacturing Technology, 1983. **32**(2): p. 573-582.
4. Shore, P. and P. Morantz, *Ultra-precision: enabling our future*. Philosophical Transactions of the Royal Society A: Mathematical, Physical and Engineering Sciences, 2012. **370**(1973): p. 3993-4014.
5. Luo, X., S. Goel, and R.L. Reuben, *A quantitative assessment of nanometric machinability of major polytypes of single crystal silicon carbide*. Journal of the European Ceramic Society, 2012. **32**(12): p. 3423-3434.
6. Liu, X., R.E. DeVor, S.G. Kapoor, and K.F. Ehmann, *The Mechanics of Machining at the Microscale: Assessment of the Current State of the Science*. Journal of Manufacturing

- Science and Engineering, 2004. **126**(4): p. 666-678.
7. Yu, D.P., Y.S. Wong, and G.S. Hong, *A novel method for determination of the subsurface damage depth in diamond turning of brittle materials*. International Journal of Machine Tools and Manufacture, 2011. **51**(12): p. 918-927.
  8. Jain, V.K., *Magnetic field assisted abrasive based micro-/nano-finishing*. Journal of Materials Processing Technology, 2009. **209**(20): p. 6022-6038.
  9. Jain, N.K. and V.K. Jain, *Modeling of material removal in mechanical type advanced machining processes: a state-of-art review*. International Journal of Machine Tools and Manufacture, 2001. **41**(11): p. 1573-1635.
  10. Brinksmeier, E. and W. Preuss, *Micro-machining*. Philosophical Transactions of the Royal Society A: Mathematical, Physical and Engineering Sciences, 2012. **370**(1973): p. 3973-3992.
  11. Ezugwu, E.O., *Key improvements in the machining of difficult-to-cut aerospace superalloys*. International Journal of Machine Tools and Manufacture, 2005. **45**(12–13): p. 1353-1367.
  12. Cai, M.B., X.P. Li, M. Rahman, and A.A.O. Tay, *Crack initiation in relation to the tool edge radius and cutting conditions in nanoscale cutting of silicon*. International Journal of Machine Tools and Manufacture, 2007. **47**(3-4): p. 562-569.
  13. Seagal, M., *Learning from silicon*. Nature, 2012. **483**: p. S43-S44.
  14. Suresh, P., P. Venkateswara Rao, and S. Deshmukh, *A genetic algorithmic approach for optimization of surface roughness prediction model*. International Journal of Machine Tools and Manufacture, 2002. **42**(6): p. 675-680.
  15. Puttick, K.E., L.C. Whitmore, P. Zhdan, A.E. Gee, and C.L. Chao, *Energy scaling transitions in machining of silicon by diamond*. Tribology International, 1995. **28**(6): p. 349-355.
  16. Kovalchenko, A., Y. Gogotsi, V. Domnich, and A. Erdemir, *Phase Transformations in Silicon Under Dry and Lubricated Sliding*. Tribology Transactions, 2002. **45**(3): p. 372-380.
  17. Blake, P.N., *PhD Thesis on Ductile-regime diamond turning of germanium and silicon*. 1988, North Carolina State University, USA.
  18. Bifano, Dow, and Scattergood, *Ductile-Regime Grinding: A New Technology for Machining Brittle Materials*. Journal of Engineering for Industry, 1991. **113**(184).
  19. Scattergood, R.O., Blake, N., *Ductile-regime machining of germanium and silicon*. Journal of the American ceramic society, 1990. **73**(4): p. 949-957.
  20. Blackley, W.S. and R.O. Scattergood, *Ductile-regime machining model for diamond turning of brittle materials*. Precision Engineering, 1991. **13**(2): p. 95-103.
  21. Ravindra, D., *Ductile mode material removal of ceramics and semiconductors*, in *Department of Mechanical and Aeronautical Engineering*. 2011, Western Michigan University: Michigan. p. 312.
  22. Morris, J.C., D.L. Callahan, J. Kulik, J.A. Patten, and R.O. Scattergood, *Origins of the Ductile Regime in Single-Point Diamond Turning of Semiconductors*. Journal of the American Ceramic Society, 1995. **78**(8): p. 2015-2020.
  23. Mylvaganam, K. and L.C. Zhang, *Nanotwinning in monocrystalline silicon upon nanoscratching*. Scripta Materialia, 2011. **65**(3): p. 214-216.
  24. Goel, S., *PhD thesis, An atomistic investigation on the nanometric cutting mechanism of hard, brittle materials*, in *Mechanical Engineering*. 2013, Heriot-Watt University: Edinburgh. p. 1-246.
  25. King, R.F. and D. Tabor, *The Strength Properties and Frictional Behavior of Brittle Solids*, in *Series A: Mathematical and Physical Science*. 1954, Proceedings of the Royal Society of London. p. 225-238.
  26. Bridgman, P.W. and I. Simon, *Effects of Very High Pressures on Glass*. Journal of Applied Physics, 1953. **24**(4): p. 405-413.
  27. Lawn, B. and R. Wilshaw, *Indentation fracture: principles and applications*. Journal of Materials Science, 1975. **10**(6): p. 1049-1081.

28. Lawn, B.R. and D.B. Marshall, *Hardness, Toughness, and Brittleness: An Indentation Analysis*. Journal of the American Ceramic Society, 1979. **62**(7-8): p. 347-350.
29. Wang, M., W. Wang, and Z. Lu, *Anisotropy of machined surfaces involved in the ultra-precision turning of single-crystal silicon—a simulation and experimental study*. The International Journal of Advanced Manufacturing Technology, 2012. **60**(5): p. 473-485.
30. Marshall, D.B. and L. B.R., *Indentation of Brittle Materials*. Microindentation Technology in Materials Science and Engineering. Vol. 889. 1986: ASTM STP.
31. Jasinevicius, R.G., J.G. Duduch, L. Montanari, and P.S. Pizani, *Dependence of brittle-to-ductile transition on crystallographic direction in diamond turning of single-crystal silicon*. Proceedings of the Institution of Mechanical Engineers, Part B: Journal of Engineering Manufacture, 2011.
32. Kovalchenko, A. and Y.V. Milman, *On the cracks self-healing mechanism at ductile mode cutting of silicon*. Tribology International, 2014.
33. Kulshreshtha, P.K., K.M. Youssef, and G. Rozgonyi, *Nano-indentation: A tool to investigate crack propagation related phase transitions in PV silicon*. Solar Energy Materials and Solar Cells, 2012. **96**(0): p. 166-172.
34. Arif, M., Z. Xinquan, M. Rahman, and S. Kumar, *A predictive model of the critical undeformed chip thickness for ductile–brittle transition in nano-machining of brittle materials*. International Journal of Machine Tools and Manufacture, 2013. **64**(0): p. 114-122.
35. Nakasuji, T., S. Kodera, S. Hara, H. Matsunaga, N. Ikawa, and S. Shimada, *Diamond Turning of Brittle Materials for Optical Components*. CIRP Annals - Manufacturing Technology, 1990. **39**(1): p. 89-92.
36. Inamura, T., N. Takezawa, Y. Kumaki, and T. Sata, *On a Possible Mechanism of Shear Deformation in Nanoscale Cutting*. CIRP Annals - Manufacturing Technology, 1994. **43**(1): p. 47-50.
37. Yan, J., Syoji, Katsuo, Kuriyagawa, Tsunemoto, Suzuki, Hirofumi, *Ductile regime turning at large tool feed*. Journal of Materials Processing Technology, 2002. **121**(2-3): p. 363-372.
38. Gilman, J.J., *Insulator-metal transitions at microindentations*. Journal of Materials Research, 1992. **7**: p. 535-538.
39. Gilman, J.J. *Metallization at Microindentations*. in *MRS Spring Meeting*. 1992: Cambridge University Press.
40. Gilman, J.J., *Mechanism of shear-induced metallization*. Czechoslovak Journal of Physics, 1995. **45**(11): p. 913-919.
41. Goel, S., X. Luo, and R.L. Reuben, *Shear instability of nanocrystalline silicon carbide during nanometric cutting*. Applied Physics Letters, 2012. **100**(23): p. 231902.
42. Bouwelen Van, F.M., L.M. Brown, and J.E. Field, *A new view on the mechanism of diamond polishing*. Industrial diamond review, 1997. **57**(1): p. 21-25.
43. Arefin, S., X.P. Li, M.B. Cai, M. Rahman, K. Liu, and A. Tay, *The Effect of the Cutting Edge Radius on a Machined Surface in the Nanoscale Ductile Mode Cutting of Silicon Wafer*. Proceedings of the Institution of Mechanical Engineers, Part B: Journal of Engineering Manufacture, 2007. **221**(2): p. 213-220.
44. Cai, M.B., X.P. Li, and M. Rahman, *Study of the mechanism of nanoscale ductile mode cutting of silicon using molecular dynamics simulation*. International Journal of Machine Tools and Manufacture, 2007. **47**(1): p. 75-80.
45. Lucca, D.A., Y.W. Seo, and R.L. Rhorer, *Energy Dissipation and Tool-Workpiece Contact in Ultra-Precision Machining*. Tribology Transactions, 1994. **37**(3): p. 651-655.
46. Leung, T.P., W.B. Lee, and X.M. Lu, *Diamond turning of silicon substrates in ductile-regime*. Journal of Materials Processing Technology, 1998. **73**(1-3): p. 42-48.
47. Marsh, E.R., E.J. Sommer, T.R.S. Deakyne, G.A. Kim, and J.A. Simonson, *Detection of orientation-dependent, single-crystal diamond tool edge wear using cutting force sensors, while spin-turning silicon*. Precision Engineering, 2010. **34**(2): p. 253-258.
48. Shibata Y., F.S., Makino E. and Ikeda M., *Ductile-regime turning mechanism of single-*

- crystal silicon*. Precision Engineering, 1996. **18**: p. 129-137.
49. O'Connor, B.P., Marsh, E. R. and Couey, J. A., *On the effect of crystallographic orientation on ductile material removal in silicon*. Precision Engineering, 2005. **29**: p. 124-132.
  50. Born, D.K. and W.A. Goodman, *An empirical survey on the influence of machining parameters on tool wear in diamond turning of large single-crystal silicon optics*. Precision Engineering, 2001. **25**(4): p. 247-257.
  51. Ichida Y. *Ductile Mode Maching of Single Crystal Silicon Using a Single Point Diamond Tool*. in *Proceedings of the first International Conference and General Meeting of the European Society for Precision Engineering and Nanotechnology (EUSPEN)*. 1999. Bremen, Germany.
  52. Buzio, R., C. Boragno, F. Biscarini, F.B. De Mongeot, and U. Valbusa, *The contact mechanics of fractal surfaces*. Nature Materials, 2003. **2**(4): p. 233-236.
  53. Bex, P.A., *Diamond Turning Tools*, in *Industrial Diamond Review*. 1975. p. 11-18.
  54. Casey, M. and J. Wilks, *Some experiments to study turning tools using the scanning electron microscope*. International Journal of Machine Tool Design and Research, 1976. **16**(1): p. 13-22.
  55. H.H. Hurt and D.L. Decker, *Tribological considerations of the diamond single-point tool*. Proceedings of SPIE, Production Aspects of Single-point Machined Optics, 1986. **508**: p. 126-131.
  56. Ikawa, N., S. S., and M. H., *Technology of Diamond Tool for Ultraprecision Metal Cutting*, in *Bulletin: Japan Society of Precision Engineering*. 1987. p. 233-238.
  57. Yuan, Z.J., J.C. He, and Y.X. Yao, *The Optimum Crystal Plane of Natural Diamond Tool for Precision Machining*. CIRP Annals - Manufacturing Technology, 1992. **41**(1): p. 605-608.
  58. Oomen, J.M. and J. Eisses, *Wear of monocrystalline diamond tools during ultraprecision machining of nonferrous metals*. Precision Engineering, 1992. **14**(4): p. 206-218.
  59. Ikawa, N., S. Shimada, and H. Tsuwa, *Microfracture of Diamond as Fine Tool Material*. CIRP Annals - Manufacturing Technology, 1982. **31**(1): p. 71-74.
  60. Komanduri, R., N. Chandrasekaran, and L.M. Raff, *Molecular dynamics simulation of atomic-scale friction*. Physical Review B, 2000. **61**(20): p. 14007-14019.
  61. Lucca, D.A., Y.W. Seo, and R. Komanduri, *Effect of Tool Edge Geometry on Energy Dissipation in Ultraprecision Machining*. CIRP Annals - Manufacturing Technology, 1993. **42**(1): p. 83-86.
  62. Komanduri, R., N. Chandrasekaran, and L.M. Raff, *Effect of tool geometry in nanometric cutting: a molecular dynamics simulation approach*. Wear, 1998. **219**(1): p. 84-97.
  63. Komanduri, R., *Some aspects of machining with negative rake tools simulating grinding*. International Journal of Machine Tool Design and Research, 1971. **11**(3): p. 223-233.
  64. Astakhov, V.P., *Fundamentals of the Selection of Cutting Tool Geometry Parameters Geometry of Single-point Turning Tools and Drills*. 2010, Springer London. p. 127-204.
  65. Komanduri, R. and L. Raff, *A review on the molecular dynamics simulation of machining at the atomic scale*. Proceedings of the Institution of Mechanical Engineers, Part B: Journal of Engineering Manufacture, 2001. **215**(12): p. 1639-1672.
  66. Komanduri, R. and W.R. Reed Jr, *Evaluation of carbide grades and a new cutting geometry for machining titanium alloys*. Wear, 1983. **92**(1): p. 113-123.
  67. Biddut A.Q., Rahman M., Neo K.S., R. K.M.R., M. Sawa, and Y. Maeda, *Performance of single crystal diamond tools with different rake angles during micro-grooving on electroless nickel plated die materials*. International Journal of Advanced Manufacturing Technology, 2007. **33**(0): p. 891-899.
  68. Krulewich D., Syn C., Davis P., Zimmermann M., Blaedel K., Carr J., and Haack J., *An empirical survey on the influence of machining parameters on tool wear in diamond turning of large single crystal silicon optics - Paper prepared for submission to ASPE 14th Annual meeting at Monterey, CA*. 1999, Lawrence Livermore National Laboratory: Livermore, USA.

69. Samuels Leonard E., *The Mechanisms of Abrasive Machining*. Scientific American, 1978. **239**(5): p. 132.
70. Patten, J.A. and W. Gao, *Extreme negative rake angle technique for single point diamond nano-cutting of silicon*. Precision Engineering, 2001. **25**(2): p. 165-167.
71. Patten, J., W. Gao, and K. Yasuto, *Ductile Regime Nanomachining of Single-Crystal Silicon Carbide*. Journal of Manufacturing Science and Engineering, 2005. **127**(3): p. 522-532.
72. Durazo-Cardenas, I., P. Shore, X. Luo, T. Jacklin, S.A. Impey, and A. Cox, *3D characterisation of tool wear whilst diamond turning silicon*. Wear, 2007. **262**(3-4): p. 340-349.
73. Fang, F.Z. and V.C. Venkatesh, *Diamond Cutting of Silicon with Nanometric Finish*. CIRP Annals - Manufacturing Technology, 1998. **47**(1): p. 45-49.
74. Yan, J., T. Asami, H. Harada, and T. Kuriyagawa, *Crystallographic effect on subsurface damage formation in silicon microcutting*. CIRP Annals - Manufacturing Technology, 2012. **61**(1): p. 131-134.
75. Komanduri, R., Ch, N. rasekaran, and L.M. Raff, *Molecular dynamics simulation of the nanometric cutting of silicon*. Philosophical Magazine Part B, 2001. **81**(12): p. 1989 - 2019.
76. Lai, M., X.D. Zhang, and F.Z. Fang, *Study on critical rake angle in nanometric cutting*. Applied Physics A, 2012. **108**(4): p. 809-818.
77. Rapaport, D., *The Art of Molecular Dynamics Simulation*. 2004: Cambridge University Press.
78. Alder, B.J. and T.E. Wainwright, J. Chem. Phys., 1957. **1208**(27).
79. Gracie, R. and T. Belytschko, *An adaptive concurrent multiscale method for the dynamic simulation of dislocations*. International Journal for Numerical Methods in Engineering, 2011. **86**(4-5): p. 575-597.
80. Oskay, C. and J. Fish, *Fatigue life prediction using 2-scale temporal asymptotic homogenization*. International Journal for Numerical Methods in Engineering, 2004. **61**(3): p. 329-359.
81. Kerfriden, P., J.C. Passieux, and S.P.A. Bordas, *Local/global model order reduction strategy for the simulation of quasi-brittle fracture*. International Journal for Numerical Methods in Engineering, 2012. **89**(2): p. 154-179.
82. Psakhie, S.G., Y. Horie, S.Y. Korostelev, A.Y. Smolin, A.I. Dmitriev, E.V. Shilko, and S.V. Alekseev, *Method of movable cellular automata as a tool for simulation within the framework of mesomechanics*. Russian Physics Journal, 1995. **38**(11): p. 1157-1168.
83. Tan, Y., D. Yang, and Y. Sheng, *Discrete element method (DEM) modeling of fracture and damage in the machining process of polycrystalline SiC*. Journal of the European Ceramic Society, 2009. **29**(6): p. 1029-1037.
84. Pen, H.M., Y.C. Liang, X.C. Luo, Q.S. Bai, S. Goel, and J.M. Ritchie, *Multiscale simulation of nanometric cutting of single crystal copper and its experimental validation*. Computational Materials Science, 2011. **50**(12): p. 3431-3441.
85. Jiwang, Y., Z. Hongwei, and K. Tsunemoto, *Effects of tool edge radius on ductile machining of silicon: an investigation by FEM*. Semiconductor Science and Technology, 2009. **24**(7): p. 075018.
86. Patten, J. and J. Jacob, *Comparison between numerical simulations and experiments for single-point diamond turning of single-crystal silicon carbide*. Journal of Manufacturing Processes, 2008. **10**: p. 28-33.
87. Aly, M.F., E. Ng, S.C. Veldhuis, and M.A. Elbestawi, *Prediction of cutting forces in the micro-machining of silicon using a "hybrid molecular dynamic-finite element analysis" force model*. International Journal of Machine Tools and Manufacture, 2006. **46**(14): p. 1727-1739.
88. Belak, J.F. and I.F. Stowers, *A Molecular Dynamics model of Orthogonal Cutting process*. Proceedings of American Society Precision Engineering Annual conference, 1990: p. 76-79.
89. Ikawa, Naoya, Shimada, Shoichi, Tanaka, and Hiroaki, *Minimum thickness of cut in*

- micromachining*. Nanotechnology, 1992. **1**(3): p. 6-9.
90. Voter, A.F. and J.D. Kress. *Atomistic Simulation of Diamond-Tip Machining of Nanoscale Features*. in *Principles of Cutting Mechanics: Applications of Ultra-Precision Machining and Grinding, 1993 Spring Topical Meeting* 1993. Tucson, AZ, USA: ASPE Proceedings.
  91. Inamura, T., S. Shimada, N. Takezawa, and N. Nakahara, *Brittle/Ductile Transition Phenomena Observed in Computer Simulations of Machining Defect-Free Monocrystalline Silicon*. CIRP Annals - Manufacturing Technology, 1997. **46**(1): p. 31-34.
  92. Rentsch, R. *Influence of Crystal Orientation on the Nanometric Cutting Process*. in *Proceedings of the First International Euspen Conference*. 1999. Bremen, Germany,.
  93. James F. Belak, I.F.S., D.B.Boercker, *Simulation of Diamond turning of silicon surfaces*. Proceedings of 7th American Society Precision Engineering Annual conference, 1992: p. 76-79.
  94. Nozaki, T., M. Doyama, Y. Kogure, and T. Yokotsuka, *Micromachining of pure silicon by molecular dynamics*. Thin Solid Films, 1998. **334**(1-2): p. 221-224.
  95. Shimada, S., N. Ikawa, T. Inamura, N. Takezawa, H. Ohmori, and T. Sata, *Brittle-Ductile Transition Phenomena in Microindentation and Micromachining*. CIRP Annals - Manufacturing Technology, 1995. **44**(1): p. 523-526.
  96. Komanduri, R., N. Chandrasekaran, and L.M. Raff, *Molecular dynamics simulation of the nanometric cutting of silicon*. Philosophical Magazine Part B, 2001. **81**(12): p. 1989 - 2019.
  97. Zhang, L.C. and K. Mylvaganam, *Nano-Tribological Analysis by Molecular Dynamics Simulation - A Review*. Journal of Computational and Theoretical Nanoscience, 2006. **3**(2): p. 167-188.
  98. Kovalchenko, A., *Studies of the ductile mode of cutting brittle materials (A review)*. Journal of Superhard Materials, 2013. **35**(5): p. 259-276.
  99. Balamane, H., T. Halicioglu, and W.A. Tiller, *Comparative study of silicon empirical interatomic potentials*. Physical Review B, 1992. **46**(4): p. 2250-2279.
  100. Plimpton, S.J. and A.P. Thompson, *Computational aspects of many-body potentials (DOI:10.1557/mrs.2012.96)*. MRS Bulletin, 2012. **37**: p. 513-521.
  101. Daw, M.S. and M.I. Baskes, *Embedded-atom method: Derivation and application to impurities, surfaces, and other defects in metals*. Physical Review B, 1984. **29**(12): p. 6443-6453.
  102. Stillinger, F.H. and T.A. Weber, *Computer simulation of local order in condensed phases of silicon*. Physical Review B, 1985. **31**(8): p. 5262-5271.
  103. Stillinger, F.H. and T.A. Weber, *Erratum: Computer simulation of local order in condensed phases of silicon [Phys. Rev. B 31, 5262 (1985)]*. Physical Review B, 1986. **33**(2): p. 1451-1451.
  104. Berendsen, H.J.C., J.R. Grigera, and T.P. Straatsma, *The missing term in effective pair potentials*. The Journal of Physical Chemistry, 1987. **91**(24): p. 6269-6271.
  105. Tersoff, J., *New empirical approach for the structure and energy of covalent systems*. Physical Review B, 1988. **37**(12): p. 6991.
  106. Tersoff, J., *Empirical interatomic potential for silicon with improved elastic properties*. Physical Review B, 1988. **38**(14): p. 9902.
  107. Tersoff, J., *Modeling solid-state chemistry: Interatomic potentials for multicomponent systems*. Physical Review B, 1989. **39**(8): p. 5566.
  108. Tersoff, J., *Erratum: Modeling solid-state chemistry: Interatomic potentials for multicomponent systems*. Physical Review B, 1990. **41**(5): p. 3248.
  109. Tersoff, J., *Carbon defects and defect reactions in silicon*. Physical Review Letters, 1990. **64**(15): p. 1757.
  110. Tersoff, J., *Chemical order in amorphous silicon carbide*. Physical Review B, 1994. **49**(23): p. 16349.
  111. Agrawal, P.M., L.M. Raff, and R. Komanduri, *Monte Carlo simulations of void-nucleated melting of silicon via modification in the Tersoff potential parameters*. Physical Review B,

2005. **72**(12): p. 125206.
112. Devanathan, R., T. Diaz de la Rubia, and W.J. Weber, *Displacement threshold energies in  $\beta$ -SiC*. Journal of Nuclear Materials, 1998. **253**(1–3): p. 47-52.
  113. Kumagai, T., S. Izumi, S. Hara, and S. Sakai, *Development of bond-order potentials that can reproduce the elastic constants and melting point of silicon for classical molecular dynamics simulation*. Computational Materials Science, 2007. **39**(2): p. 457-464.
  114. Bazant, M.Z., E. Kaxiras, and J. Justo, *Environment-dependent interatomic potential for bulk silicon*. Physical Review B, 1997. **56**(14): p. 8542.
  115. Lucas, G., M. Bertolus, and L. Pizzagalli, *An environment-dependent interatomic potential for silicon carbide: calculation of bulk properties, high-pressure phases, point and extended defects, and amorphous structures*. Journal of Physics: Condensed Matter, 2010. **22**(3): p. 035802.
  116. Baskes, M.I., J.S. Nelson, and A.F. Wright, *Semiempirical modified embedded-atom potentials for silicon and germanium*. Physical Review B, 1989. **40**(9): p. 6085-6100.
  117. Brenner, D.W., *Empirical potential for hydrocarbons for use in simulating the chemical vapor deposition of diamond films*. Physical Review B, 1990. **42**(15): p. 9458-9471.
  118. Stuart, S.J., A.B. Tutein, and J.A. Harrison, *A reactive potential for hydrocarbons with intermolecular interactions*. The Journal of Chemical Physics, 2000. **112**(14): p. 6472-6486.
  119. van Duin, A.C.T., S. Dasgupta, F. Lorant, and W.A. Goddard, *ReaxFF: A Reactive Force Field for Hydrocarbons*. The Journal of Physical Chemistry A, 2001. **105**(41): p. 9396-9409.
  120. Erhart, P. and K. Albe, *Analytical potential for atomistic simulations of silicon, carbon, and silicon carbide*. Physical Review B, 2005. **71**(3): p. 035211.
  121. Yu, J., S.B. Sinnott, and S.R. Phillpot, *Charge optimized many-body potential for the Si/SiO<sub>2</sub> system*. Physical Review B, 2007. **75**(8): p. 085311.
  122. Zhou, X.W. and F.P. Doty, *Embedded-ion method: An analytical energy-conserving charge-transfer interatomic potential and its application to the La-Br system*. Physical Review B, 2008. **78**(22): p. 224307.
  123. Bartók, A.P., M.C. Payne, R. Kondor, and G. Csányi, *Gaussian Approximation Potentials: The Accuracy of Quantum Mechanics, without the Electrons*. Physical Review Letters, 2010. **104**(13): p. 136403.
  124. de Brito Mota, F., J.F. Justo, and A. Fazzio, *Structural properties of amorphous silicon nitride*. Physical Review B, 1998. **58**(13): p. 8323.
  125. Matsunaga, K. and Y. Iwamoto, *Molecular Dynamics Study of Atomic Structure and Diffusion Behavior in Amorphous Silicon Nitride Containing Boron*. Journal of the American Ceramic Society, 2001. **84**(10): p. 2213-2219.
  126. Matsunaga, K., C. Fisher, and H. Matsubara, *Tersoff Potential Parameters for Simulating Cubic Boron Carbonitrides*. Japanese Journal of Applied physics, 2000. **39**: p. L48-L51.
  127. Pastewka, L., A. Klemen, P. Gumbsch, and M. Moseler, *Screened empirical bond-order potentials for Si-C*. Physical Review B, 2013. **87**(20): p. 205410.
  128. Pastewka, L., P. Pou, R. Pérez, P. Gumbsch, and M. Moseler, *Describing bond-breaking processes by reactive potentials: Importance of an environment-dependent interaction range*. Physical Review B, 2008. **78**(16): p. 161402.
  129. Ikawa, N., S. Shimada, H. Tanaka, and G. Ohmori, *An Atomistic Analysis of Nanometric Chip Removal as Affected by Tool-Work Interaction in Diamond Turning*. CIRP Annals - Manufacturing Technology, 1991. **40**(1): p. 551-554.
  130. Nordlund, K., J. Keinonen, and T. Mattila, *Formation of Ion Irradiation Induced Small-Scale Defects on Graphite Surfaces*. Physical Review Letters, 1996. **77**(4): p. 699.
  131. Goel, S., *A topical review on "The current understanding on the diamond machining of silicon carbide"*. Journal of Physics D: Applied Physics, 2014. **47**(24): p. 243001.
  132. Goel, S., A. Stukowski, X. Luo, A. Agrawal, and R.L. Reuben, *Anisotropy of single-crystal 3C-SiC during nanometric cutting*. Modelling and Simulation in Materials Science and Engineering, 2013. **21**(6): p. 065004.

133. Zhang, Z.G., F.Z. Fang, X.T. Hu, and C.K. Sun, *Molecular dynamics study on various nanometric cutting boundary conditions*. Journal of Vacuum Science & Technology B, 2009. **27**(3): p. 1355-1360.
134. Goel, S., X. Luo, and R.L. Reuben, *Wear mechanism of diamond tools against single crystal silicon in single point diamond turning process*. Tribology International, 2013. **57**(0): p. 272-281.
135. Pizani, P.S., R. Jasinevicius, J.G. Duduch, and A.J.V. Porto, *Ductile and brittle modes in single-point-diamond-turning of silicon probed by Raman scattering*. Journal of Materials Science Letters, 1999. **18**(14): p. 1185-1187.
136. Stukowski, A., *Structure identification methods for atomistic simulations of crystalline materials*. Modelling and Simulation in Materials Science and Engineering, 2012. **20**(4): p. 045021.
137. Cheong, W.C.D. and L.C. Zhang, *Molecular dynamics simulation of phase transformations in silicon monocrystals due to nano-indentation*. Nanotechnology, 2000. **11**(3): p. 173.
138. Ackland, G.J. and A.P. Jones, *Applications of local crystal structure measures in experiment and simulation*. Physical Review B, 2006. **73**(5): p. 054104.
139. Francis Brent Neal, J., *PhD Thesis on Molecular dynamics simulations of adhesion and nanoindentation of Gallium Arsenide*, in *The Department of Physics and Astronomy*. 2002, Louisiana State University.
140. Goel, S., X. Luo, R.L. Reuben, and H. Pen, *Influence of temperature and crystal orientation on tool wear during single point diamond turning of silicon*. Wear, 2012. **284–285**(0): p. 65-72.
141. Pei, Q.X., C. Lu, and H.P. Lee, *Large scale molecular dynamics study of nanometric machining of copper*. Computational Materials Science, 2007. **41**(2): p. 177-185.
142. Kelchner, C.L., S.J. Plimpton, and J.C. Hamilton, *Dislocation nucleation and defect structure during surface indentation*. Physical Review B, 1998. **58**(17): p. 11085.
143. Goel, S., W.B. Rashid, X. Luo, A. Agrawal, and V. Jain, *A theoretical assessment of surface defect machining and hot machining of nanocrystalline silicon carbide*. Journal of Manufacturing Science and Engineering, 2014.
144. Komanduri, R., N. Chandrasekaran, and L.M. Raff, *M.D. Simulation of nanometric cutting of single crystal aluminum—effect of crystal orientation and direction of cutting*. Wear, 2000. **242**(1–2): p. 60-88.
145. Pastewka, L., S. Moser, P. Gumbsch, and M. Moseler, *Anisotropic mechanical amorphization drives wear in diamond*. Nature Materials, 2011. **10**(1): p. 34-38.
146. Uddin, M.S., K.H.W. Seah, X.P. Li, M. Rahman, and K. Liu, *Effect of crystallographic orientation on wear of diamond tools for nano-scale ductile cutting of silicon*. Wear, 2004. **257**(7-8): p. 751-759.
147. Chen, H.P., R.K. Kalia, A. Nakano, P. Vashishta, and I. Szlufarska, *Multimillion-atom nanoindentation simulation of crystalline silicon carbide: Orientation dependence and anisotropic pileup*. Journal of Applied Physics, 2007. **102**(6).
148. Wang, C., K. Cheng, N. Nelson, W. Sawangsri, and R. Rakowski, *Cutting force-based analysis and correlative observations on the tool wear in diamond turning of single-crystal silicon*. Proceedings of the Institution of Mechanical Engineers, Part B: Journal of Engineering Manufacture, 2014: p. 0954405414543316.
149. Zykova-Timan, T., D. Ceresoli, and E. Tosatti, *Peak effect versus skating in high-temperature nanofriction*. Nature Materials, 2007. **6**(3): p. 230-234.
150. Patten J.A., Cherukuri H., and J. Yan, *Ductile Regime Machining of Semiconductors and Ceramics*, in *High Pressure Surface Science and Engineering*, Y.G. Gogotsi and V. Domnich, Editors. 2003, Taylor and Francis, CRC Press: Philadelphia, Pennsylvania, USA. p. 639.
151. Domnich, V. and Y. Gogotsi, *Phase transformations in silicon under contact loading*. Reviews on advanced materials science, 2001. **3**(1).

152. Zarudi, I., L. Zhang, W. Cheong, and T. Yu, *The difference of phase distributions in silicon after indentation with Berkovich and spherical indenters*. Acta Materialia, 2005. **53**(18): p. 4795-4800.
153. Mylvaganam, K., L. Zhang, P. Eyben, J. Mody, and W. Vandervorst, *Evolution of metastable phases in silicon during nanoindentation: mechanism analysis and experimental verification*. Nanotechnology, 2009. **20**(30): p. 305705.
154. Trenkle, J.C., C.E. Packard, and C.A. Schuh, *Hot nanoindentation in inert environments*. Review of Scientific Instruments, 2010. **81**(7): p. 073901-13.
155. Gridneva, I.V., Y.V. Milman, and V.I. Trefilov, *Phase transition in diamond-structure crystals during hardness measurements*. physica status solidi (a), 1972. **14**(1): p. 177-182.
156. Jamieson, J.C., *Crystal Structures at High Pressures of Metallic Modifications of Silicon and Germanium*. Science, 1963. **139**(3556): p. 762-764.
157. Jasinevicius, R.G., J.G. Duduch, L. Montanari, and P.S. Pizani, *Phase transformation and residual stress probed by Raman spectroscopy in diamond-turned single crystal silicon*. Proceedings of the Institution of Mechanical Engineers, Part B: Journal of Engineering Manufacture, 2008. **222**(9): p. 1065-1073.
158. Yan, J.W., H. Takahashi, J. Tamaki, X. Gai, and T. Kuriyagawa, *Transmission electron microscopic observation of nanoindentations made on ductile-machined silicon wafers*. Applied Physics Letters, 2005. **87**(21).
159. Ge, D., V. Domnich, and Y. Gogotsi, *High-resolution transmission electron microscopy study of metastable silicon phases produced by nanoindentation*. Journal of Applied Physics, 2003. **93**(5): p. 2418-2423.
160. Budnitzki, M. and M. Kuna, *A thermomechanical constitutive model for phase transformations in silicon under pressure and contact loading conditions*. International Journal of Solids and Structures, 2012. **49**(11): p. 1316-1324.
161. Vodenitcharova, T. and L. Zhang, *A new constitutive model for the phase transformations in mono-crystalline silicon*. International Journal of Solids and Structures, 2004. **41**(18): p. 5411-5424.
162. Smith, G., E. Tadmor, N. Bernstein, and E. Kaxiras, *Multiscale simulations of silicon nanoindentation*. Acta Materialia, 2001. **49**(19): p. 4089-4101.
163. Smith, G., E. Tadmor, and E. Kaxiras, *Multiscale simulation of loading and electrical resistance in silicon nanoindentation*. Physical Review Letters, 2000. **84**(6): p. 1260.
164. Kim, D. and S. Oh, *Atomistic simulation of structural phase transformations in monocrystalline silicon induced by nanoindentation*. Nanotechnology, 2006. **17**(9): p. 2259.
165. Wang, Y., S. Ruffell, K. Sears, A.P. Knights, J.E. Bradby, and J.S. Williams. *Electrical properties of Si-XII and Si-III formed by nanoindentation*. in *Optoelectronic and Microelectronic Materials and Devices (COMMAD), 2010 Conference on*. 2010.
166. Jardret, V., H. Zahouani, J.L. Loubet, and T.G. Mathia, *Understanding and quantification of elastic and plastic deformation during a scratch test*. Wear, 1998. **218**(1): p. 8-14.
167. Jasinevicius, R.G., J.G. Duduch, and P.S. Pizani, *Structure evaluation of submicrometre silicon chips removed by diamond turning*. Semiconductor Science and Technology, 2007. **22**(5): p. 561.
168. Cahn, R.W., *Metallic solid silicon*. Nature, 1992. **357**(6380): p. 645-646.
169. Chrobak, D., N. Tymiak, A. Beaver, O. Ugurlu, W.W. Gerberich, and R. Nowak, *Deconfinement leads to changes in the nanoscale plasticity of silicon*. Nat Nano, 2011. **6**(8): p. 480-484.
170. Cross, G.L.W., *Silicon nanoparticles: Isolation leads to change*. Nat Nano, 2011. **6**(8): p. 467-468.
171. Yury, G., Z. Guohui, K. Sang-Song, and C. Sabri, *Raman microspectroscopy analysis of pressure-induced metallization in scratching of silicon*. Semiconductor Science and Technology, 2001. **16**(5): p. 345.
172. Goel, S. and A. Anupam, *Effect of the crystal structure in influencing the material removal*

- mechanism during nanomachining of silicon (submitted)*. 2014.
173. Goel, S., N.H. Faisal, X. Luo, J. Yan, and A. Agrawal, *Nanoindentation of polysilicon and single crystal silicon: Molecular dynamics simulation and experimental validation*. Journal of Physics D: Applied Physics, 2014. **47**(27): p. 275304.
  174. Deb, S.K., M. Wilding, M. Somayazulu, and P.F. McMillan, *Pressure-induced amorphization and an amorphous–amorphous transition in densified porous silicon*. Nature, 2001. **414**(6863): p. 528-530.
  175. Yan, J., H. Takahashi, J.i. Tamaki, X. Gai, H. Harada, and J. Patten, *Nanoindentation tests on diamond-machined silicon wafers*. Applied Physics Letters, 2005. **86**(18): p. 181913.
  176. Wang, Y., J. Shi, and C. Ji, *A numerical study of residual stress induced in machined silicon surfaces by molecular dynamics simulation*. Applied Physics A, 2014. **115**(4): p. 1263-1279.
  177. Li, M. and T. Xu, *Topological and atomic scale characterization of grain boundary networks in polycrystalline and nanocrystalline materials*. Progress in Materials Science, 2011. **56**(6): p. 864-899.
  178. Sumitomo, T., H. Huang, and L. Zhou, *Deformation and material removal in a nanoscale multi-layer thin film solar panel using nanoscratch*. International Journal of Machine Tools and Manufacture, 2011. **51**(3): p. 182-189.
  179. Wang, Z.Y. and K.P. Rajurkar, *Wear of CBN tool in turning of silicon nitride with cryogenic cooling*. International Journal of Machine Tools and Manufacture, 1997. **37**(3): p. 319-326.
  180. Zong, W.J., Y.H. Huang, Y.L. Zhang, and T. Sun, *Conservation law of surface roughness in single point diamond turning*. International Journal of Machine Tools and Manufacture, 2014. **84**(0): p. 58-63.
  181. Brinksmeier, E., J.T. Cammett, W. König, P. Leskovar, J. Peters, and H.K. Tönshoff, *Residual Stresses — Measurement and Causes in Machining Processes*. CIRP Annals - Manufacturing Technology, 1982. **31**(2): p. 491-510.
  182. Wong, C.J., *Fracture and Wear of Diamond Cutting Tools*. Journal of Engineering Materials and Technology, 1981. **103**(4): p. 341-345.
  183. Paul, E., C.J. Evans, A. Mangamelli, M.L. McGlaufflin, and R.S. Polvani, *Chemical aspects of tool wear in single point diamond turning*. Precision Engineering, 1996. **18**(1): p. 4-19.
  184. Jackson, M. and J. Morrell, *Machining Brittle Materials Using Nanostructured Diamond Tools*, in *Machining with Nanomaterials*. 2009, Springer US. p. 1-30.
  185. Jasinevicius, R.G., J.G. Duduch, and A.J.V. Porto, *Investigation on diamond turning of silicon crystal - generation mechanism of surface cut with worn tool*. Journal of the Brazilian Society of Mechanical Sciences, 2001. **23**: p. 241-252.
  186. Li, X.P., T. He, and M. Rahman, *Tool wear characteristics and their effects on nanoscale ductile mode cutting of silicon wafer*. Wear, 2005. **259**(7-12): p. 1207-1214.
  187. Khurshudov, A.G., K. Kato, and H. Koide, *Wear of the AFM diamond tip sliding against silicon*. Wear, 1997. **203-204**: p. 22-27.
  188. Yan, J., Syoji, Katsuo, Tamaki, Jun'ichi, *Some observations on the wear of diamond tools in ultra-precision cutting of single-crystal silicon*. Wear, 2003. **255**(7-12): p. 1380-1387.
  189. Wilks, J., *Performance of diamonds as cutting tools for precision machining*. Precision Engineering, 1980. **2**(2): p. 57-70.
  190. Maekawa, K. and A. Itoh, *Friction and tool wear in nano-scale machining--a molecular dynamics approach*. Wear, 1995. **188**(1-2): p. 115-122.
  191. Cheng, K., X. Luo, R. Ward, and R. Holt, *Modeling and simulation of the tool wear in nanometric cutting*. Wear, 2003. **255**: p. 1427-1432.
  192. Cai, M.B., X.P. Li, and M. Rahman, *Study of the Mechanism of Groove Wear of the Diamond Tool in Nanoscale Ductile Mode Cutting of Monocrystalline Silicon*. Journal of Manufacturing Science and Engineering, 2007. **129**(2): p. 281-286.
  193. Cai, M.B., X.P. Li, and M. Rahman, *Characteristics of "dynamic hard particles" in nanoscale ductile mode cutting of monocrystalline silicon with diamond tools in relation to tool groove wear*. Wear, 2007. **263**(7-12): p. 1459-1466.

194. Narulkar, R., S. Bukkapatnam, L.M. Raff, and R. Komanduri, *Graphitization as a precursor to wear of diamond in machining pure iron: A molecular dynamics investigation*. Computational Materials Science, 2009. **45**(2): p. 358-366.
195. Zhiguo Wang, Y.L., Mingjun Chen, Zhen Tong, Jiaxuan Chen. *Analysis about diamond tool wear in nano-metric cutting of single crystal silicon using molecular dynamics method*. 2010: SPIE.
196. Fung, K., C. Tang, C.F. Cheung, and W. Law. *Molecular Dynamics Simulation of Plastic Deformation of Diamond at an Elevated Temperature*. in *Key Engineering Materials*. 2015: Trans Tech Publ.
197. Beyers, R., *Thermodynamic considerations in refractory metal-silicon-oxygen systems*. Journal of Applied Physics, 1984. **56**(1): p. 147-152.
198. Cheng, Z., *Reaction kinetics and structural evolution for the formation on nanocrystalline silicon carbide via carbothermal reduction*. MSc Thesis- Materials Science & Engineering, Georgia Institute of Technology, 2004.
199. Viscomi, F.a.H., L., *Kinetic and Mechanistic Study on the Formation of Silicon Carbide from Silica Flour and Coke Breeze*. Journal of Metals, 1978(6): p. 21-24.
200. Weimer, A.W., Nilsen, K. J., Cochran, G. A., and Roach, R. P., *Kinetics of Carbothermal Reduction Synthesis of Beta Silicon Carbide*. AIChE Journal, 1993. **39**(3): p. 493-502.
201. Pastewka, L., M. Mrovec, M. Moseler, and P. Gumbsch, *Bond order potentials for fracture, wear, and plasticity*. MRS Bulletin-Three decades of many-body potentials in materials research, 2012. **37**(5): p. 493-503.
202. Fineberg, J., *Diamonds are forever - or are they?* Nature Materials, 2011. **10**.
203. Rigney, D. and S. Karthikeyan, *The Evolution of Tribomaterial During Sliding: A Brief Introduction*. Tribology Letters, 2010. **39**(1): p. 3-7.
204. Zhang, Z., J. Yan, and T. Kuriyagawa, *Study on tool wear characteristics in diamond turning of reaction-bonded silicon carbide*. The International Journal of Advanced Manufacturing Technology, 2011. **57**(1): p. 117-125.
205. Albrecht, P., *New Developments in the Theory of the Metal-Cutting Process: Part I. The Ploughing Process in Metal Cutting*. Journal of Engineering for Industry, 1960. **82**(4): p. 348-357.
206. Woon, K.S., M. Rahman, K.S. Neo, and K. Liu, *The effect of tool edge radius on the contact phenomenon of tool-based micromachining*. International Journal of Machine Tools and Manufacture, 2008. **48**(12-13): p. 1395-1407.
207. Gilman, J.J., *Mechanochemistry*. Science, 1996. **274**(5284): p. 65-65.
208. Zong, W.J., T. Sun, D. Li, K. Cheng, and Y.C. Liang, *XPS analysis of the groove wearing marks on flank face of diamond tool in nanometric cutting of silicon wafer*. International Journal of Machine Tools and Manufacture, 2008. **48**(15): p. 1678-1687.
209. Goel, S., A. Stukowski, G. Goel, X. Luo, and R.L. Reuben, *Nanotribology at high temperatures*. Beilstein Journal of Nanotechnology, 2012. **3**: p. 586-588.
210. Goel, S., S.S. Joshi, G. Abdelal, and A. Agrawal, *Molecular dynamics simulation of nanoindentation of Fe<sub>3</sub>C and Fe<sub>4</sub>C*. Materials Science and Engineering: A, 2014. **597**(0): p. 331-341.
211. Henriksson, K.O.E., C. Björkas, and K. Nordlund, *Atomistic simulations of stainless steels: a many-body potential for the Fe-Cr-C system*. Journal of Physics: Condensed Matter, 2013. **25**(44): p. 445401.
212. Narulkar, R., *Investigations on the mechanism of wear of single crystal diamond tool in nanometric cutting of iron using molecular dynamics and the development of generalised potential energy surfaces(GPES) based on ab initio calculations.*, in *Mechanical Engineering*. 2009, Oklahoma State University: Oklahoma.
213. Komanduri, R. and M.C. Shaw, *Wear of synthetic diamond when grinding ferrous metals*. Nature, 1975. **255**(5505): p. 211-213.
214. Ravindra, D., J. Patten, and R. Jacobsen, *Hybrid laser ablation-single point diamond*

- turning machining process for CVD–silicon carbide ceramics*. International Journal of Manufacturing Research, 2013. **8**(3): p. 227-249.
215. John A. Patten, Jerry Jacob, Biswarup Bhattacharya, Andrew Grevstad, Ning Fang, and E.R. Marsh, *Chapter 2: Numerical simulations and cutting experiments on single point diamond machining of semiconductors and ceramics*, in *Semiconductor Machining at the Micro-Nano Scale*, J. Yan and J.A. Patten, Editors. 2007, Transworld Research Network: Trivandrum-695 023, Kerala, India.
  216. Ravindra, D. and J.A. Patten, *Chapter 4: Ductile regime material removal of silicon carbide(SiC)*, in *Silicon Carbide: New Materials, Production methods and application*, S.H. Vanger, Editor. 2011, Nova Publishers: Trivandrum, India. p. 141-167.
  217. Rashid, W.B., S. Goel, X. Luo, and J.M. Ritchie, *The development of a surface defect machining method for hard turning processes*. Wear, 2013. **302**(1–2): p. 1124-1135.
  218. Rashid, W.B., S. Goel, X. Luo, and J.M. Ritchie, *An experimental investigation for the improvement of attainable surface roughness during hard turning process*. Proceedings of the Institution of Mechanical Engineers, Part B: Journal of Engineering Manufacture, 2013. **227**(2): p. 338-342.
  219. Bartarya, G. and S.K. Choudhury, *Influence of machining parameters on forces and surface roughness during finish hard turning of EN 31 steel*. Proceedings of the Institution of Mechanical Engineers, Part B: Journal of Engineering Manufacture, 2013: p. 0954405413500492.
  220. Brinksmeier, E. and R. Gläbe, *Advances in Precision Machining of Steel*. CIRP Annals - Manufacturing Technology, 2001. **50**(1): p. 385-388.
  221. Evans, C. and J.B. Bryan, *Cryogenic Diamond Turning of Stainless Steel*. CIRP Annals - Manufacturing Technology, 1991. **40**(1): p. 571-575.
  222. Casstevens, J.M., *Diamond turning of steel in carbon-saturated atmospheres*. Precision Engineering, 1983. **5**(1): p. 9-15.
  223. Brehl, D.E. and T.A. Dow, *Review of vibration-assisted machining*. Precision Engineering, 2008. **32**(3): p. 153-172.
  224. Shamoto, E. and T. Moriwaki, *Ultraprecision Diamond Cutting of Hardened Steel by Applying Elliptical Vibration Cutting*. CIRP Annals - Manufacturing Technology, 1999. **48**(1): p. 441-444.
  225. Moriwaki, T. and E. Shamoto, *Ultraprecision Diamond Turning of Stainless Steel by Applying Ultrasonic Vibration*. CIRP Annals - Manufacturing Technology, 1991. **40**(1): p. 559-562.
  226. Yan, J., Z. Zhang, and T. Kuriyagawa, *Effect of Nanoparticle Lubrication in Diamond Turning of Reaction-Bonded SiC*. International Journal of Automation Technology, 2011. **5**(3): p. 307-312.
  227. Inada, A., S. Min, and H. Ohmori, *Micro cutting of ferrous materials using diamond tool under ionized coolant with carbon particles*. CIRP Annals - Manufacturing Technology, 2011. **60**(1): p. 97-100.
  228. Yan, J., Z. Zhang, and T. Kuriyagawa, *Tool wear control in diamond turning of high-strength mold materials by means of tool swinging*. CIRP Annals - Manufacturing Technology, 2010. **59**(1): p. 109-112.
  229. Tang, X., K. Nakamoto, K. Obata, and Y. Takeuchi, *Ultraprecision micromachining of hard material with tool wear suppression by using diamond tool with special chamfer*. CIRP Annals - Manufacturing Technology, 2013. **62**(1): p. 51-54.
  230. Zareena, A.R. and S.C. Veldhuis, *Tool wear mechanisms and tool life enhancement in ultra-precision machining of titanium*. Journal of Materials Processing Technology, 2012. **212**(3): p. 560-570.
  231. Kawasegi, N., H. Sugimori, H. Morimoto, N. Morita, and I. Hori, *Development of cutting tools with microscale and nanoscale textures to improve frictional behavior*. Precision Engineering, 2009. **33**(3): p. 248-254.

232. Chang, W., J. Sun, X. Luo, J.M. Ritchie, and C. Mack, *Investigation of microstructured milling tool for deferring tool wear*. *Wear*, 2011. **271**(9–10): p. 2433-2437.
233. Fujisaki, K., H. Yokota, N. Furushiro, Y. Yamagata, T. Taniguchi, R. Himeno, A. Makinouchi, and T. Higuchi, *Development of ultra-fine-grain binderless cBN tool for precision cutting of ferrous materials*. *Journal of Materials Processing Technology*, 2009. **209**(15-16): p. 5646-5652.
234. Goel, S., X. Luo, R.L. Reuben, and W.B. Rashid, *Replacing diamond cutting tools with CBN for efficient nanometric cutting of silicon*. *Materials Letters*, 2012. **68**(0): p. 507-509.
235. Fang, F.Z., Y.H. Chen, X.D. Zhang, X.T. Hu, and G.X. Zhang, *Nanometric cutting of single crystal silicon surfaces modified by ion implantation*. *CIRP Annals - Manufacturing Technology*, 2011. **60**(1): p. 527-530.
236. To, S., H. Wang, and E.V. Jelenković, *Enhancement of the machinability of silicon by hydrogen ion implantation for ultra-precision micro-cutting*. *International Journal of Machine Tools and Manufacture*, 2013. **74**(0): p. 50-55.
237. Jiwang, Y., S. Shin, I. Hiromichi, and I. Koji, *Recovery of microstructure and surface topography of grinding-damaged silicon wafers by nanosecond-pulsed laser irradiation*. *Semiconductor Science and Technology*, 2009. **24**(10): p. 105018.
238. Liang, Y., D. Li, Q. Bai, S. Wang, and M. Chen. *Molecular Dynamics Simulation of Elliptical Vibration Cutting*. in *Nano/Micro Engineered and Molecular Systems, 2006. NEMS'06. 1st IEEE International Conference on*. 2006: IEEE.
239. Sun, J., X. Luo, W. Chang, J. Ritchie, J. Chien, and A. Lee, *Fabrication of periodic nanostructures by single-point diamond turning with focused ion beam built tool tips*. *Journal of Micromechanics and Microengineering*, 2012. **22**(11): p. 115014.
240. Jayasena, B., C.D. Reddy, and S. Subbiah, *Separation, folding and shearing of graphene layers during wedge-based mechanical exfoliation*. *Nanotechnology*, 2013. **24**(20): p. 205301.
241. Shaw, M.C. and A. Vyas, *Chip Formation in the Machining of Hardened Steel*. *CIRP Annals - Manufacturing Technology*, 1993. **42**(1): p. 29-33.
242. Shaw, M.C. and A. Vyas, *The Mechanism of Chip Formation with Hard Turning Steel*. *CIRP Annals - Manufacturing Technology*, 1998. **47**(1): p. 77-82.
243. Danyluk, S. and R. Reaves, *Influence of fluids on the abrasion of silicon by diamond*. *Wear*, 1982. **77**(1): p. 81-87.
244. Rentsch, R. and I. Inasaki, *Effects of fluids on the surface generation in material removal processes - Molecular dynamics simulation*. *Cirp Annals-Manufacturing Technology*, 2006. **55**(1): p. 601-604.